AD-A235 372

(2)

GL-TR-90-0328

CBSD Version II
Component Models of the IR Celestial Background

John P. Kennealy and Gene A. Glaudell

Mission Research Corporation
One Tara Boulevard
Nashua, NH 03062-2801

7 December 1990

DTIC
ELECTE
MAY 0 6 1991
S E D

Scientific Report No. 1

APPROVED FOR PUBLIC RELEASE; DISTRIBUTION UNLIMITED

GEOPHYSICS LABORATORY
AIR FORCE SYSTEMS COMMAND
UNITED STATES AIR FORCE
HANSCOM AIR FORCE BASE, MASSACHUSETTS 01731-5000

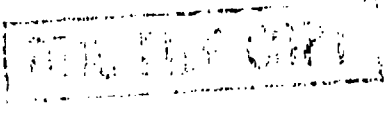

91 5 06 076

"This technical report has been reviewed and is approved for publication"

DAVID S. AKERSTROM
CONTRACT MANAGER

STEPHAN D. PRICE
BRANCH CHIEF

FOR THE COMMANDER

R. EARL GOOD
DIVISION DIRECTOR

This report has been reviewed by the ESD Public Affairs Office (PA) and is releasable to the National Technical Information Service (NTIS).

Qualified requestors may obtain additional copies from the Defense Technical Information Center. All others should apply to the National Technical Information Service.

If your address has changed, or if you wish to be removed from the mailing list, or if the addressee is no longer employed by your organization, please notify GL/DAA, Hanscom AFB, MA 01731. This will assist us in maintaining a current mailing list.

Do not return copies of this report unless contractual obligations or notices on a specific document requires that it be returned.

REPORT DOCUMENTATION PAGE

Form Approved
OMB No 0704 0188

Public reporting burden for this collection of information is estimated to average 1 hour per response, including the time for reviewing instructions, searching existing data sources, gathering and maintaining the data needed, and completing and reviewing the collection of information. Send comments regarding this burden estimate or any other aspect of this collection of information, including suggestions for reducing this burden, to Washington Headquarters Services, Directorate for information Operations and Reports, 1215 Jefferson Davis Highway, Suite 1204, Arlington, VA 22202-4302, and to the Office of Management and Budget, Paperwork Reduction Project (0704-0188), Washington, DC 20503

1. AGENCY USE ONLY (Leave blank)	2. REPORT DATE	3. REPORT TYPE AND DATES COVERED
	7 December 1990	Scientific Report #1

4. TITLE AND SUBTITLE
CBSD Version II Component Models of the IR Celestial Background

5. FUNDING NUMBERS
PE 63220C
PR S321 TA 18 WU AC
Contract F19628-88-C-0014

6. AUTHOR(S)
John P. Kennealy and Gene A. Glaudell

7. PERFORMING ORGANIZATION NAME(S) AND ADDRESS(ES)
Mission Research Corporation
One Tara Blvd
Nashua, NH 03062

8. PERFORMING ORGANIZATION REPORT NUMBER

9. SPONSORING/MONITORING AGENCY NAME(S) AND ADDRESS(ES)
Geophysics Laboratory
Hanscom AFB, MA 01731-5000

Contract Manager: David Akerstrom/OPC

10. SPONSORING/MONITORING AGENCY REPORT NUMBER
GL-TR-90-0328

11. SUPPLEMENTARY NOTES

12a. DISTRIBUTION/AVAILABILITY STATEMENT
Approved for public release; distribution unlimited

12b. DISTRIBUTION CODE

13. ABSTRACT (Maximum 200 words)

CBSD Version II addresses the development of algorithms and software which implement realistic models of all the primary celestial background phenomenologies, including solar system, galactic, and extra-galactic features. During 1990, the CBSD program developed and refined IR scene generation models for the zodiacal emission, thermal emission from asteroids and planets, and the galactic point source background. Chapters in this report are devoted to each of those areas. Ongoing extensions to the point source module for extended source descriptions of nebulae and HII regions are briefly discussed. Treatment of "small" galaxies will also be a natural extension of the current CBSD point source module. Although no CBSD module yet exists for inter-stellar IR cirrus, MRC has been working closely with the Royal Aerospace Establishment in England to achieve a data-based understanding of cirrus fractal characteristics. The CBSD modules discussed in Chapters 2, 3, and 4 are all now operational and have been employed to generate a significant variety of scenes. CBSD scene generation capability has been well accepted by both the IR astronomy community and the DoD user community and directly supports the SDIO SSGM program.

14. SUBJECT TERMS	15. NUMBER OF PAGES
Infrared Celestial Background Model Scenes Stars Zodiacal Asteroids	130
	16. PRICE CODE

17. SECURITY CLASSIFICATION OF REPORT	18. SECURITY CLASSIFICATION OF THIS PAGE	19. SECURITY CLASSIFICATION OF ABSTRACT	20. LIMITATION OF ABSTRACT
Unclassified	Unclassified	Unclassified	SAR

CBSD Version II
Component Models of the IR Celestial Background

Accession For
NTIS GRA&I
DTIC TAB
Unannounced
Justification
By
Distribution/
Availability Codes
Dist | Avail and/or Special
A-1

CONTENTS

1	INTRODUCTION	P. 1
2	THE CBSD ZODIACAL EMISSION MODULE	P. 5
3	THE CBSD POINT SOURCE BACKGROUND MODULE	P. 36
	Appendix 3-1: SKY Version 3 User Guide	P. 92
	Appendix 3-2: CBPSIMG5 Code Listing	P. 105
4	THE CBSD ASTEROIDS, SUN, MOON, AND PLANETS MODULE	P. 117
5	SUMMARY	P. 125

1 INTRODUCTION

1.1 DATA AND MODELS

During CBSD Phase-I, the major CBSD "deliverables" objectives were montages of CBSD re-processed IRAS Sky Flux Plates. The CBSD "re-processing" emphasized de-striping and flat-fielding of standard NASA/IRAS Sky Flux Plates.

The purpose of the de-striping was to attenuate the visibility of striping artifacts, which were a consequence of incomplete detector bias/gain compensation in the original generation of Sky Flux Plates. The purpose of the flat-fielding was to remove the dominating, date-dependent zodiacal emission background contributions to the scenes described by the Sky Flux Plates. Beginning in 1989, these interim CBSD products were significant in that they represented the best available scene/image data product descriptions of the complex IR celestial background.

During 1991, the CBSD Phase-I products will begin to become superseded by new NASA-standard IRAS data products which are currently referred to as "Super Sky Flux Plates." In conjunction with CBSD Phase-II products, they will be a new and useful resource for describing IR celestial backgrounds. The "Super Sky Flux Plates" are being generated at NASA's CalTech/JPL IPAC (Infrared Processing & Analysis Center).

In the context of CBSD development, MRC has been working closely with IPAC to access the most up-to-date IRAS data products available; e.g. MRC has also been a "beta" test site for one of IPAC's new Zodiacal History File products, and MRC has been given pre-release samples of Super Sky Flux. In this introduction to CBSD Phase-II work, it makes sense to describe the nature of the "Super Sky Flux Plates," so that CBSD users will have an understanding of how CBSD scene generation capability complements IRAS image data. The following is an unofficial pre-release summary of Super Sky Flux:

Plates for ecliptic latitudes >50° are scheduled to be available in Spring 1991; full-sky coverage is scheduled to be available in December 1991.

Pixel size will be 1.5 arc-minutes, compared to 2 arc-minutes in the current generation of IRAS Sky Flux Plates.

Plate size will be 12.5° × 12.5°, compared to Sky Flux's 16.5° × 16.5°;

Striping has been greatly reduced by pre-processing the raw scan data specifically to minimize detector-to-detector and scan-to-scan artifacts;

The time-dependent zodiacal emission contribution is being removed;

In addition to individual HCON Plate sets, a three HCON co-add plate set is being developed; however, regions within ±30° of the ecliptic plane may not be included in the co-add plate set sent to NSSDC for general distribution.

Super Sky Flux will constitute the best available all-sky IRAS image data. Nevertheless, relative to highly general IR celestial background scene requirements, there are still significant limitations; e.g.

the spatial resolution of Super Sky Flux images will be about 4 arc-minutes (or about 1 milli-radian), coarse relative to the CBSD requirement of 5-10 arc-seconds (e.g. a few tens of micro-radians);

the Super Sky Flux spectral coverage and spectral resolution are fixed by the four broad IRAS bands, centered at 12, 25, 60, and 100 μm, whereas CBSD must be able to generate scenes anywhere in the 2-30μm spectral range, with a spectral resolution of 0.1μm;

the CBSD must generate scenes with a flux threshold about 50 times lower than the IRAS (12 and 25μm) sensitivity limit.

Phase-II CBSD must provide a IR celestial background scene description capability which is consistent with existing data such as IRAS Super Sky Flux, but which is not limited to the spatial, spectral, and sensitivity domains of existing data. This requirement can only be satisfied by a set of models which employ sound scientific judgment to extend the domain of model utility beyond the constraints of existing data.

1.2 THE CBSD MULTI-COMPONENT MODEL

CBSD Phase-II works to address the above-stated objective via development of algorithms and software which implement realistic models of all the primary celestial background phenomenologies. These are summarized in Figure 1.2-1, which also illustrates the natural division into solar system, galactic, and extra-galactic features.

During the past year, the CBSD program has developed and refined IR scene generation models for the zodiacal emission, thermal emission from asteroids and planets, and the galactic point source background. Separate chapters in this report are devoted to each of those areas.

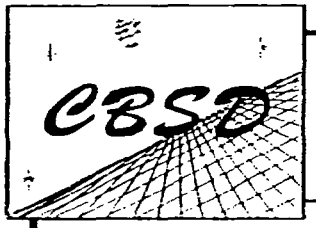

IR Background Components

- **Solar System Components**
  - Planets, Satellites, & Asteroids
  - Zodiacal Dust (Broad & Bands)
  - Cometary Dust Trails
- **Galactic Components**
  - Stellar Sources
  - Cirrus Structures
  - HII Regions
  - Nebulae
- **Extra-Galactic Components**
  - Large Galaxies
  - Small Galaxies

In Chapter 3, which addresses the point source scene generation module, ongoing extensions to that module for extended source descriptions of nebulae and HII regions are briefly discussed.

As is also indicated in Chapter 3, the CBSD treatment of "small" galaxies will be a natural extension of the point source module's reliance on the NASA/Ames SKY model.

In addition, MRC has had discussions with IPAC for the purpose of accessing digital forms of IPAC's published IRAS data base on large galaxies. During 1991, MRC will assimilate that data base into CBSD such that about 30 of the largest galaxies will be individually described in CBSD in a form consistent with the IRAS data.

Although it is not covered in this report because of its preliminary status, a CBSD module for cometary dust trails has been developed by Sykes et al at Steward Observatory (University of Arizona) and is now being tested by MRC. This module attempts to describe extended (tens of degrees) dust trails associated with 120 comets by employing the high-quality IRAS Tempel-2 data as a basis model.

Although no CBSD module yet exists for inter-stellar IR cirrus, MRC has been working closely with Jones et al at RAE in England, to achieve a data-based understanding of cirrus fractal characteristics. MRC has provided RAE with CBSD-processed versions of IRAS Sky Flux plate data in several cirrus-dominated regions and RAE has begun to make progress in deriving useful fractal paramaterizations from these data. Most recently, MRC has also provided RAE with copies of pre-release Super Sky Flux for similar analyses.

The CBSD modules discussed in Chapters 2, 3, and 4 are all now operational and have been employed to generate a significant variety of scenes. Some of those scenes have been specifically generated for comparison with IRAS plates, and the results have been quite satisfactory. Those results, whose most effective illustration require color capability, have now been widely shown and discussed at various meetings. The CBSD scene generation capability has been well accepted by both the IR astronomy community and the potential DoD user community.

Early versions of the CBSD zodiacal and point source modules were delivered to (June 1990) and are now employed within Version 1 of the SDIO Strategic Scene Generator Model (SSGM). The most recent versions of these CBSD modules and the CBSD asteroids/planets module, described in subsequent chapters, will be integrated with Version 2 of the SSGM during the first half of 1991.

2 THE CBSD ZODIACAL EMISSION MODULE

2.0 CBZODY STATUS UPDATE

Much of 1990 has been spent in the testing, cleanup, and retesting of CBZODY; in a careful review of the IRAS ZOHF database and evaluation of a new point-source removed version of ZOHF; in the development of software to extract and fit an optimal subset of ZOHF observations; and in a literature search to collate the results of other studies of zodiacal emission models and to determine the current understanding of all aspects of the zodiacal dust cloud. We present results of this work below.

2.1 INTRODUCTION

The CBSD Zodiacal Emission Model code (CBZODY) simulates the contribution of thermal emission from the solar system dust cloud to the 2 - 30 μm infrared celestial background (IRCB). This emission dominates the diffuse IR background over most of this waveband (scattering of sunlight by the zodiacal dust becomes an important contribution to the background for wavelengths $\lambda < 4\,\mu$m).

The apparent zodiacal brightness drops by a factor of roughly 3 between the ecliptic plane at 90° solar elongation (Sun-Earth-Observation angle E) and the ecliptic poles ($I_\nu \approx 80$ MJy/sr in the IRAS 25 μm band, and 1 MJy/sr = 10^6 Janskys/steradian). Figures 3-5 show typical IRAS scans in all 4 wavebands. Infrared and optical studies suggest that the zodiacal dust cloud is a disk-like structure slightly inclined to the Earth's orbital plane ($i \approx 2°$) with an ascending node Ω estimated to be between 40° - 110° depending on the data and methods used. Because the dust cloud is inclined with respect to the Earth's orbit and neither the cloud nor the Earth's orbit are circularly symmetric about the Sun, the relative geometry of the Earth, Sun, and dust cloud depends on the Earth's orbital position. Therefore, the apparent zodiacal contribution to the IR sky varies with time. [For brief, somewhat dated reviews of IR and optical work see Hauser (1988) and Giese (1980), respectively. For an extensive pre-IRAS reviews see Lienert (1975), and Weinberg and Sparrow (1978)].

In addition to the large-scale dust cloud emission, analyses of observations from the Infrared Astronomical Satellite (IRAS) have revealed narrow bands of emission which occur in symmetric pairs above and below the zodiacal cloud symmetry plane ($i \approx 1° - 10°$ for the most prominent bands). These structures contain several percent of the peak zodiacal brightness. [See Sykes *et.al.* (1989) for review.] The bands are thought to be tori of dust particles associated with different families of asteroids. Observations of both diffuse and banded emission are consistent with dynamical models of dust originating from solar system objects, most likely comets and asteroids. [Dohnanyi (1978) reviews interplanetary dust particle dynamics]. However, current dynamical models of the dust contain many more parameters than can be constrained by available observations.

CBZODY simulates both the diffuse zodiacal dust cloud and dust band contributions to the IRCB with simple physical models of the dust number density distribution and the dust emission spectrum based on available scientific data and current theories of solar system dust phenomena. The use of simple physical models instead of phenomenological descriptions of observations, or complex dynamical models, enables CBZODY to predict the zodiacal contribution to the IRCB at geometries and wavelengths where observations are limited or non-existent, while minimizing the number of parameters and computation time used to model the IRCB. This makes CBZODY a valuable tool to plan strategies for future observations, and to test, improve, and compare models of the zodiacal dust complex.

The following sections discuss various aspects of the CBZODY module. Section 2 describes CBZODY capabilities. Section 3 gives a rough sketch of the structure of the CBZODY module. Section 4 describes the models of dust cloud and bands used in CBZODY. Section 5 discusses validation of these models using available observations. Section 6 describes the improvements made in the CBZODY code.

2.2 CBZODY CAPABILITIES

CBZODY simulates space-based observations of the zodiacal thermal emission brightness density in Janskys/steradian (Jy/sr) for user-specified spectral filter, sky regions, and dates including Universal Time (UT) of observation. Some model parameters and assumptions can also be altered at run time. Observation parameters can be input interactively from the keyboard or read in from a parameter file. Output can be to a terminal screen, ASCII files, or FITS format image files. Spectral filter response for λ = 1 - 30 μm at $\Delta\lambda$ = 0.1 μm spectral resolution is specified in an ASCII file. Sky regions can be gnomonic projections of patches of the sky in equatorial coordinates similar to the IRAS Skyflux plates, or sky brightness can be obtained for lists of arbitrary points on the sky in equatorial (α, δ), ecliptic (λ, β), or differential ecliptic (λ-λ_{sun}, β) coordinate systems. Model parameters can be specified in a separate input parameter file.

The wavelength-dependent volumetric emissivity ϵ_λ of the model dust particle population as a function of heliocentric distance D is also tabulated in a user-specified ASCII file. This emissivity table, supplied by Bill Reach (UC Berkeley) depends on the detailed properties of the dust particle population (spatial variations in particle composition, structure, size distribution) and is based on an analysis of emissivity of dust near the Earth's orbit using IRAS broad-band colors [Reach, 1988].

In addition to the above capabilities, code for fitting the CBZODY model parameters to the IRAS Zodiacal Observation History File (ZOHF) data product, and for testing CBZODY as a whole and as individual subroutines are also being developed.

CBZODY is intended to be completely Fortran 77 ANSI-compliant (F77).

2.3 CBZODY CODE OVERVIEW

The following is a brief pseudo-code description of how CBZODY computes the dust cloud and dust band brightnesses in a specified region of the sky.

First, CBZODY reads in all necessary user input and performs one-time computations (initializations, Earth's orbital position, etc.) Some one-time computations (for example, the band-limited volumetric emissivity ϵ_b vs. D table) are flagged for first-pass execution inside repeatedly called subroutines.

Second, CBZODY enters a loop appropriate to the desired input/output mode (gnomonic projection of sky patch, keyboard pixel coordinate list, *etc.*). The sky coordinates are transformed to the dust model input coordinate system (differential ecliptic), and passed in the call to the LOS brightness computation subroutine (DUST3).

Third, for each pixel, the brightness is computed by integrating the dust cloud model emissivity along the LOS. This involves numerically integrating the product of the model dust number-density distribution $n(R,z)$ and an interpolation of the table of band-limited volumetric emissivity $\epsilon_b(D)$.

Fourth, the contribution of each dust band is computed. This involves determining the intersection of the LOS with a thin-ribbon model of the dust bands (see discussion of dust band model), looking up the normalized brightness density in the latitudinal profile table for each band, and multiplying by the appropriate geometric and spectral band scaling factors.

This pixel-by-pixel brightness density computation repeats for each pixel coordinate pair requested.

2.4 CBZODY MODEL OF THE ZODIACAL DUST COMPLEX

CBZODY describes the zodiacal dust complex as a multi-component system consisting of a diffuse cloud of dust distributed throughout the inner solar system and several (currently three) pairs of dust bands nominally associated with specific asteroid families (Eos, Koronis, and Themis). Each component's dust particle population characteristics are assumed homogeneous throughout space.

There has been apparent ambiguity pertaining to coordinate systems in early versions of CBZODY. This reflects both poorly written and inaccurately commented original code, the traditional Fortran restrictions on variable names, and conflicting definitions and incorrect citations in the literature. A brief aside on coordinate nomenclature for zodiacal dust cloud geometry will hopefully clear the fog (or at least point out some of the pitfalls).

Figure 1 presents the Sun-Earth-LOS geometry for a specific location P in the dust cloud with geometric quantities labelled. The origin of much of the problem is the extension of ecliptic plane geometric terminology beyond the plane. For example, "elongation" has been used for both "solar" (E) and "ecliptic" ($\lambda-\lambda_{sun}$) elongation, which are only equivalent in the ecliptic plane. We will use "differential ecliptic longitude" for "ecliptic elongation" ($\lambda-\lambda_{sun}$) to avoid confusion since the quantity is simply related to ecliptic longitude, and retain solar elongation. Another example is confusion between distance from the Sun (r in the literature, D here) and distance from the Sun projected into the dust cloud symmetry plane (R here). Again these are identical distances for in-plane measurements, but <u>not</u> for out-of-plane observations.

Misinterpretations have resulted from confusing these quantities. Our definitions of distance quantities are discussed in the model descriptions below and shown in Figure 1. We have tried to avoid these pitfalls in our definitions, and have revamped CBZODY variable names where necessary within the constraints of Fortran 77's 6-character case-insensitive variable names.

The CBZODY model for the dust cloud number-density distribution is azimuthally symmetric about its plane of symmetry, and hence completely described by cylindrical coordinates at constant azimuth (R,z). The zodiacal dust cloud symmetry plane is specified by its inclination angle (i) and ascending node (Ω) with respect to the ecliptic plane. It is also useful to define

$$D = (R^2 + z^2)^{1/2},$$

as the distance to the Sun, and β_{sun} as the heliocentric latitude measured from the symmetry plane of the dust cloud. Note that the definitions of D and R are reversed in the original CBZODY code, which was another source of confusion.

The density model $n(R,z)$ is separable into the product of two functions

$$n(R,z) = n(D, \beta_{sun}) = f(D) \cdot f(\beta_{sun}) \ ;$$

$$f(D) = n_0 \cdot D^{-1} \ ;$$

(n_0 = density at D = 1 AU, β_{sun} = 0°) .

Note that

$$\beta_{sun} = \arctan(z/R) \ .$$

This is the standard form of most zodiacal dust cloud density models to date. Note that the original version of the CBZODY code used R^{-1} in place of D^{-1} in the power-law term. This was changed to D^{-1} in the current version of the code to conform with the standard physical model of the dust cloud (see below). Computations show that this change has little effect on the model density contours near the Earth. Murdock and Price (1985) state that D^{-1} is the best-fit power-law model for Zodiacal Infrared Project (ZIP) IR rocket observations in the ecliptic plane, but that the fit is not satisfactory over the entire range of solar elongations (E = 22° - 180°).

The simplest dynamical model of the dust cloud hypothesizes that solar radiation drag in the form of the Poynting-Robertson (P-R) effect and corpuscular drag from the solar wind causes dust particles to spiral inward from solar system sources (comets and/or asteroids) on time-scales of 10^4 to 10^5 years. This drag force preserves orbital inclination and therefore β_{sun}, reduces the eccentricity of orbits, and tends toward a steady-state D^{-1} radial dust density distribution for a constant source of dust. These properties are independent of particle size and composition as long as P-R drag is the dominant perturbing force on the Sun's central gravitational field. However, particles from the same source will be segregated by composition and size because of the differing rates of infall, and dust populations are expected to evolve as a result of collisions and solar heat-induced structural changes.

A number of models have been proposed for the latitudinal density distribution $f(\beta_{sun})$, but to date none of them has fit satisfactorily over the all regions of the sky observed, nor consistently from waveband to waveband. CBZODY uses a Lorentzian latitudinal function

$$f(\beta_{sun}) = \Gamma^2 / (\Gamma^2 + \tan(\beta_{sun})^2 \ ,$$

or in cylindrical coordinates

$$f(R,z) = (1 + (z/\Gamma R)^2) \ ,$$

where Γ is the value of $\tan(\beta)$ corresponding to the half-width-half-max (HWHM) for $f(\beta_{sun})$ ($\Gamma \approx z_{\mathrm{HWHM}}$, R = 1 AU). Also note that

$$\sin(\beta_{sun}) = z/D \ ,$$

a term which also appears in some $f(\beta_{sun})$ models.

This Lorentzian density distribution shares properties of both the classical ellipsoidal and fan models of previous optical and IR studies studies (see Giese *et.al.*, 1986; Giese and Kneißel, 1989 for reviews). Both models take the standard form

$$n(D,\beta_{sun}) = D^{-\nu} f(\beta_{sun})$$

with latitudinal density distribution functions:

Fan Model -

$$f(\beta_{sun}) = \exp(-\Gamma_F |\sin(\beta_{sun})|) \ ;$$

Ellipsoidal Model -

$$f(\beta_{sun}) = (1 + (\Gamma_E \sin(\beta_{sun}))^2)^{-\nu/2} \ .$$

There are various versions of the fan model, qualitatively similar, possessing density contours which are pinched at small R, and approach a cusp at the point of maximum radial extent R_{max} for a given density contour. The fan model provides a consistent fit over a wide range of solar elongations, but it fails to fit well at all latitudes because of its unphysical cusp in the symmetry plane. This can be seen in fits to IRAS ZOHF scans (Rowan-Robinson *et.al.*, 1990).

The ellipsoidal model roughly fits the data at 90° solar elongation, although a lack of brightness at intermediate latitudes β_{sun} has been noted in zodiacal light studies (Giese *et.al.*, 1986). The CBZODY Lorenztian model has constant density contours which retain the successful features of the fan model while removing the unphysical cusp. This can be seen by considering constant density contours in the R-z plane [Figure 6]. The constant density contours approach an ellipsoidal model near their maximum extent. They are broader than ellipsoidal contours in the z-direction at intermediate R, but then reach a peak HWHM and start dropping back towards the symmetry plane as R approaches zero. Note that qualitatively, the Lorentzian model has more in common with the fan model than the ellipsoidal model, although in functional form it is easily mistaken for the ellipsoidal model.

The model for the volumetric emissivity of the dust assumes that the dust population is physically homogeneous throughout the solar system (same size distribution, same composition). This is not realistic, but is a reasonable simplifying assumption in the absence of sufficient data. The dynamics of the dust are expected to be size and composition dependent (P-R drag, radiation pressure, secular planetary perturbations), as is the evolution of the dust particle population

(collisions, solar heating). However, the effects of any inhomogenities may be reduced by the near-earth domination of LOS brightness, particularly near the ecliptic poles. In-plane brightnesses may be more dependent on spatial variations of dust particle properties because of the slow fall-off of emissivity with distance (see below). Also, studies suggest that particles of a small range of sizes will dominate the IR emission [Reach, 1988; Gustafson, 1990] (size $\approx$ 3 μm for typical particle size distributions and compositions). More sophisticated models of spatial variations of particle properties are probably not justified by available data, but can be added to CBZODY through the volumetric emissivity database file to study the sensitivity of CBZODY to these unknown properties of the dust.

One implicit model parameter that has been little discussed in previous fits of IR dust cloud models to observations is how the dust cloud density distribution is cutoff at large radii. Currently, CBZODY arbitrarily cuts off the dust cloud on the boundaries of cylinder with radius R = 6 AU and height Δz = $\pm$6 AU about symmetry plane. The apparent LOS brightness distribution is not sensitive to the choice of cutoff boundaries in the vertical direction since the density distribution is strongly concentrated towards the symmetry plane. However, the LOS brightness integral does not converge as rapidly in the ecliptic plane. In fact, the LOS dust density integral by itself diverges logarithmically ($n(R,z=0) \propto D^{-1}$, and the LOS brightness integral only converges because of the decrease in volumetric emissivity with distance ($\epsilon_\lambda \propto D^{-1.5}$ for $\lambda \approx 25\,\mu$m) [Figure 7]. Simple computations using these heliocentric distance dependencies suggest that $\approx$ 13% of the contribution to the LOS brightness comes from D = 3 - 6 AU and $\approx$ 7% comes from D = 4 - 6 AU (E = 180°) for a 6 AU cutoff. This is an important point, since the primary source of dust may be inside 4 AU (dust bands or short-period comets).

Note that this is not as much of an issue for optical studies since the amount of scattered light is suppressed by the proportionality to the solar flux itself ($\propto D^{-2}$) and the scattering function. How this directly relates to the IRAS observations is discussed in section 2.5.

The emission from each pair of dust bands is modelled as a thin, Sun-centered, toroidal ribbon with a radius equal to the perihelion distance of the asteroid family associated with the band pair. The circular symmetry and infinitesimal thickness allows each pair of bands to be described by a 1-D surface brightness profile in heliocentric latitude about the dust band symmetry plane. The profile is generated from a projection of Sykes (1990) 3-D dust band model convolved with a gaussian distribution of inclinations consistent with those of the nominal asteroid family. The current normalizations represent best-guesses consistent with high-pass filtered IRAS observations in the 25 μm band. Note that such a normalization scheme is only semi-quantitative, and that final normalization will be determined by a self-consistent fit to IRAS observations together with the CBZODY dust cloud model. We have found that the original dust band model is typically a factor of 2 - 3 below the dust cloud model residuals, but the qualitative structure of the band model appears consistent with the residuals [Figures 11-12]. A gray-body emissivity

spectrum with temperature characteristic of the associated asteroid family is assumed.

2.5 MODEL FITTING AND VALIDATION

IRAS observations are being used to verify that the CBZODY model of the zodiacal emission satisfactorally simulates available observations. This is being accomplished by finding the best-fit model to a well-understood subset of the IRAS data, verifying that the model yields acceptable residuals for this data, and examining the residuals for a larger set of the IRAS data to guide further refinements of the model. Other observations (for example, ZIP) would also be useful for evaluating the model fit at a wider range of solar elongations.

The IRAS low-resolution Zodiacal Observation History File data product (ZOHF) is being used to derive best-fit parameters for the CBZODY dust cloud model (IRAS Explanatory Supp., 1988). The ZOHF consists of processed one-dimensional scans of the sky binned into approximately 0.5° x 0.5° pixels in all four IRAS bands (effective wavelengths $\lambda_c \approx 12$, 25, 60, 100 μm). Only the 12 and 25 μm bands are being used for fitting, since contamination from galactic sources becomes a problem at 60 μm and dominates the sky at 100 μm. However, the 60 and 100 μm bands still contain useful color information, particularly in some relatively uncontaminated scans through the galactic anticenter.

There are several sources of systematic uncertainties in the data that can be summarized phenomonologically in the conversion from raw data-number (*DN*) to brightness densities (*I*)

$$I = GAIN \cdot DN + OFFSET$$

In principle, gain and offset parameters can fluctuate both between different scans and across single scans. Scan-to-scan fluctuations in both parameters appear to exist at the 5% level (Deul and Wolstencroft, 1988). In-scan fluctuations are ignored here, since they would be difficult to separate from real spatial variations in the zodiacal emission. However, it would be prudent to estimate the effect of small offset drifts (< 5%) on the results. There is also an overall factor of 2 discrepancy between IRAS and ZIP observations of the zodiacal emission which has not been resolved.

These systematic uncertainties in gain and offset are handled by treating them as uninteresting parameters which are always chosen to minimize the fit statistic. The standard deviation of the best-fit values for a range of scans should verify the estimated magnitude of the scan-to-scan fluctuations. 1-sigma ZOHF pixel-to-pixel statistical fluctuations are at the 0.01 - 0.02 MJy/sr level for 12 and 25 μm bands respectively, and are dominated by systematic uncertainties and the background contamination discussed below.

The real limitation in fitting the model to the data is the background contamination from infrared emission outside the solar system. There are several approaches to this problem. The simplest approach is to exclude from fitting those data points which are likely or known to be contaminated. This is the method currently used in CBZODY fits. All points within galactic latitude $\beta_{gal} = \pm 15°$ are excluded to

eliminate contamination by galactic emission concentrated towards the galactic plane. Also, all points within ecliptic latitudes $\beta = \pm 15°$ are excluded to eliminate the influence of the dust bands on the initial fit of the zodiacal dust cloud. This restriction can be lifted if fitting the dust band and dust cloud models simultaneously. Bright point sources are rare enough to be handled by hand for small numbers of scans, but a new IPAC data product, the Bright Point Source Removed ZOHF, can be used to identify pixels contaminated by bright point sources automatically. Regions around other well-known IR sources (for example, the Magellanic Clouds) are also excluded.

An alternative approach for handling background contamination is to do some sort of lower envelope fit in place of a least-squares residuals fit. This operates on the principle that background contamination is always positive, so data points which exceed model predictions are simply not used in fitting. This fit method has the added advantage of rejecting unphysical models (those which overestimate emission). However, lower envelope fit estimates are not robust in the presence of systematic and statistical fluctuations which significantly depress data points. Such effects (for, example, in-scan drifts in gain and offset) are known to be present in IRAS scans.

What can IRAS tell us about the zodiacal emission model parameters? To understand that we must consider the nature of the IRAS database. IRAS scans were restricted to solar elongation angles $E \approx 60° - 120°$, with only a few scans taken at elongations outside $E = 80° - 100°$ and a majority of the scans concentrated near $E = 90°$. Note that 90° scans are taken at a constant ecliptic longitude $\lambda = \lambda_{earth} \pm 90°$. So, IRAS effectively used the Earth's orbital motion to scan the sky. The IRAS mission was divided into 3 operational periods: a brief (approximately 1 month) initial set of scans at a wide range of solar elongations E; a 6-month double survey of the entire sky at $E = 90° \pm 10°$ degrees (HCON1 and HCON2); 3-months of a single survey starting at extreme elongations ($E \approx 60°$ and 120°) and slowly approaching $E = 90°$ (HCON3). [Figure 2]

Single scans can be used to put some constraints on the half-width r and normalization n_0 of the model density distribution, but the zodiacal emission must be observed throughout the Earth's orbit to determine the ascending node and inclination of the dust cloud symmetry plane. Since the emission varies with elongation, the initial fit uses scans at a single value of elongation ($E = 90°$) from a fairly uniform sampling of points on the Earth's orbit (18 positions over approximately 6 months). At each orbital position, the most nearly pole-to-pole scans were selected (typically ±1°, see Figure 2). The use of $E = 90°$ scans minimizes the variation of heliocentric distance D along the LOS, hence minimizing the sensitivity of best-fit estimates of Ω, i, and r to radial gradients in dust density and volumetric emissivity. The $E = 90°$ scan sample can be complemented by $E = 80°$ and 100° samples with similar 6-month coverage of the Earth's orbit at some cost in coverage near the ecliptic poles.

Note that the scan sample will not be uniform in the sense that the near-galactic plane regions excluded from scan fits varies with Earth's orbital position. The

effects on coverage of ecliptic latitude resulting from this masking out of the galactic plane should be considered in the analysis of fit results.

Actually, there are two sets of scan samples, since scans taken on the leading side of the Earth's orbit exhibit systematic asymmetries from trailing-side scans. These differences are best handled by fitting the two sets separately and comparing the results to determine if the observed asymmetries have significant effects on the best-fit parameters.

There are at least two other useful scan samples that can be culled from the survey. The last 3 months of operation (HCON3) produced a nearly continuous survey of elongations from 60° - 120° over a smaller interval of the Earth's orbit ($\Delta\lambda_{earth} < 90°$), and the initial month of the survey provided a complementary set of extreme solar elongation scans separated by roughly one-half orbit from the HCON3 extreme elongation scans.

The extreme solar elongation scans test the validity of the best-fit model beyond $E \approx 80° - 100°$. These scans provide some constraint on the radial power-law index of the density distribution, but this dependence is difficult to separate from radial variations in dust particle properties. The radial density variations are probably better constrained by the wide range of solar elongations observed in ZIP data.

In summary, $E = 80°$, 90°, and 100° samples are being used to derive best-fit parameters for the CBZODY model. The resulting best-fit model will be compared with extreme solar elongation scans ($E \approx 90° \pm 30°$) to determine the model's applicablity to these extreme elongations. The results of comparison of the model with the IRAS ZOHF database will determine the next step in the modelling process.

The 12 and 25 μm band observations will differ in sensitivity to contributions to the LOS emissivity integral from different regions of the zodiacal dust complex. The dust temperature near the Earth is estimated at $T_{dust} \approx 250K - 300K$ (peak blackbody brightness wavelength $\lambda_{peak} \approx 12\,\mu m$), and $T_{dust} \propto D^{-1/2}$. As D increases from 1 to 4 AU, λ_{peak} will increase from 12 to 25 μm. Therefore, the dust volumetric emissivity at $\lambda = 12\,\mu m$ will drop more quickly with $D > 1$ AU than at $\lambda = 25\,\mu m$ ($12\,\mu m < \lambda_{peak} < 25\,\mu m$). The net result is that the 12 μm band will be relatively more sensitive than the 25 μm band to LOS brightness integral contributions from near-Earth dust, and that the 25 μm band will be relatively more sensitive to dust outside the Earth's orbit, particularly dust near $D \approx 4$ AU (if there is any out there) [Figure 7].

Preliminary fits of the CBZODY model have been done to a small number of individual IRAS ZOHF scans. These results are only semi-quantitative, in the sense that some important model parameters were not allowed to vary. For example, no offset parameter was used, ascending node Ω and inclination i were

fixed at typical values ($\Omega = 77°$, $i = 1.7°$), and multiple scans were not fit simultaneously. Nevertheless, some useful insights can be made from these preliminary fits.

For $E = 90°$, the latitudinal HWHM $\Gamma \approx 0.25$ (12μm) to 0.32 (25μm). This is consistent with most other model fits to both IR and optical observations, and the results seem to be fairly robust (insensitive to the exact choice of other model parameters). Overall, the model fits 12 μm scans better than 25 μm scans, particularly near the ecliptic plane, where the model significantly underrepresents the observed brightness. This may be a manifestation of the greater sensitivity of the 25 μm band to dust at larger R, particularly in light of the dependence of near-plane model brightness densities on a cutoff in the dust number density (currently $R = 6$ AU). The systematically larger best-fit Γ for the 25 μm band probably arises from this large cutoff radius, since it sharpens the model scan profile near-ecliptic peak, forcing a larger best-fit HWHM Γ to compensate for this. Note that $\Gamma_{25} > \Gamma_{12}$ is true at all solar elongations. Ascending node $\Omega = 77°$ gives satisfactory fits to the 12 μm scans, but smaller values of Ω appear more appropriate for 25 μm scans, as observed in previous studies. See [Figures 8-10].

At smaller solar elongations ($E \approx 60°$), the 12 μm band band does not fit as well as at $E = 90°$. This is consistent with the discussion of relative sensitivity of the two bands (the 12 μm band is more sensitive to deviations from the model inside the Earth's orbit).

A larger solar elongation scan profile ($E = 115°$) exhibits much more asymmetry about the ecliptic plane than the model in both bands. Varying Ω does not improve the fit significantly. This may be a manifestation of deviations of the true dust cloud density distribution from the model symmetry assumptions. Variations in Ω and i with D are predicted from studies of the effects of planetary secular perturbations on dust dynamics, and may have been observed in the inner solar system in zodiacal light studies (which are relatively more sensitive to inner solar system dust because of the D^{-2} solar flux dependence).

The above discussion was primarily concerned with the dust cloud model ... what about the dust band model? Since the current dust band model is very qualitative, it would only confuse the issue to fit the dust cloud and bands simultaneously to the near ecliptic plane data. However, it is in this region that a modified lower envelope fit to the scans would be of use. It is highly undesirable to have the dust cloud model brightness densities exceed the observed brightness here, but we really don't know exactly what the true dust bands look like. Spatial frequency filtering shows distinct bands, but miss any fairly smooth dust band structure, which does appear evident in high resolution scans [Figure 13] (perhaps a large number of low brightness bands with a range of inclinations). Rather than having our very uncertain dust band model drive the dust cloud model fit in this region, we can simply reject any dust cloud model which overestimates the observed near-plane brightness density. If the dust cloud model can simultaneously fit scan data away from the ecliptic plane without overestimating in-plane brightness density, then it will be reasonable to fit the dust band model to the observed residuals. This

will yield a more accurate normalization for the dust band emission than currently available.

Once a satisfactory dust cloud model is generated, the dust bands can be studied in more detail by using a higher resolution data product, such as IPAC's high-resolution ZOHF, or GEISHA's RSPLINE.

Comparison of the current best-fit dust cloud model residuals with the dust band model reveals that the location and qualitative features of the dust band model are consistent with the residuals in scans where the dust cloud model is doing a good job of subtracting the true dust cloud emission. However, the overall normalization of the dust band model appears to be a factor of 2 - 3 too low at 25 μm and perhaps lower at 12 μm. This is not surprising considering the qualitative nature of the model.

The CBZODY-IRAS best-fit model results will both answer some questions and raise others about current and future models of the zodiacal dust complex. How well can a model density distribution with azimuthal symmetry (single Ω, i) fit IRAS observations in both 12 and 25 μm bands? How well does the model fit at smaller solar elongations, and how can it be improved here? What are the asymmetries at large solar elongations telling us about the dust density distribution? How can we cut off the dust density distribution at large radii in a manner consistent with observations? Probably the most important question will be: what observations need to be made to better constrain zodiacal dust complex models?

2.6 CLEANUP AND TESTING

While the basic architecture and coding of all computational tasks necessary to simulate the zodiacal emission already existed in working form for CBZODY, it was necessary to bring some order and consistency to such a complex piece of software. Users of previous versions of CBZODY (v4.0) have been essential in identifying possible errors, inconsistencies, and improvements. To summarize the cleanup efforts:

- Ambiguous, redundant, and conflicting variable names have been altered and clarified (within the limits of the Fortran 77 six-character rule), and misleading or incorrect comments have been rewritten.

- Redundant computations have been eliminated by storing results or moving computations up or down in the program hierarchy.

- One-time computations of some parameters by subroutines are now passed in argument lists to improve readability and clarify input dependencies, and to allow re-use elsewhere in the code (for example, for testing, fitting, *etc.*)

- Julian day computations have been corrected, tested, and extended to include the decimal fraction of the day from Universal Time input. This is necessary to determine the position of the Earth to better than 1° (≈ 1 day)

- The Earth's ecliptic longitude computation was rewritten to be consistent with standard practice for ephemeral computations.

- The volumetric emissivity interpolation was changed from a naive Lagrange polynomial interpolation to a more efficient and robust spline interpolation.

- The Gaussian quadrature LOS integration of the product of dust density and emissivity is also being replaced, probably with a cubic-spline quadrature. This ensures reasonable behavior at the endpoints of the integration (there is no guarantee that the high-order quadrature polynomials will not deviate significantly from the model emissivity values at the endpoints of the integration). It also allows for an intelligent choice of quadrature points considering volumetric emissivity database spacing. An issue which needs to be considered is the behavior of the emissivity profiles along LOS's. At small elongation, we expect a peak in the LOS emissivity at the point of closest approach to the Sun. Depending on the spatial resolution of the quadrature points, the integration across the peak could be poorly approximated. Also, as discussed in sections 4 and 5, the termination of the LOS integration is a non-trivial matter. These points need to be investigated further.

- Computation of zodiacal symmetry plane coordinates along a line-of-sight are being reduced from a series of redundant trignometric computations to a single set of trig computations for each LOS and a linear transformation plus translation for each integration point along the line of sight.

- The main program module for CBZODY has been modified to accomodate the different possible modes of operation (for example, gnomonic projection, coordinate list (keyboard or file), 1-D scan, ZOHF scan format) in a single program.

- The entire coding development effort is being transferred to a Unix platform (Sun Sparcstation) to automate the maintenance of the program including testing, update history, validation and model fitting, and released source code generation. The code is also tested on a PC/AT for compatibility and performance comparisons.

BIBLIOGRAPHY

Dohnanyi, J. S. 1978, in *Cosmic Dust*, ed. J. A. M. McDonnell (New York: Wiley), p.527.

Deul, E. R., and Wolstencroft, R. D. 1988, *As.Ap.*, 196, 277.

Giese, R. H. 1980, in *IAU Symposium 90, Solid Particles in the Solar System*, ed. I. Halliday and B. A. McIntosh (Boston: Reidel), p.1

Giese, R. H., and Kneißel, B. 1989, *Icarus*, 81, 369.

Giese, R. H., Kneißel, B., and Rittich U. 1986, *Icarus*, 68, 395.

Gustafson, B. 1990, in *Fall 1990 IRCB Review Meeting Minutes*.

Hauser, M. G. 1988, in *Proc. Third Internat. IRAS Conf., Comets to Cosmology*, ed. A. Lawrence (Lecture Notes in Physics; Berlin: Springer-Verlag), p.27.

IRAS Catalogs and Atlases, Explanatory Supplement. 1988, ed. C. Beichman, G. Neugebauer, H. J. Habing, P. E. Clegg, and T. J. Chester, (Washington, D.C.: GPO).

Lienert, C. 1975, *Space Sci.Rev.*, **18**, 281.

Murdock, T. L., and Price S. D. 1985, *A.J.*, 90, 375.

Reach, W. T. 1988, *Ap.J.*, **335**, 468.

Rowan-Robinson, M., Hughes, J., Vedi, K., and Walker, D. W. 1990, (preprint), published in *M.N.R.A.S.*.

Sykes, M. V. 1990, (preprint 935, Steward Obs., U. of Arizona), published in *Icarus*.

Sykes, M. V., Greenberg, R., Dermott, S. F., Nicholson, P. D., Burns, J. A., and Gautier, T. N. 1989, in *Asteroids II*, ed. R. P. Binzel, T. Gehrels, and M. S. Matthews, (Tucson:U. of Arizona), p.336.

Weinberg, J. L., and Sparrow, J. G. 1978, in *Cosmic Dust*, ed. J. A. M. McDonnell (New York: Wiley), p.75.

FIGURE CAPTIONS

1. Sun-Earth-LOS geometry with labelled geometric parameters. For simplicity i = 0° for the cylindrical coordinate system of the dust cloud. The actual model R-z coordinates will be inclined with respect the the ecliptic coordinates. (Adapted from Lienert, 1975).

2. Coverage of solar elongation over the IRAS mission. The top plot includes all scans in the ZOHF data product. The bottom plot includes only those scans which come within 1° of half-scan poles (i = 90°). These poles are not the same as the ecliptic poles for E = 90°.

3-5. Examples of IRAS ZOHF scans at E = 60°, 90°, and 115° in all four IRAS bands. These are the same scans shown in the comparison with the CBZODY model.

6. Cross-sections of Lorentzian dust cloud model constant density contours for Γ = 0.25. The top plot is the upper half of an R-z plane slice. The lower plot is perpendicular to the R-z plane and approximately tangent to the earth's orbit. The axes are not identically scaled to accomodate the flatness of the density contours.

7. CBZODY volumetric emissivity model. The top plot shows the relative emissivity profiles beyond the earth's orbit for IRAS bands 1 and 2. The bottom plot shows spectral emissivities at several heliocentric distances.

8-10. Preliminary CBZODY model fits to IRAS ZOHF scans at 3 representative solar elongations. Fixed parameters: i = 1.7°, Ω = 77°. Free parameters: Γ, overall normalization. No allowance has been made for detector offset corrections. Best-fit Γ's are discussed in text. The 115° scan is quite asymmetric, and requires further study.

11-12. Comparison of Residuals for E = 90° and 115° models with the original CBZODY dust band model. Larger solar elongations enhance the contrast between the dust bands and the diffuse dust cloud emission. The dust band structure is evident in the 115° scan.

13. GEISHA RSPLINE high resolution scans at large E for single detectors. The dust bands manifest themselves as shoulders and corners in the scan profile. An accurate physical model of the diffuse dust cloud contribution is necessary to determine true dust band contribution (including low spatial frequency components).

Sun–Earth–LOS Geometry

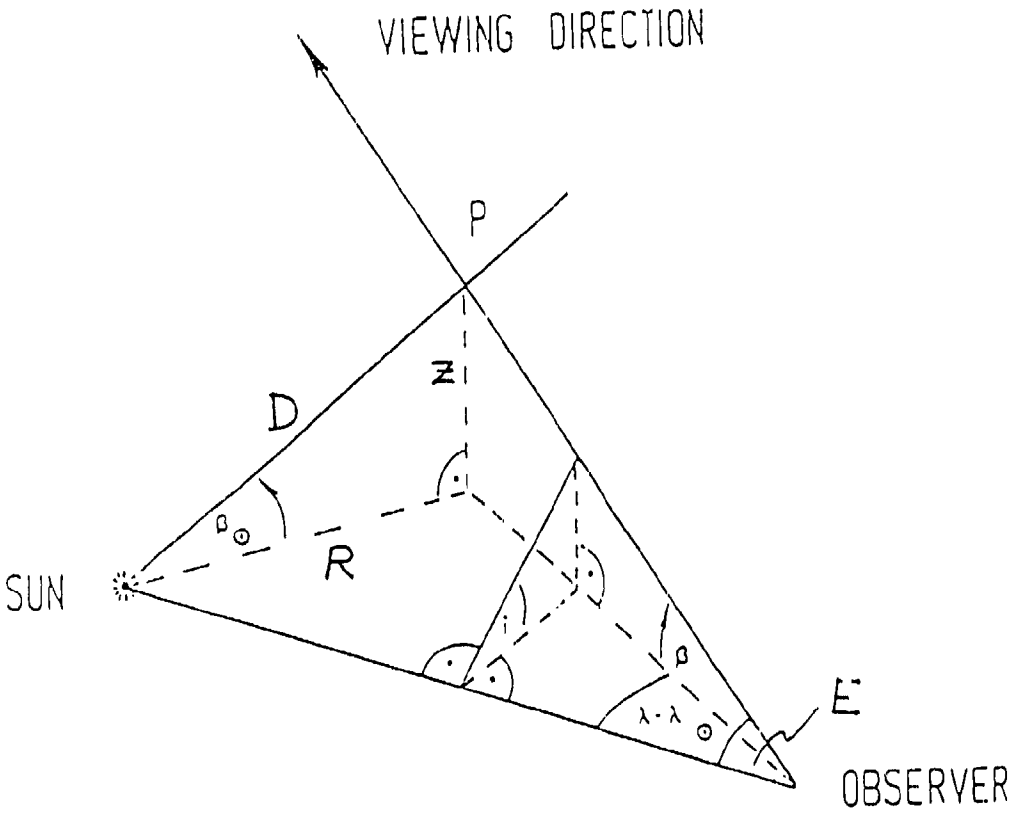

Figure 1

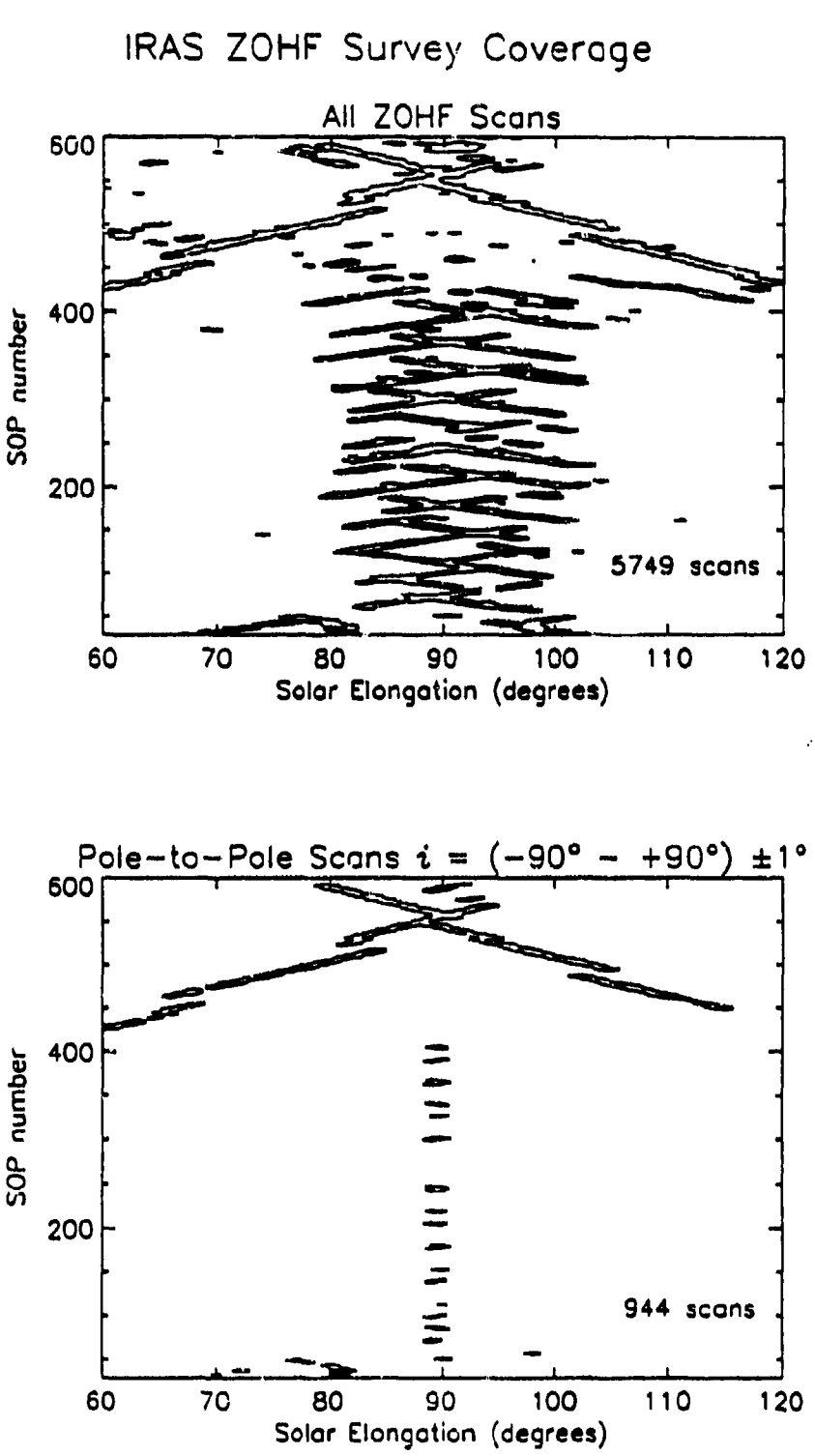
IRAS ZOHF Survey Coverage
All ZOHF Scans
600
400
200
SOP number
5749 scans
60
70
80
90
100
110
120
Solar Elongation (degrees)
Pole-to-Pole Scans i = (-90° - +90°) ±1°
600
400
200
SOP number
944 scans
60
70
80
90
100
110
120
Solar Elongation (degrees)

Figure 2

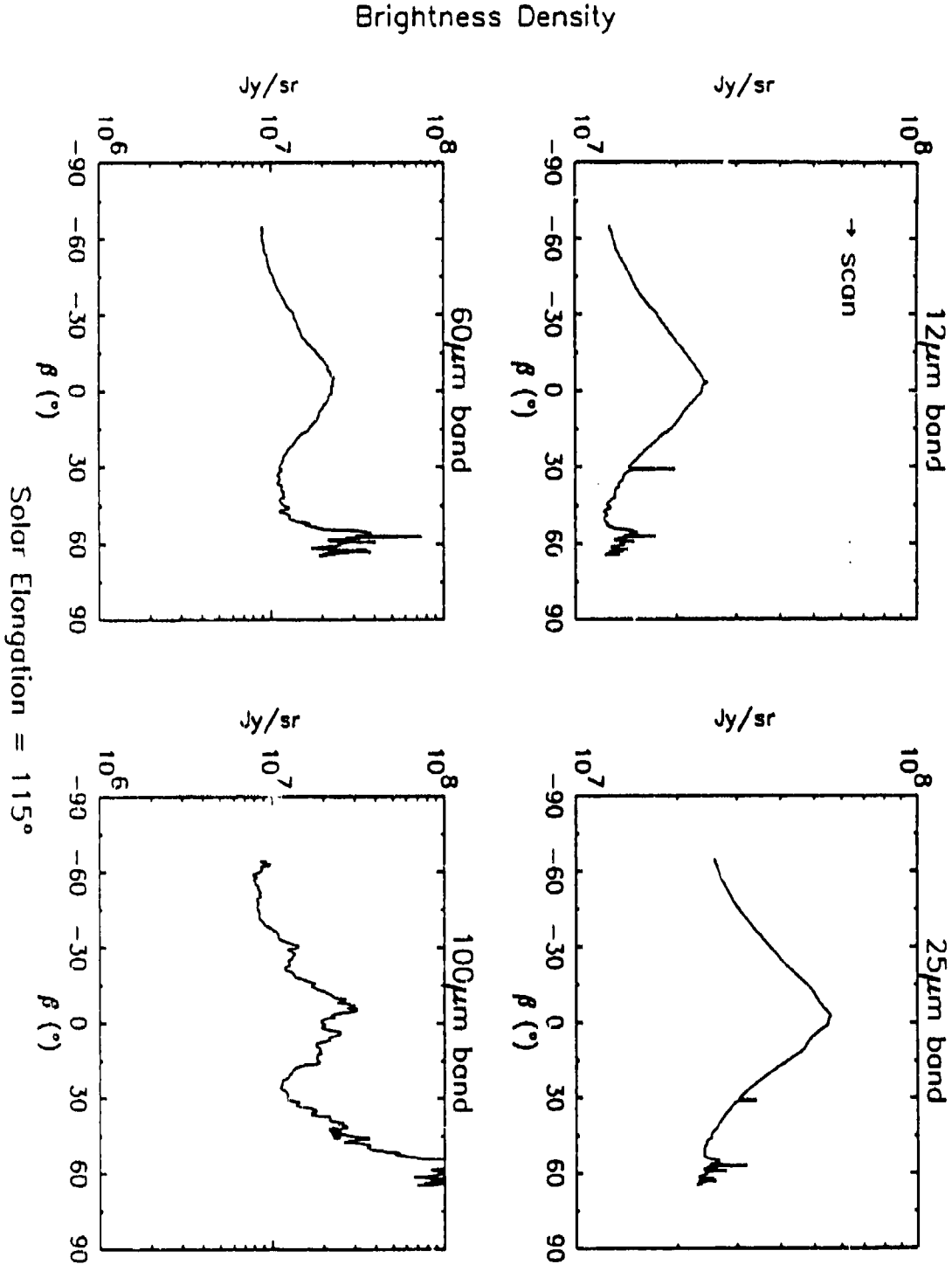
Brightness Density
IRAS ZOHF Sample Scan Profiles
Jy/sr
12μm band
→ scan
25μm band
60μm band
100μm band
β (°)
Solar Elongation = 115°

Figure 3

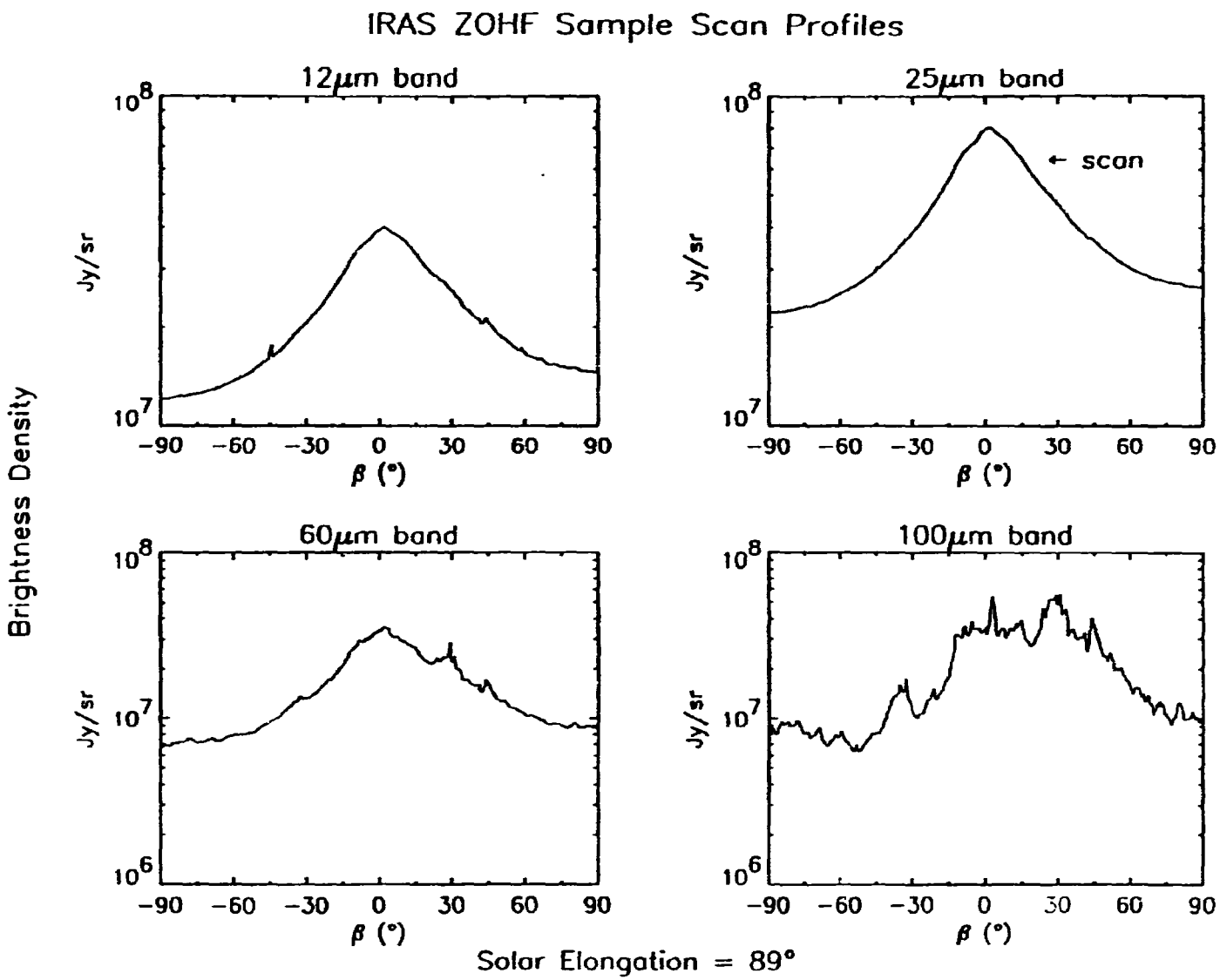
IRAS ZOHF Sample Scan Profiles
12μm band
25μm band
60μm band
100μm band
← scan
Brightness Density
Jy/sr
β (°)
Solar Elongation = 89°

Figure 4

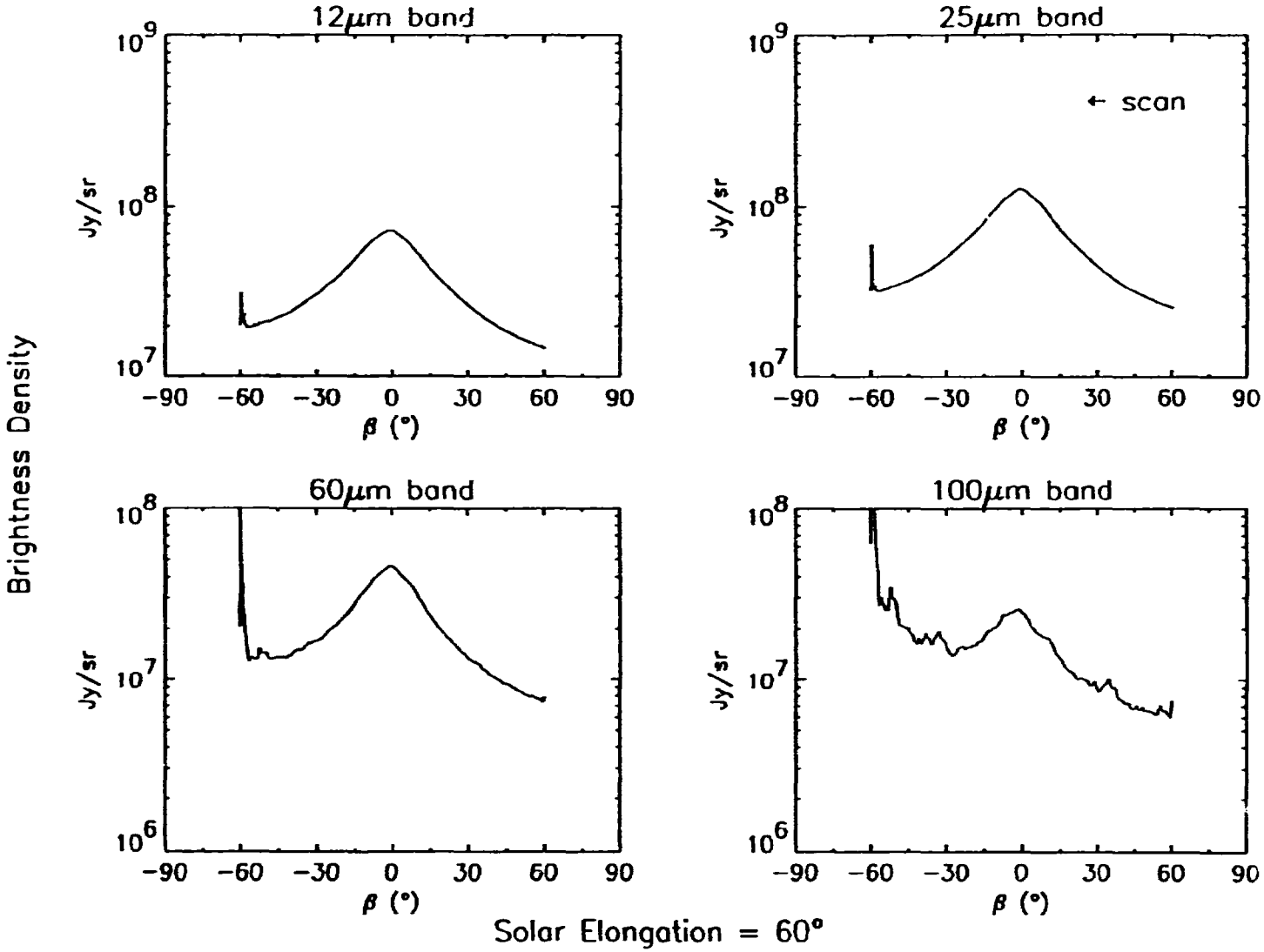
IRAS ZOHF Sample Scan Profiles
12μm band
25μm band
60μm band
100μm band
← scan
Brightness Density
Jy/sr
β (°)
Solar Elongation = 60°

Figure 5

Dust Number Density Contours

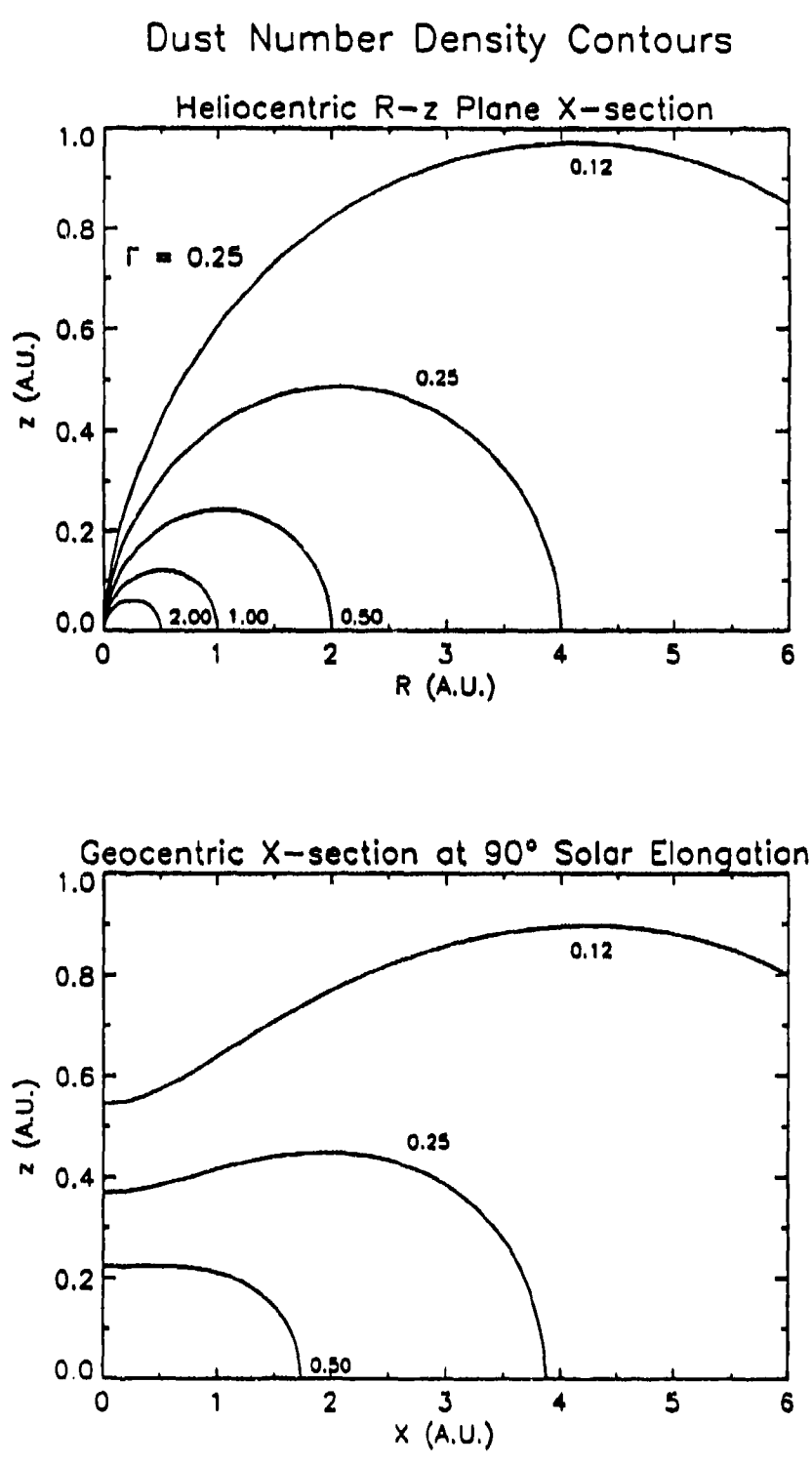

Figure 6

Dust Volumetric Emissivity Model

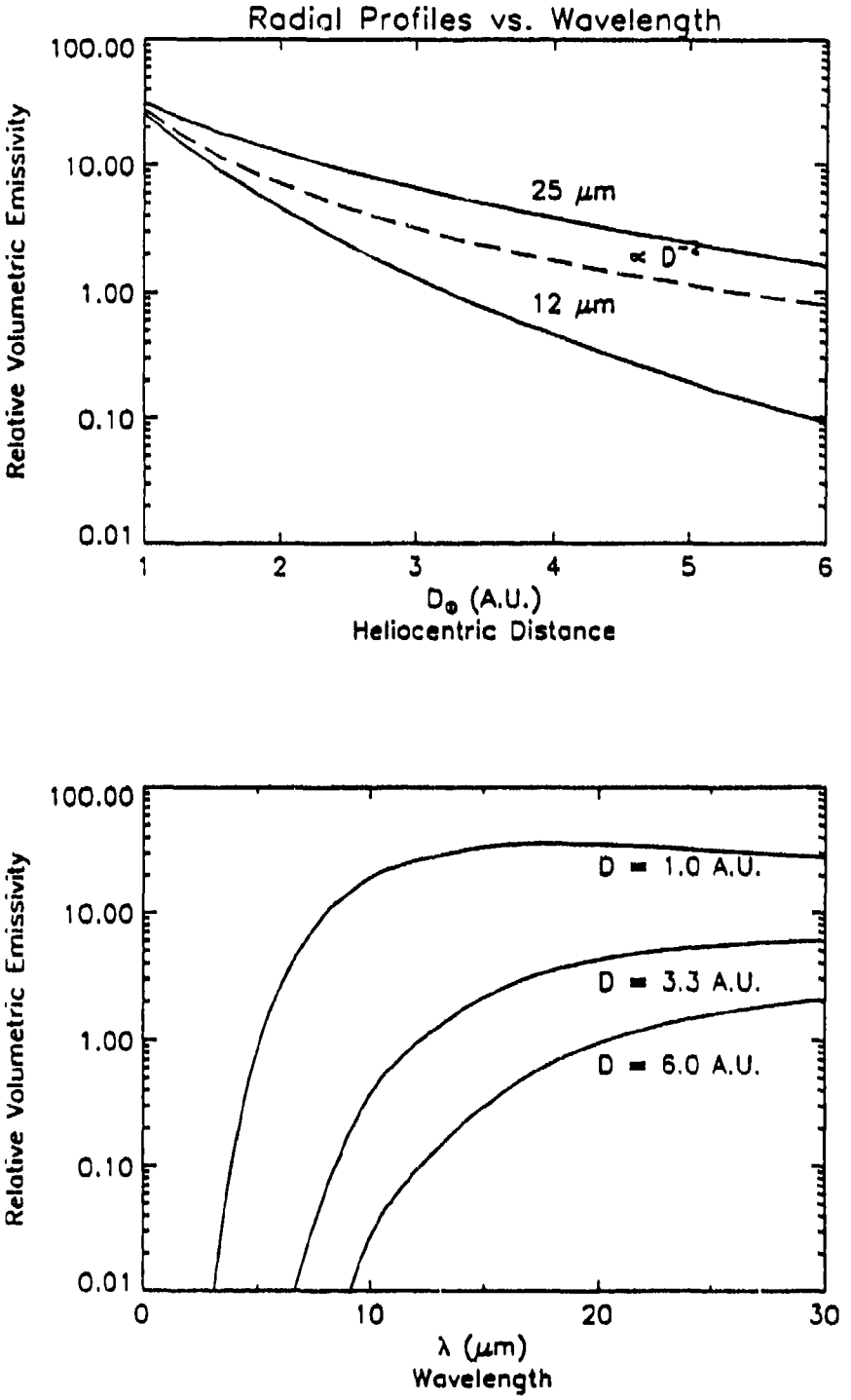

Figure 7

Dust Cloud Model – IRAS ZOHF Scan Comparison

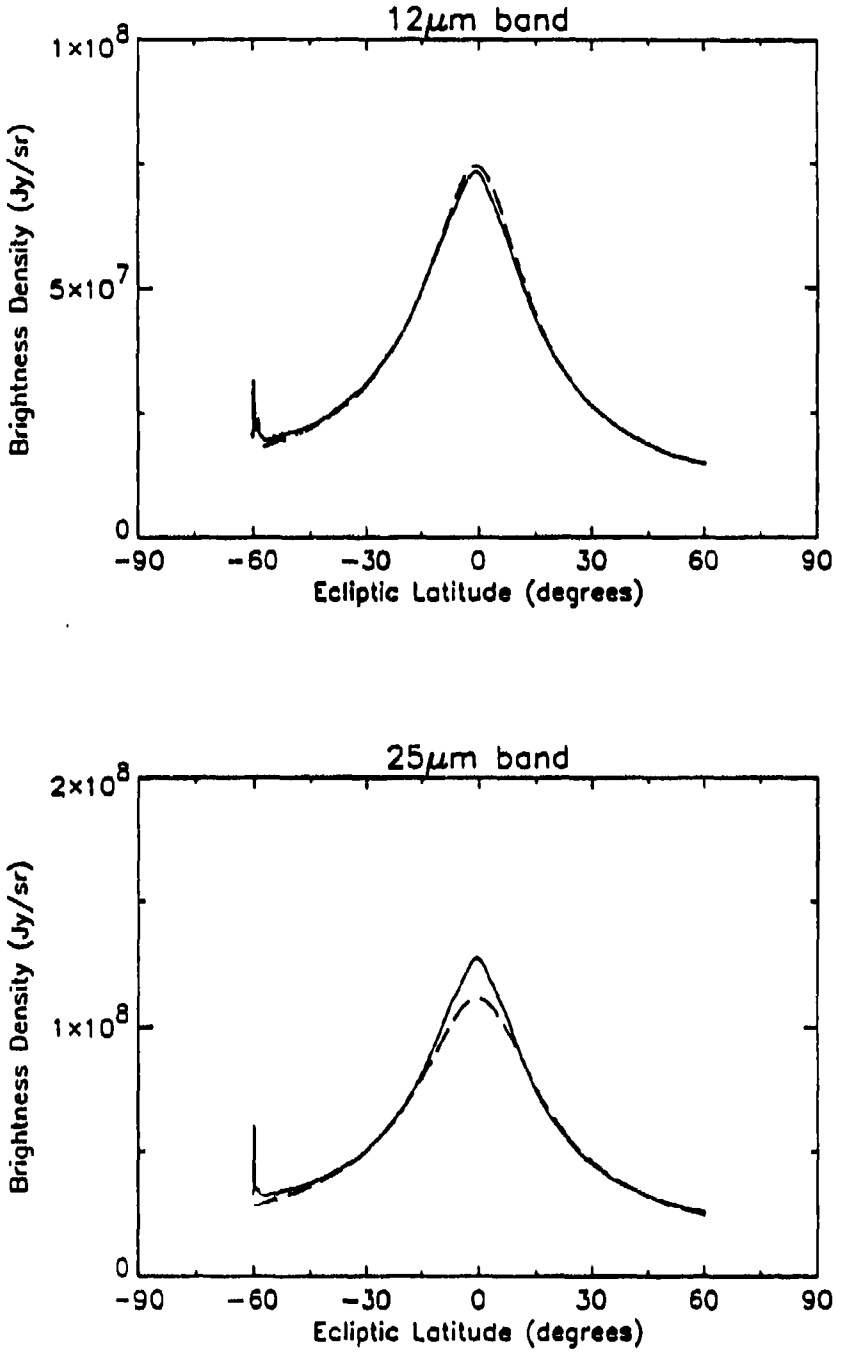

Solar Elongation = 60°

Figure 8

Dust Cloud Model – IRAS ZOHF Scan Comparison

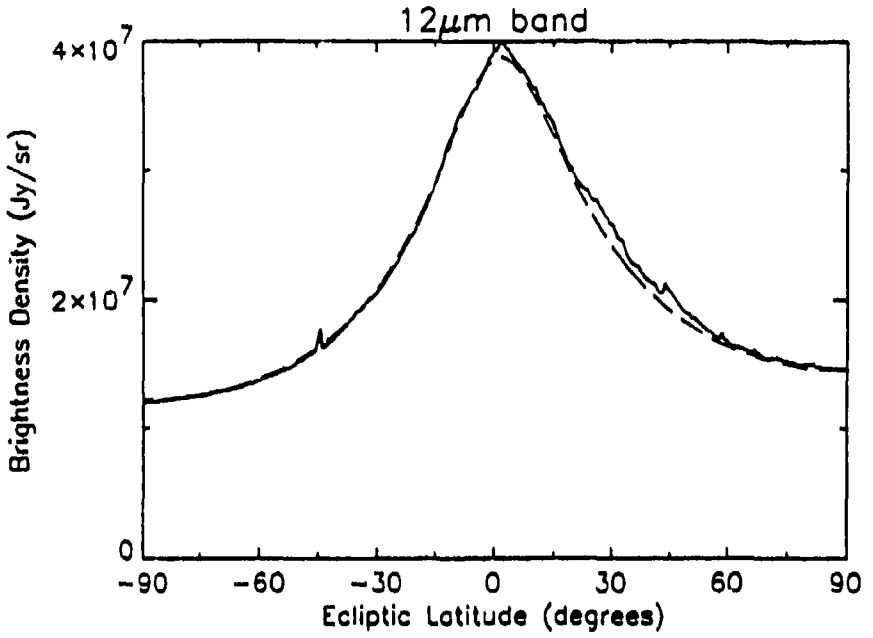

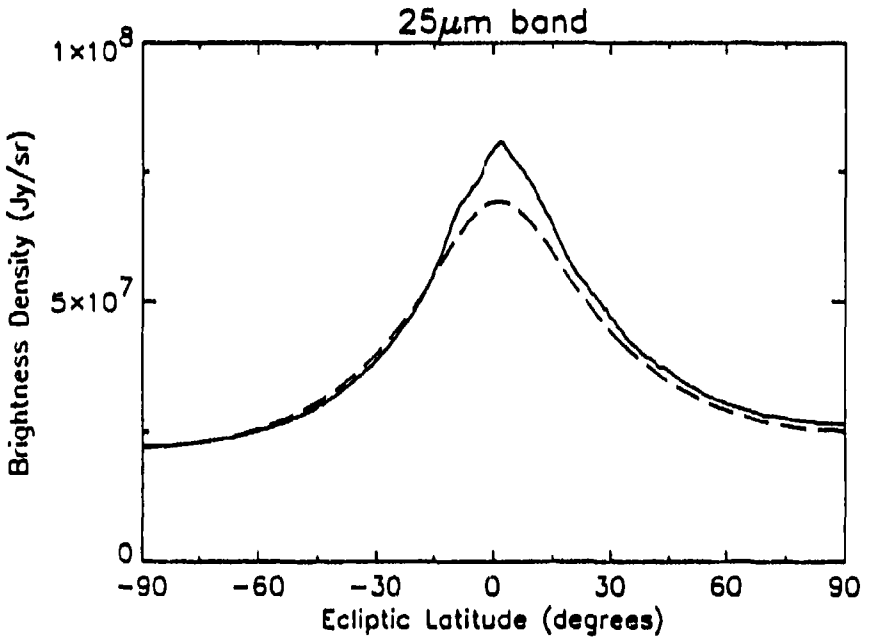

Solar Elongation = 90°

Figure 9

Dust Cloud Model – IRAS ZOHF Scan Comparison

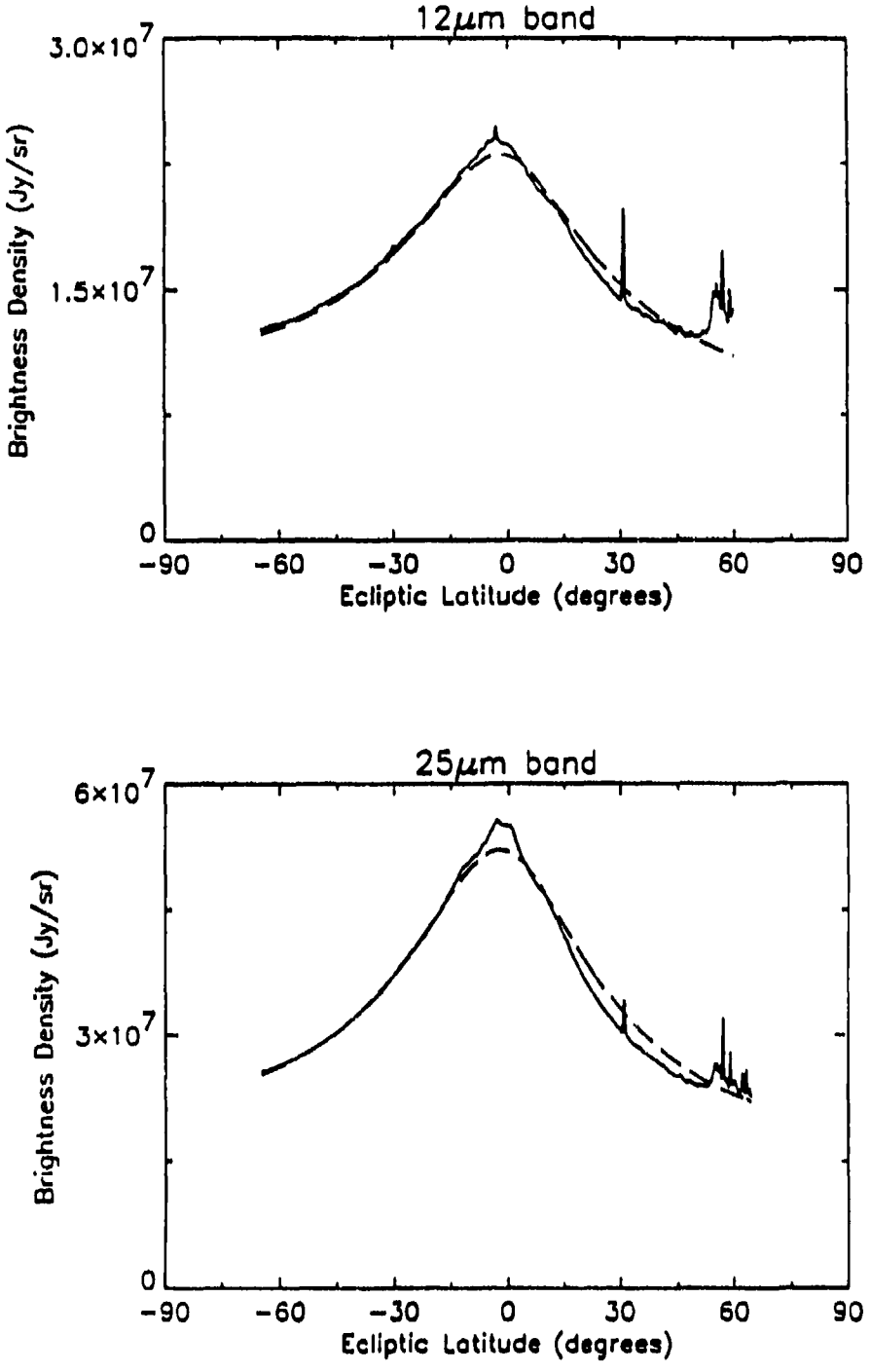

Solar Elongation = 115°

Figure 10

Dust Band Model vs. Dust Cloud Model Residuals

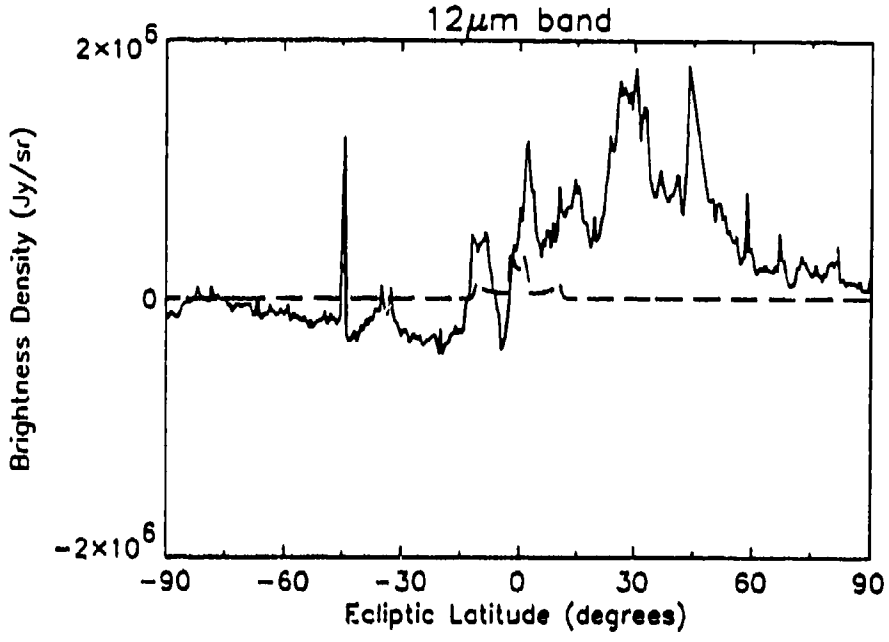

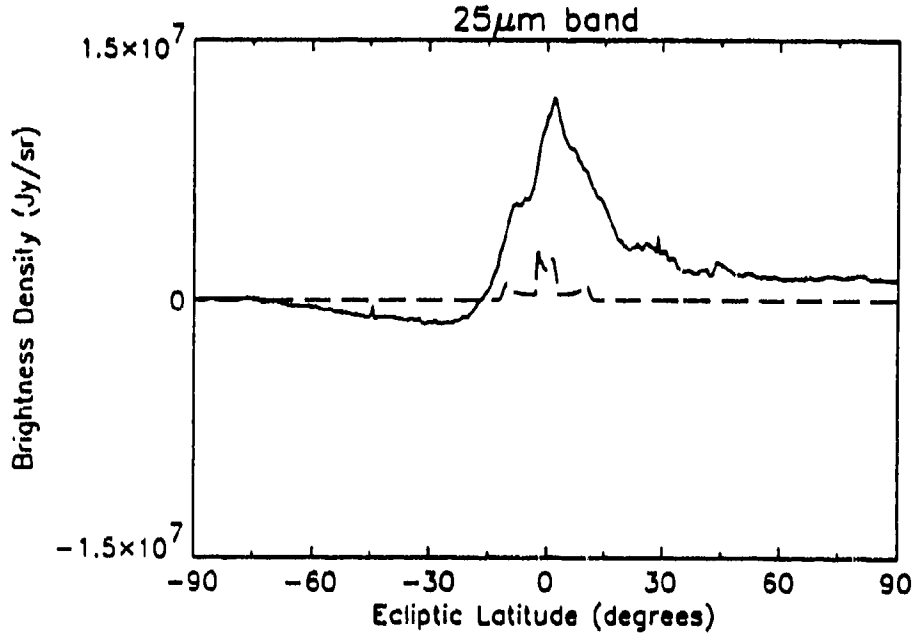

Solar Elongation = 90°

Figure 11

Dust Band Model vs. Dust Cloud Model Residuals

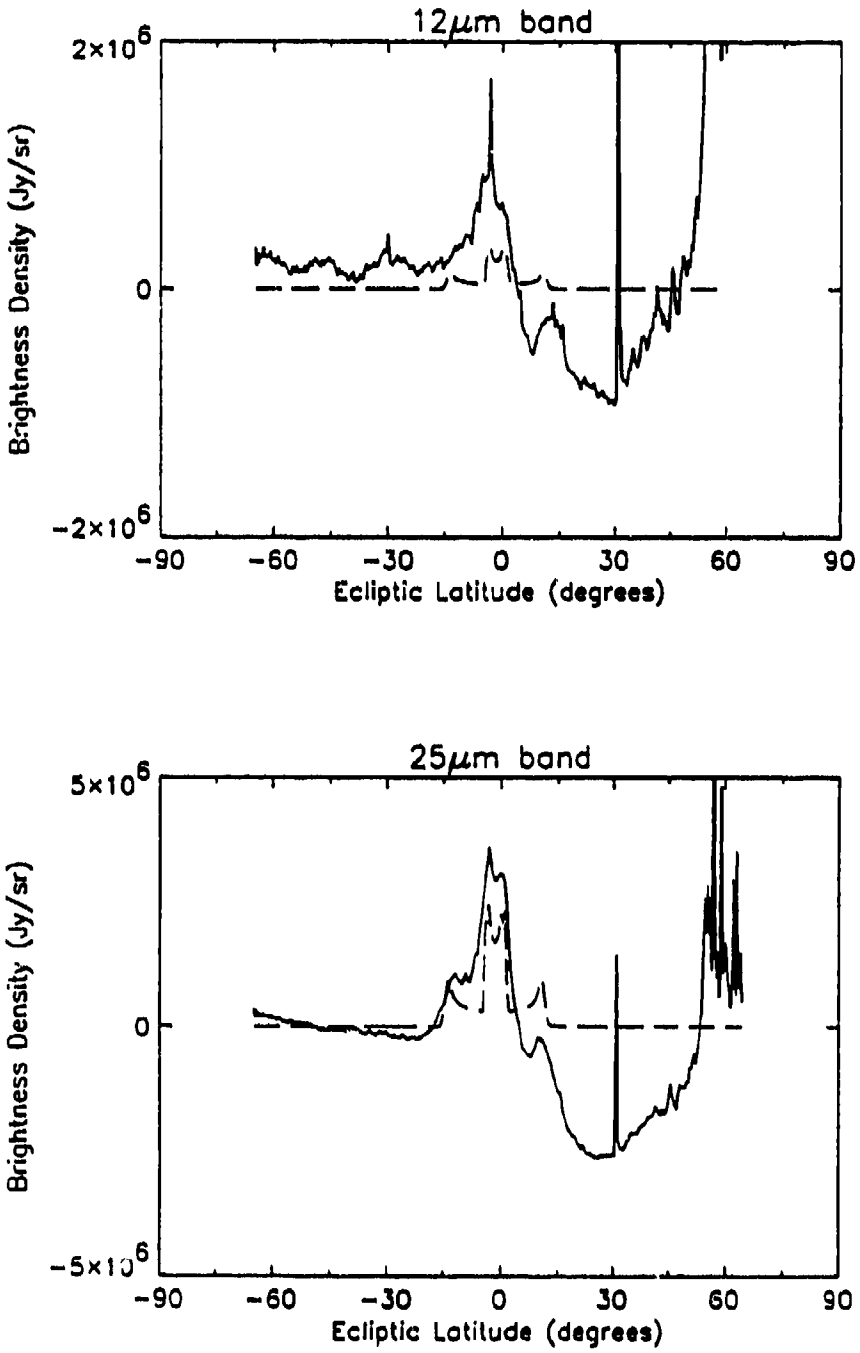

Solar Elongation = 115°

Figure 12

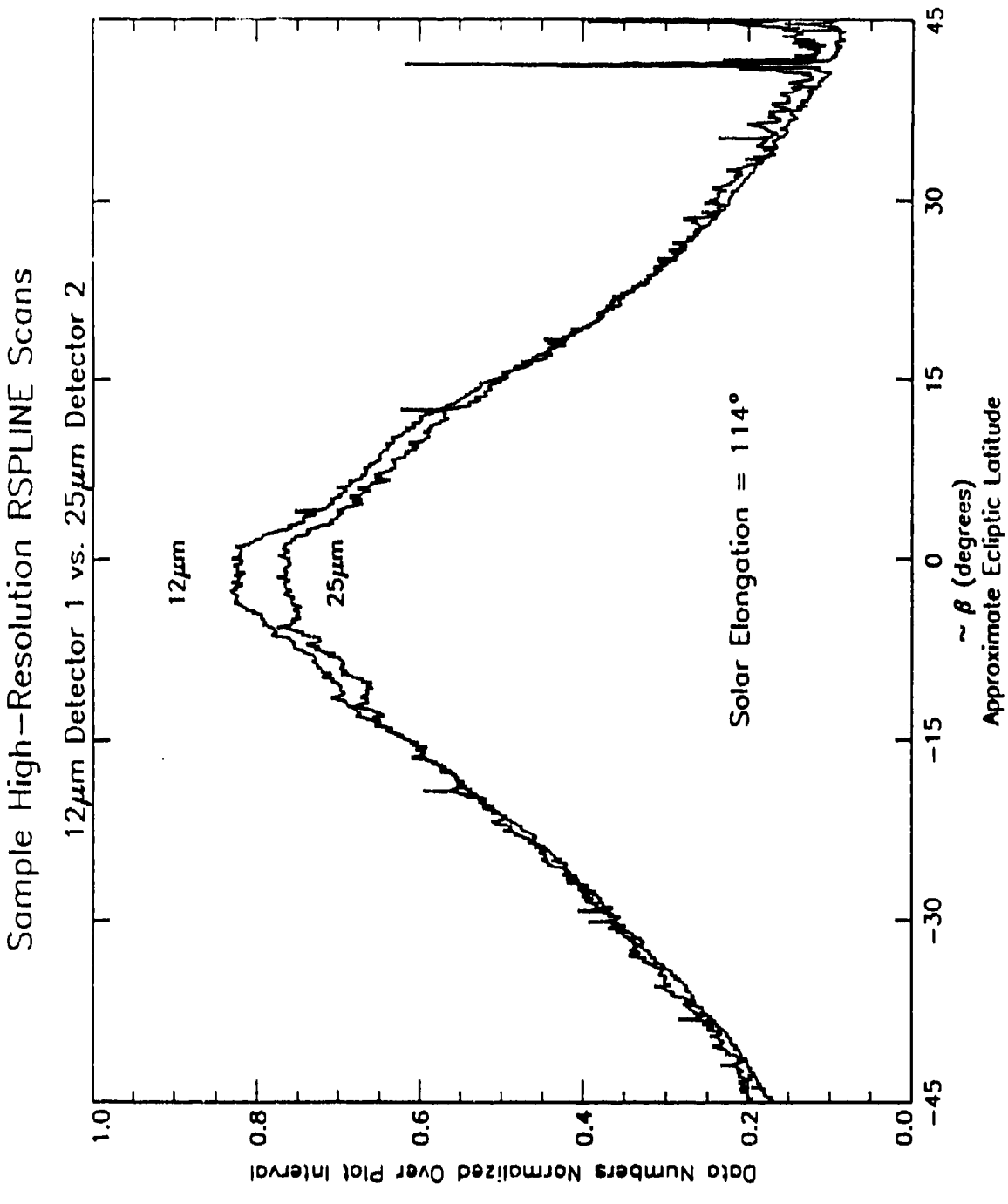
Sample High-Resolution RSPLINE Scans
12μm Detector 1 vs. 25μm Detector 2
12μm
25μm
Solar Elongation = 114°
Data Numbers Normalized Over Plot Interval
1.0
0.8
0.6
0.4
0.2
0.0
-45
-30
-15
0
15
30
45
~ β (degrees)
Approximate Ecliptic Latitude

Figure 13

3 THE CBSD POINT SOURCE BACKGROUND MODULE

3.1 INTRODUCTION

One of the most important segments of the IR celestial background is obviously the emission from point sources. Although spatially and spectrally limited data bases existed prior to the IRAS mission (most notably, the Two Micron Sky Survey and the AFGL measurements), the IRAS mission included a sensitive survey of the entire sky (~95% complete) at four different wavelengths (12, 25, 60, and 100μm). One of the most important data products resulting from the IRAS mission is the IRAS Point Source Catalog (PSC), which includes data on approximately 246,000 sources characterized by IRAS survey measurements.

Despite the comprehensiveness of the IRAS PSC, by itself it does not even begin to satisfy most requirements for general infrared celestial background scene characterization and scene generation. It is useful to explain the reasons for this statement. An uninvolved technologist could easily believe that the IRAS data base, by itself, is sufficiently comprehensive, complete, and reliable, as to be able to satisfy most DoD celestial background point source scene requirements. Because IRAS Band 1, nominally centered at 12μm, is near the middle of the currently defined range of CBSD operability (2-30μm), the Band 1 PSC is a prime source of CBSD information. An examination of this data can also help illustrate the limitations of the PSC relative to CBSD requirements.

SUMMARY OF IRAS PSC BAND 1 CONTENT

DATA SOURCE	R.A. Range	Total Points	Flux Quality		
			Low	Med	High
File 1	0°- 60°	21835	11089	203	10543
File 2	60°- 120°	37619	17346	356	19917
File 3	120°- 180°	28854	10939	450	17465
File 4	180°- 240°	34011	11586	494	21931
File 5	240°- 300°	90965	23279	1703	65983
File 6	300°- 360°	32605	12863	626	19116
TOTALS		**245889**	**87102**	**3832**	**154955**

From this table, one can immediately see that only about 60% of the IRAS PSC entries are considered high-quality in Band 1. In general, where the PSC indicates that the flux is low-quality, this implies that the given Band 1 flux is an upper limit for a point source which has been less ambiguously identified in another spectral band. Moreover, it has been estimated by some that perhaps as many as a third of the PSC entries actually correspond to "knots" or other discontinuous features in the general IR cirrus background, most prominent in IRAS Bands 3 and 4.

There are also other important issues pertaining to the direct utility of the PSC relative to CBSD scene generation requirements.

First, it is useful to note that the Band 1 spectral responsivity half-power points are at approximately 8μm and 15μm (the comparable Band 2 limits are 19μ and 30μm). Although the CBSD must be able to generate point source scenes at any wavelength in the 2-30μm range, with a spectral finesse of better than 1μm, each IRAS data set represents an integral over a fixed spectral band whose spectral bandwidth is many microns.

Second, the IRAS Band 1 instrumental detection limit was a few tenths of a Jansky, whereas the CBSD sensitivity threshold must be a few milli-Jansky.

Third, in the galactic plane and several other regions, IRAS was confusion-limited. Therefore, the IRAS point source survey is not complete in all regions down to the instrumental sensitivity limit. In much of the galactic plane, for example, the point source catalog is complete only down to a few Jansky. This point is emphatically illustrated by Figure 3.1-1, which shows the distribution of IRAS PSC sources with Band 1 fluxes < 1 Jansky along the inner plane. The almost complete void along the plane here is one manifestation of the confusion problem.

Fourth, and intimately related to the third point above, the IRAS spatial finesse of a few arc-minutes is clearly insufficient relative to the CBSD requirement of a few arc-seconds.

Thus, despite the constraints imposed by the IRAS instrumentation and the IRAS survey strategy, the IRAS PSC is the best single data source available for characterization of the IR point source background. However, it is not directly useful for satisfying scene generation requirements of the type which must be addressed by the CBSD.

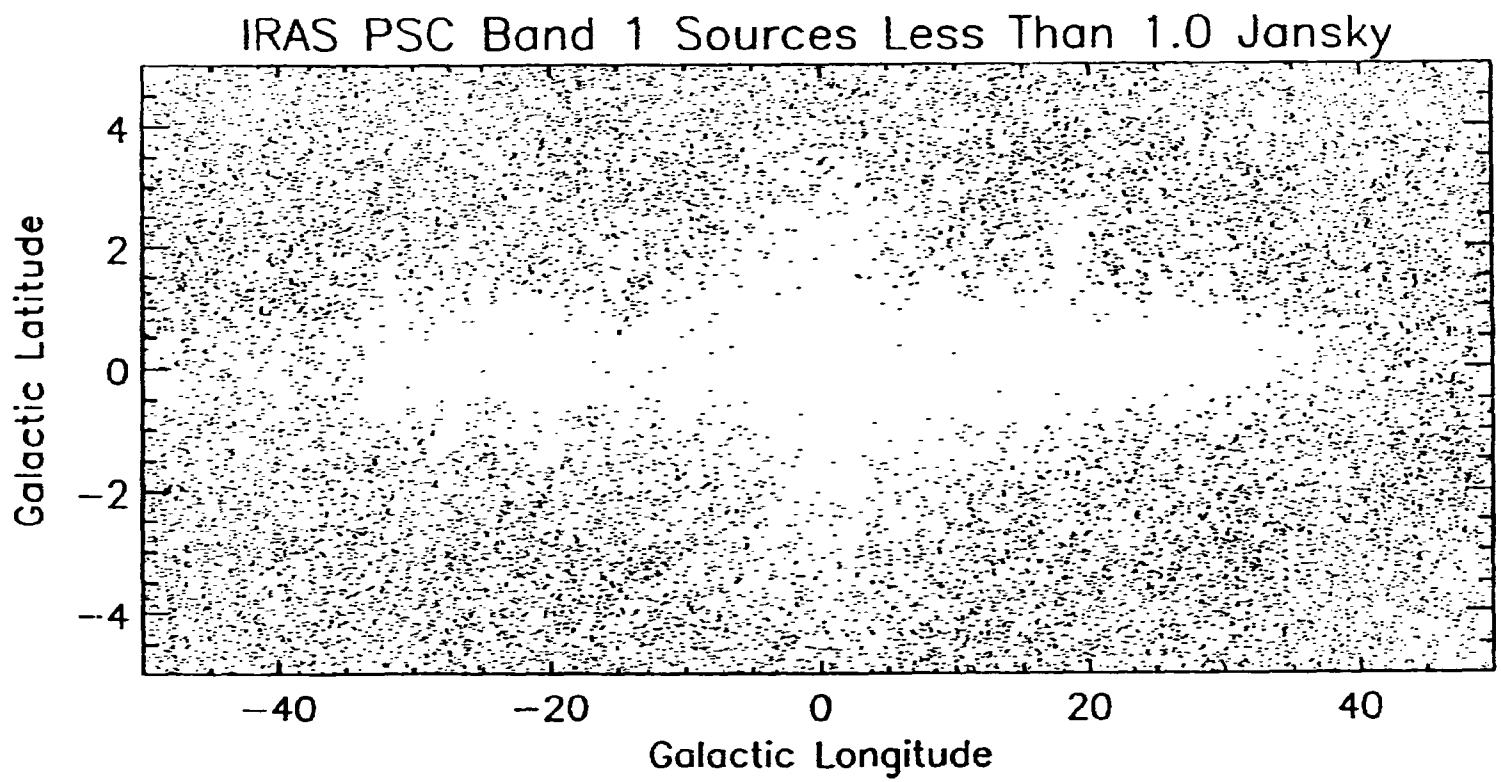
IRAS PSC Band 1 Sources Less Than 1.0 Jansky
Galactic Latitude
4
2
0
−2
−4
−40
−20
0
20
40
Galactic Longitude

3.2 THE NASA/AMES "SKY" MODEL

With Air Force support and technical direction from the Air Force Geophysics Laboratory, the NASA/Ames Research Center and Jamieson Science & Engineering undertook the development of an IR model of the point source sky which would be consistent with IRAS point source data but would not be subject to the limitations of the data. Initially delivered in early 1989, SKY "comprises geometrically and physically realistic representations of the galactic disk, bulge, spheroid, spiral arms (including the 'local arm'), molecular ring, and the extragalactic sky."

In some ways, this division of the galaxy into these five components, as well as the details of their associated luminosity functions, evolved from an older galactic point source model developed by Price and Walker at the Air Force Geophysics Laboratory in the 1970's.

Guided somewhat by a parallel Monte Carlo simulation of the galaxy at 12μm (by Volk et al at NASA/Ames), SKY models each of the galactic components by up to 87 different spectral classes of point sources. Each spectral class is characterized by different scale heights, space densities, and absolute magnitudes at B, V, J, H, K, 12μm, and 25μm. The spectral classes defined in and used by SKY are the result of color-color analyses of the IRAS Low Resolution Spectrometer (LRS) data base.

An additional module of SKY also describes the extra-galactic background as a mix of "red" and "blue" normal galaxies, quasars, and Seyferts. However, in SKY the galaxies are assumed to have an isotropic distribution.

> **From the CBSD perspective, the greatest value of SKY is that it predicts, for any specified line of sight, the number of point sources per unit angular area (e.g. per square degree) per magnitude interval for each of the spectral classes.**

The statistical descriptions of point source distributions embodied within SKY have been validated by Jamieson Science and Engineering, via comparison of SKY cumulative point source counts (versus 12μm and 25μm magnitudes) with the IRAS PSC, Faint Source Catalog (FSC), and Serendipitous Survey Catalog (SSC). Figures 3.2-1 and 3.2-2 synopsize some of the global comparisons with the PSC; in the unshaded zones, the agreement is said to be in the $\pm$25% range.

Within the CBSD program, SKY has been employed since Spring 1989 as the basis for the CBSD point source background module. The methods employed within CBSD for the use of SKY are discussed in later sections of this chapter. All of the CBSD work up until the present employs Version 2 of SKY. At the present time, the CBSD program has begun to assimilate Version 3 of SKY, which was preliminarily released in September 1990. Attached as an Appendix to this report is a brief description of the SKY Version 3 software which was provided to MRC on

Validation of NASA/Ames SKY Model

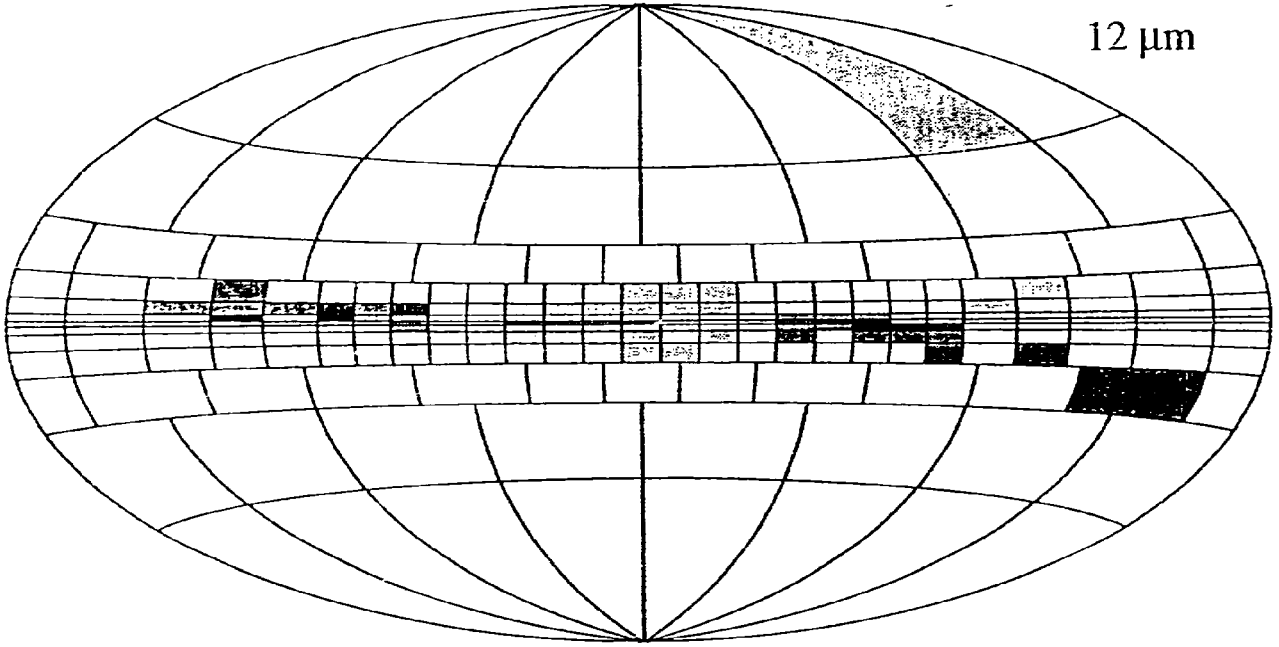

Black: PSC > 2*SKY MdGry: PSC > 1.5*SKY LtGry: PSC < SKY

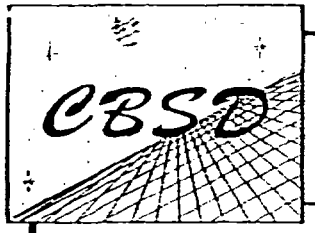

Validation of NASA/Ames SKY Model

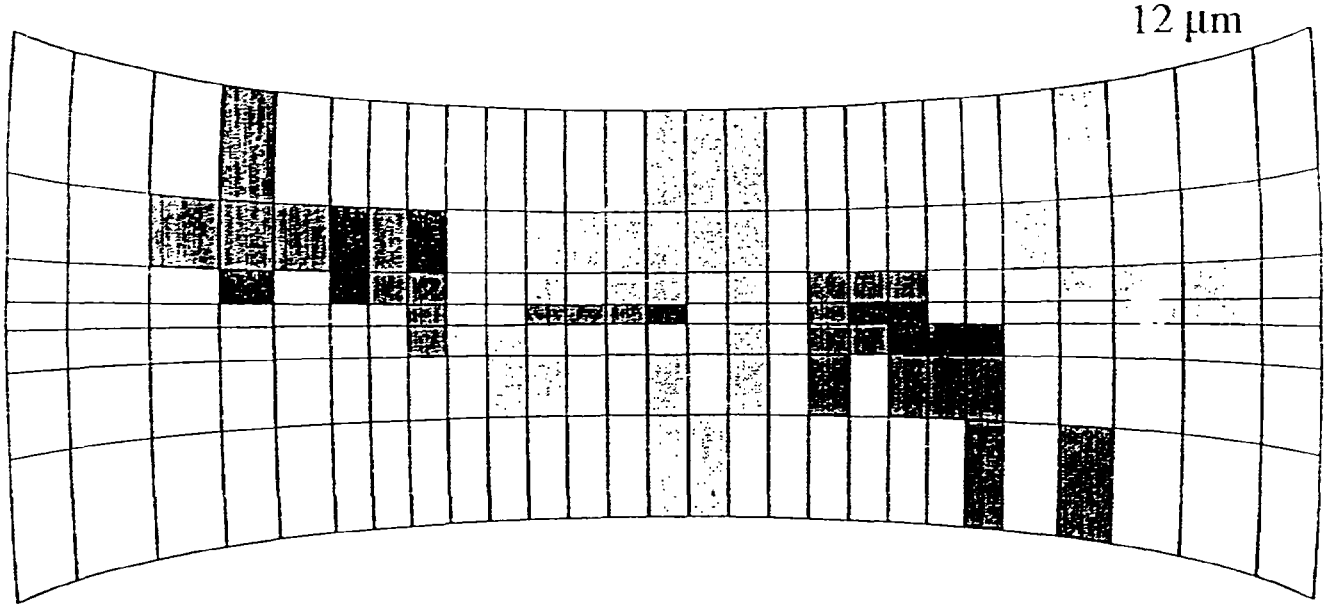

Black: PSC > 2*SKY MdGry: PSC > 1.5*SKY LtGry: PSC < SKY

magnetic media. In the following section, the spectral data base integrated with Version 3 of SKY is summarized.

MRC experience with the SKY software has generally been quite satisfactory, although there are some minor problems which have been repeated from Version 2 to Version 3, and which are somewhat of a major nuisance. Jamieson Science & Engineering is delivering the SKY software in the VAX-Fortran language, which is at variance with ANSI-Standard Fortran-77 in several ways. The most serious and most time-consuming to repair are:

(1) ANSI-Standard Fortran-77 supports a maximum of 19 continuation lines to a single statement. In all of its many long "DATA" statements, describing the spatial and spectral characteristics of the 87 point source classes, SKY employs >20 continuation lines.

(2) Throughout, SKY makes use of VAX Fortran capability for using, e.g.

```
        DO K=1,87     {or DO WHILE (K.LT.87)}
         .
         .
        ENDDO
```

instead of the ANSI-standard "labelled" DO,

```
        DO label K=1,87
         .
         .
label   continue
```

Although these seem like minor nuisances, in fact they have required many hours of tedious clean-up in order for the code to be ANSI-compliant.

3.3 THE SPECTRAL DATA BASE

As already noted, the NASA/Ames SKY model makes use of results from a spectral classification schema to describe the point source background as a mix of 91 different types of sources, each having different spectral characteristics. An integral part of the SKY software is a library of template spectra for each of the 91 different source types. These 91 spectral classes include 82 sub-classes of stars, two classes of planetary nebulae ("red" and "blue"), two classes of reflection nebulae ("red" and "blue"), HII regions, and four classes of extra-galactic sources ("red" galaxies, "blue" galaxies, Seyferts, and quasars).

The primary source data for the SKY template spectra was the IRAS LRS (*Low-Resolution Spectrometer*) data base. The NASA/Ames group derived "typical" template spectra for each of the 91 spectral classes, thereby "digesting" the much larger LRS data base. However, because the LRS covered only the spectral range of 7.7-22.7μm, the template spectra delivered with Versions 1 & 2 of SKY also were limited to this same spectral range.

Perhaps the most important aspect of SKY Version 3 is that the template spectra now cover the spectral range of 2-35μm. In order to extend the spectral range beyond the limits of the IRAS LRS data base, Cohen et al employed whatever complementary, reliable spectral data they could find and fitted together such data with the LRS data. For cases where no reliable data existed, they employed astronomical judgement to extrapolate the LRS data.

Because MRC has already begun the process of integrating SKY.v3 into the CBSD, prior to the availability of any NASA documentation on the spectral extensions to SKY, it was deemed useful to include CBSD hard-copy presentations of the newest spectral template library within this report.

Each of the spectra on the following pages is identified by a spectral class name. Names for the stellar classes are generally recognizable as variants of traditional astronomical class names. For additional clarification, note that:

HIIREG	means	HII Regions
NORMAL1	means	"Blue" Standard Galaxies
NORMAL2	means	"Red" Standard Galaxies
PNBLUE	means	"Blue" Planetary Nebulae
PNRED	means	"Red" Planetary Nebulae
RNBLUE	means	"Blue" Reflection Nebulae
RNRED	means	"Red" Reflection Nebulae

CBSD plots of the 91 template spectra are presented on the next 23 pages, ordered alphabetically by their SKY class names.

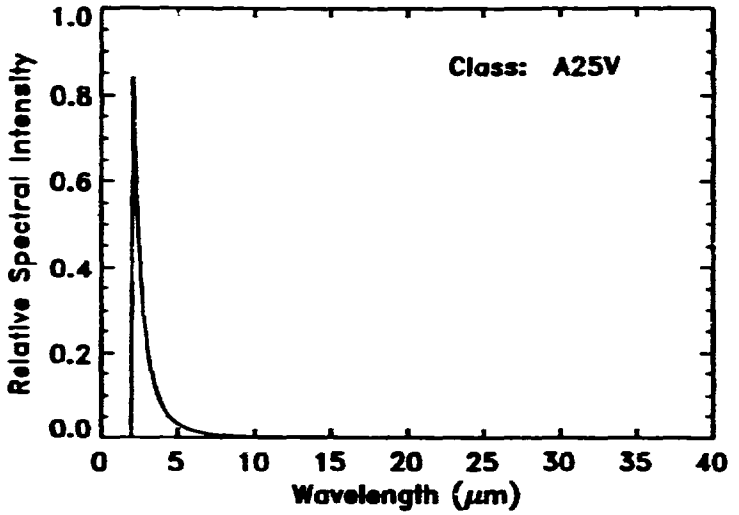
Class: A25V
Relative Spectral Intensity
1.0
0.8
0.6
0.4
0.2
0.0
0 5 10 15 20 25 30 35 40
Wavelength (μm)

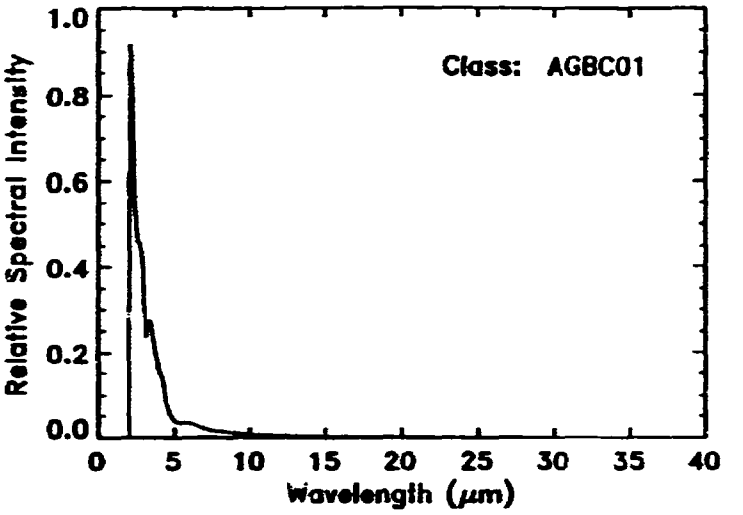
Class: AGBC01
Relative Spectral Intensity
1.0
0.8
0.6
0.4
0.2
0.0
0 5 10 15 20 25 30 35 40
Wavelength (μm)

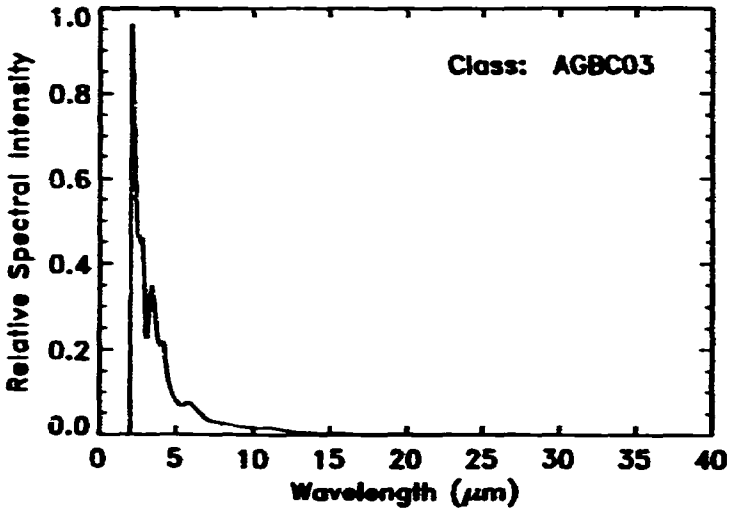
Class: AGBC03
Relative Spectral Intensity
1.0
0.8
0.6
0.4
0.2
0.0
0 5 10 15 20 25 30 35 40
Wavelength (μm)

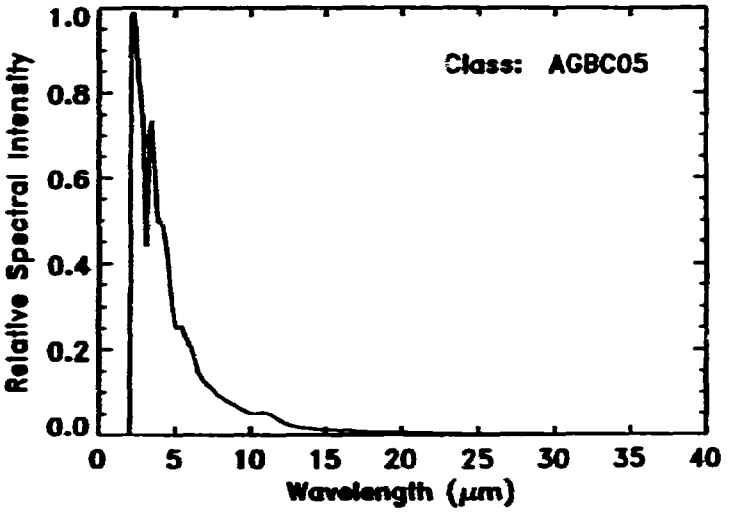
Class: AGBC05
Relative Spectral Intensity
1.0
0.8
0.6
0.4
0.2
0.0
0 5 10 15 20 25 30 35 40
Wavelength (μm)

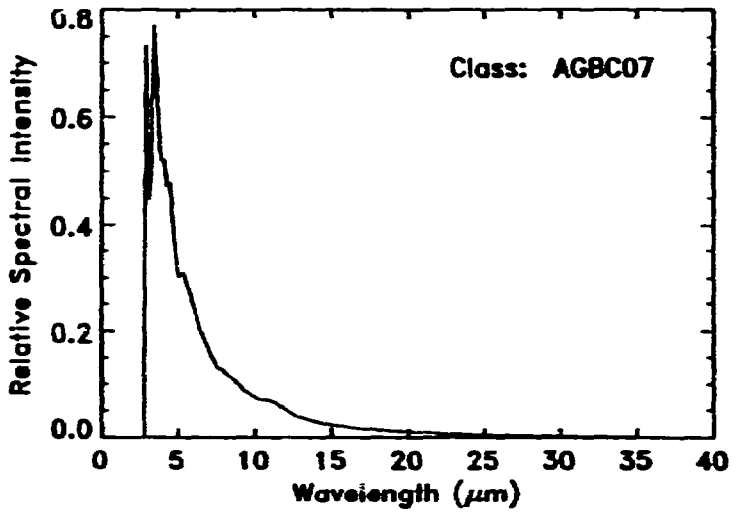
Class: AGBC07
Relative Spectral Intensity
Wavelength (μm)
0.0
0.2
0.4
0.6
0.8
0
5
10
15
20
25
30
35
40

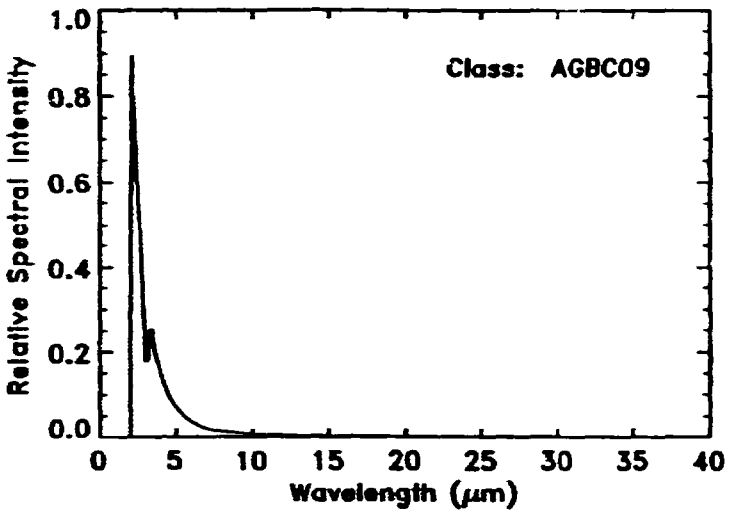
Class: AGBC09
Relative Spectral Intensity
Wavelength (μm)
0.0
0.2
0.4
0.6
0.8
1.0
0
5
10
15
20
25
30
35
40

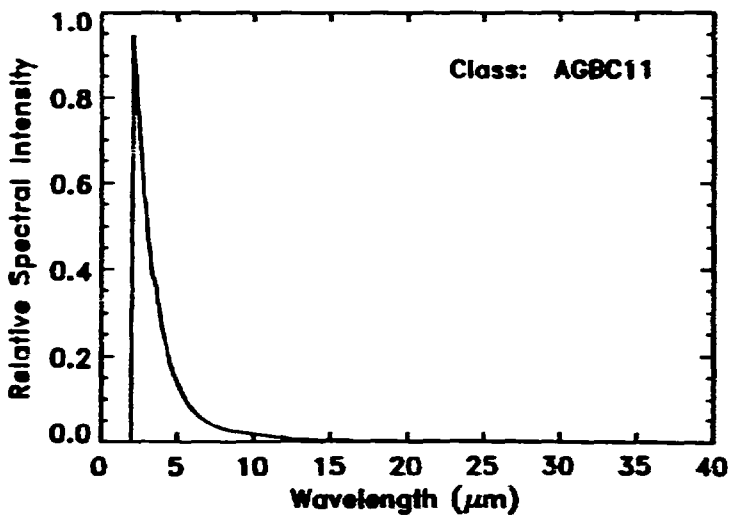
Class: AGBC11
Relative Spectral Intensity
Wavelength (μm)
0.0
0.2
0.4
0.6
0.8
1.0
0
5
10
15
20
25
30
35
40

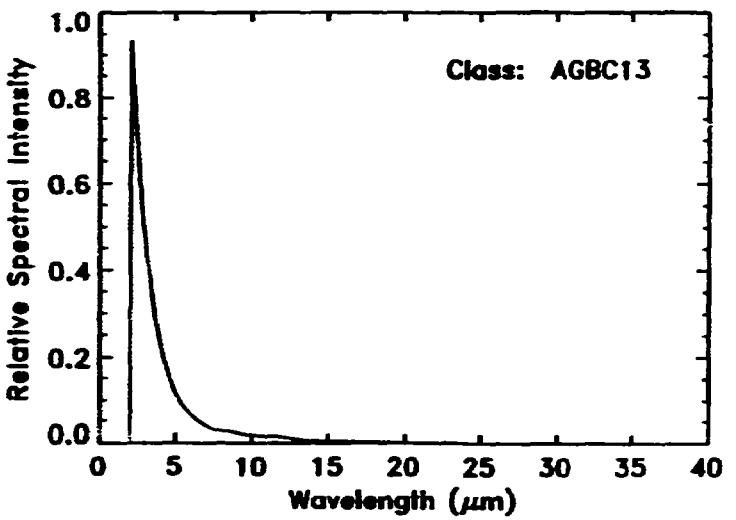
Class: AGBC13
Relative Spectral Intensity
Wavelength (μm)
0.0
0.2
0.4
0.6
0.8
1.0
0
5
10
15
20
25
30
35
40

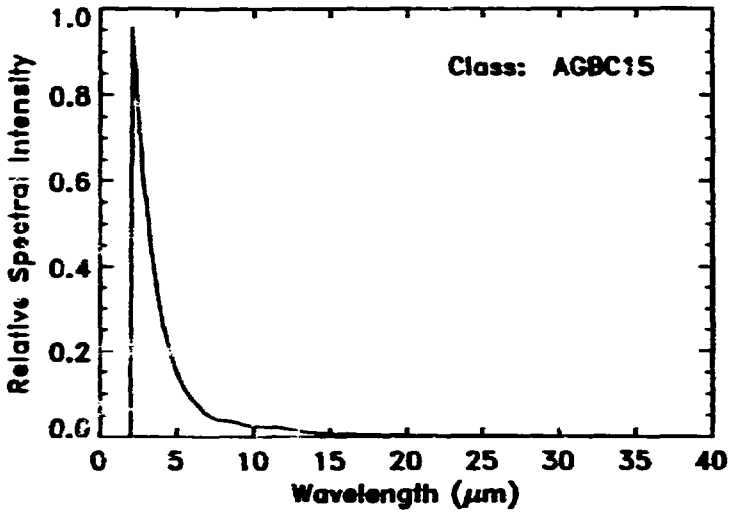
Class: AGBC15
Relative Spectral Intensity
Wavelength (μm)
0.0
0.2
0.4
0.6
0.8
1.0
0
5
10
15
20
25
30
35
40

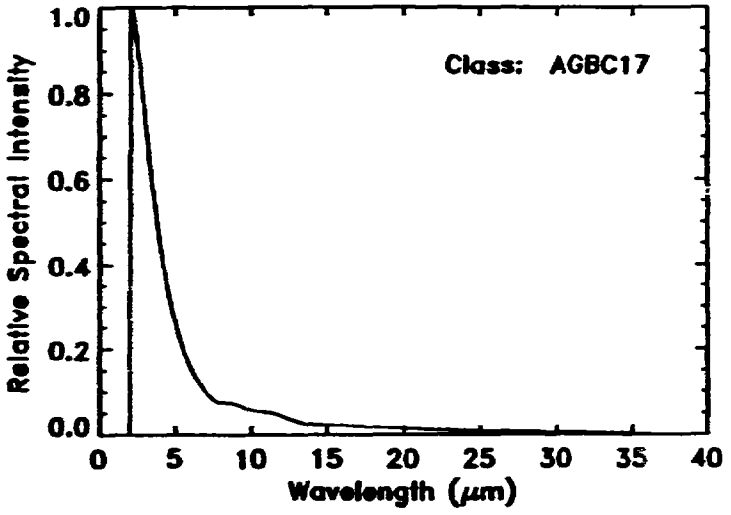
Class: AGBC17
Relative Spectral Intensity
Wavelength (μm)
0.0
0.2
0.4
0.6
0.8
1.0
0
5
10
15
20
25
30
35
40

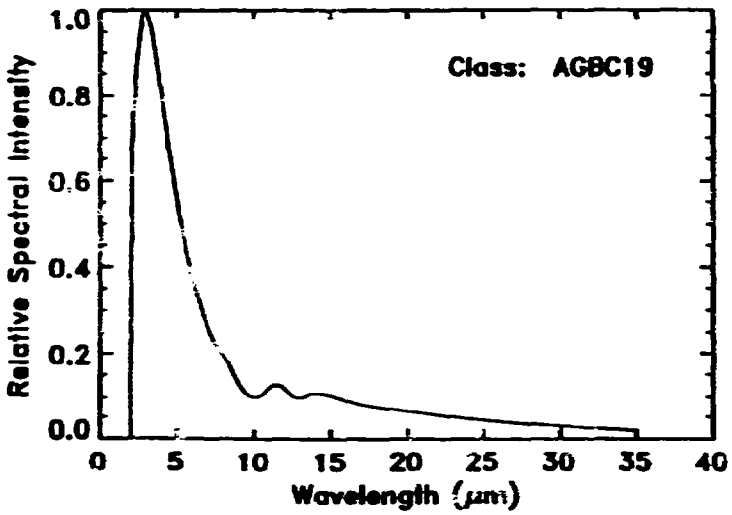
Class: AGBC19
Relative Spectral Intensity
Wavelength (μm)
0.0
0.2
0.4
0.6
0.8
1.0
0
5
10
15
20
25
30
35
40

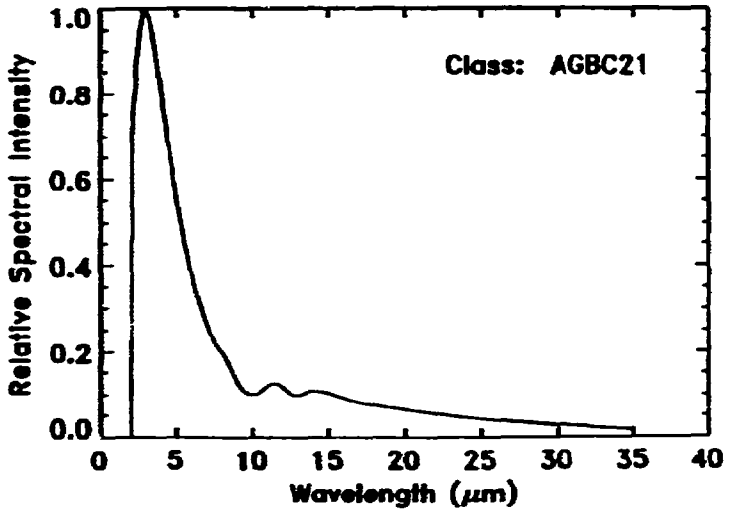
Class: AGBC21
Relative Spectral Intensity
Wavelength (μm)
0.0
0.2
0.4
0.6
0.8
1.0
0
5
10
15
20
25
30
35
40

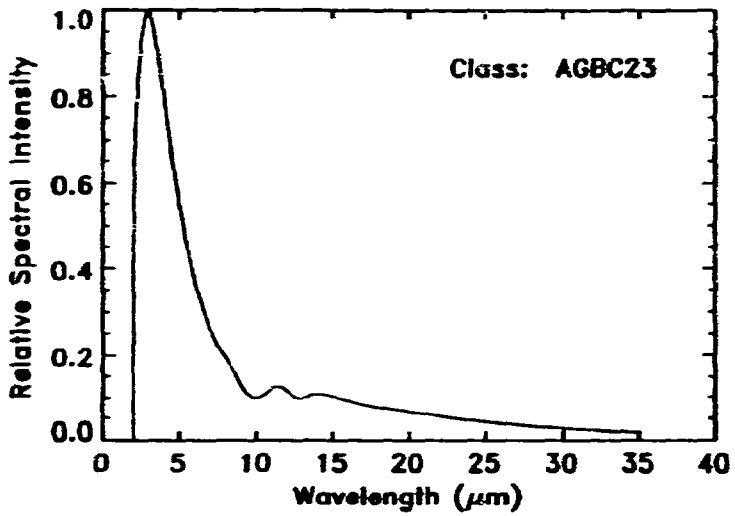
Class: AGBC23
Relative Spectral Intensity
Wavelength (μm)
1.0
0.8
0.6
0.4
0.2
0.0
0
5
10
15
20
25
30
35
40

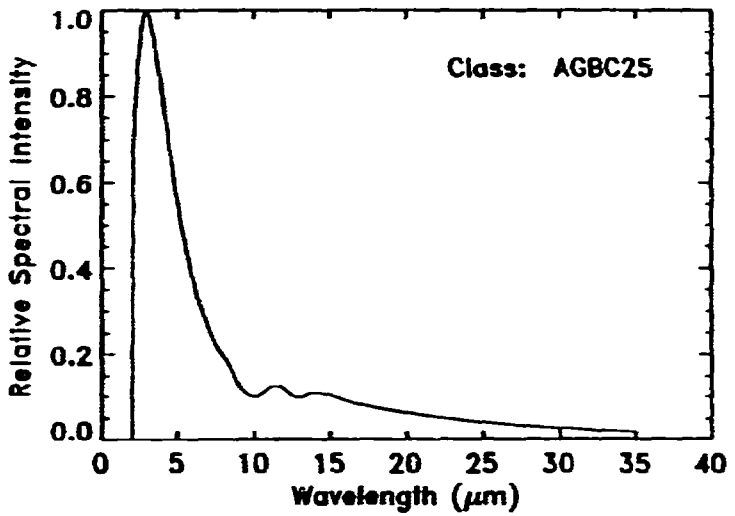
Class: AGBC25
Relative Spectral Intensity
Wavelength (μm)
1.0
0.8
0.6
0.4
0.2
0.0
0
5
10
15
20
25
30
35
40

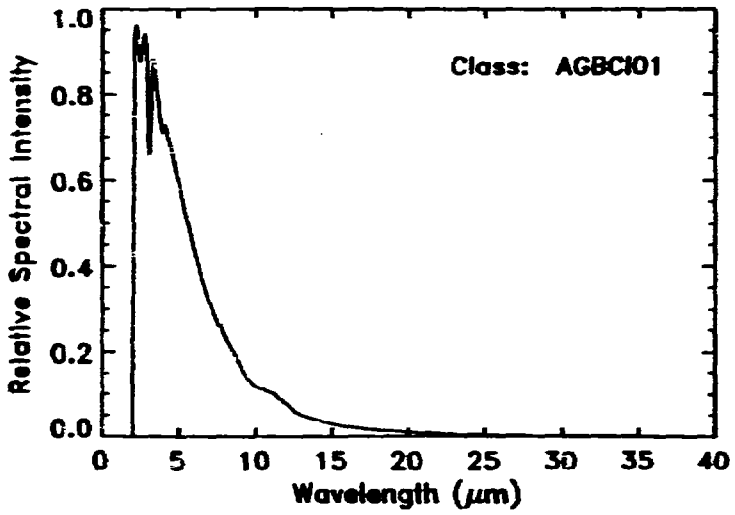
Class: AGBCI01
Relative Spectral Intensity
Wavelength (μm)
1.0
0.8
0.6
0.4
0.2
0.0
0
5
10
15
20
25
30
35
40

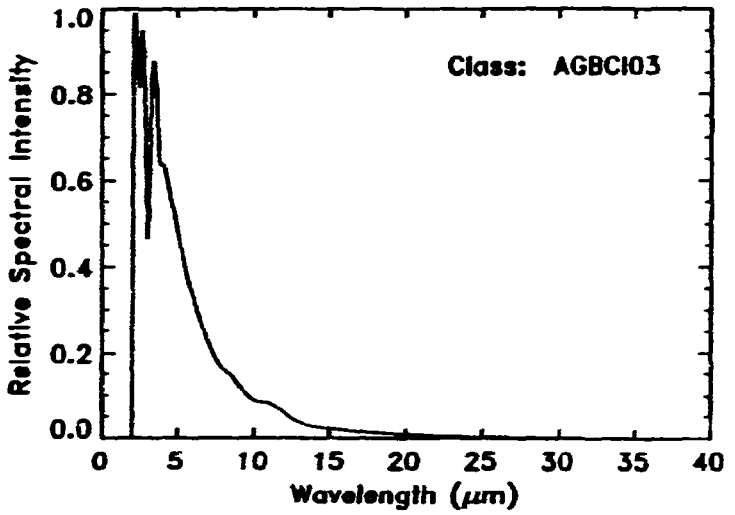
Class: AGBCI03
Relative Spectral Intensity
Wavelength (μm)
1.0
0.8
0.6
0.4
0.2
0.0
0
5
10
15
20
25
30
35
40

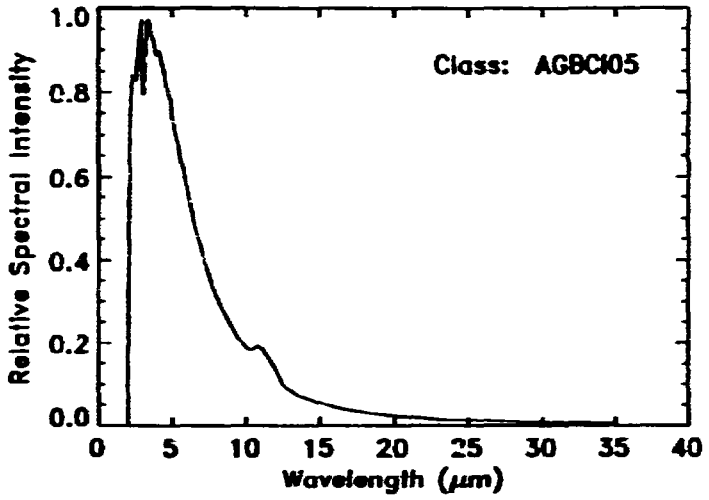
Class: AGBCI05
Relative Spectral Intensity
1.0
0.8
0.6
0.4
0.2
0.0
0
5
10
15
20
25
30
35
40
Wavelength (μm)

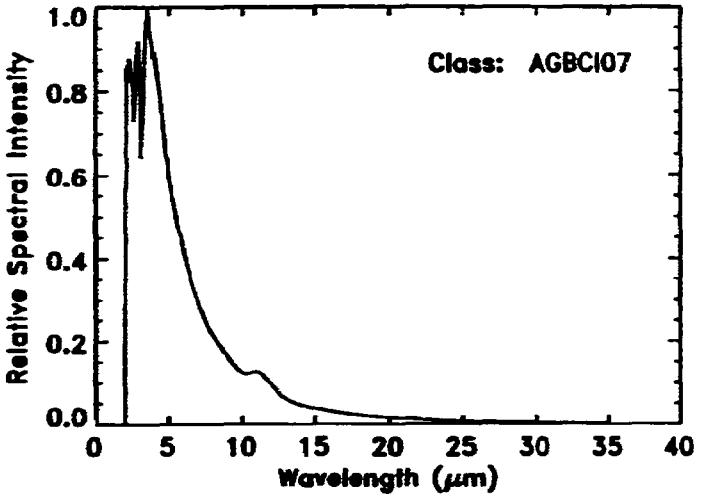
Class: AGBCI07
Relative Spectral Intensity
1.0
0.8
0.6
0.4
0.2
0.0
0
5
10
15
20
25
30
35
40
Wavelength (μm)

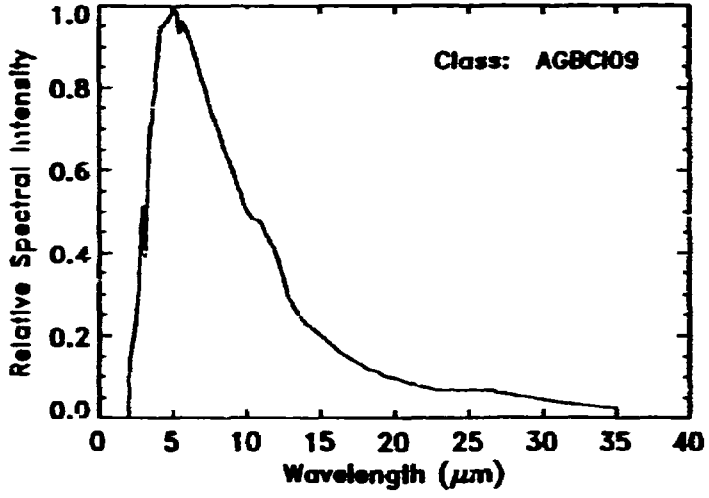
Class: AGBCI09
Relative Spectral Intensity
1.0
0.8
0.6
0.4
0.2
0.0
0
5
10
15
20
25
30
35
40
Wavelength (μm)

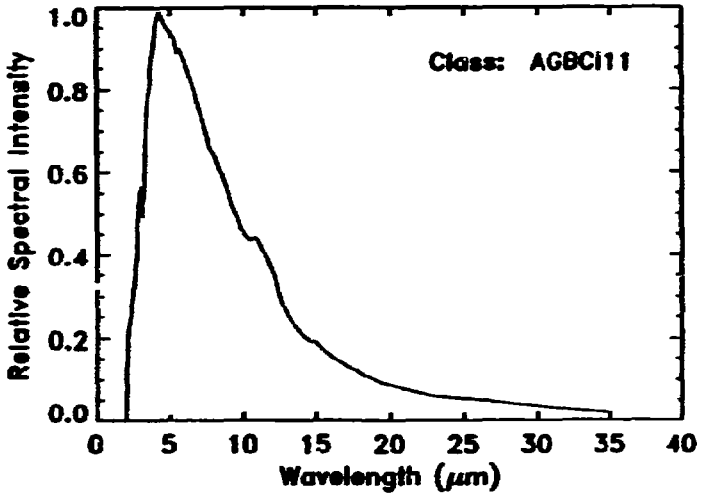
Class: AGBCI11
Relative Spectral Intensity
1.0
0.8
0.6
0.4
0.2
0.0
0
5
10
15
20
25
30
35
40
Wavelength (μm)

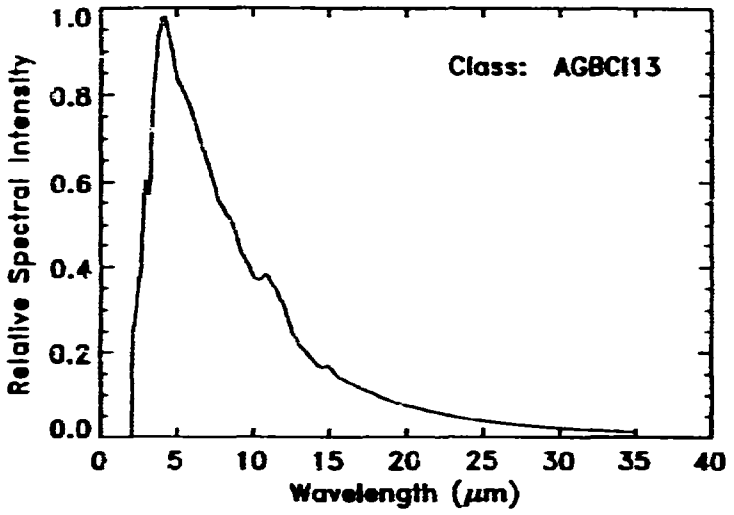
Class: AGBCI13
Relative Spectral Intensity
Wavelength (μm)
0.0
0.2
0.4
0.6
0.8
1.0
0
5
10
15
20
25
30
35
40

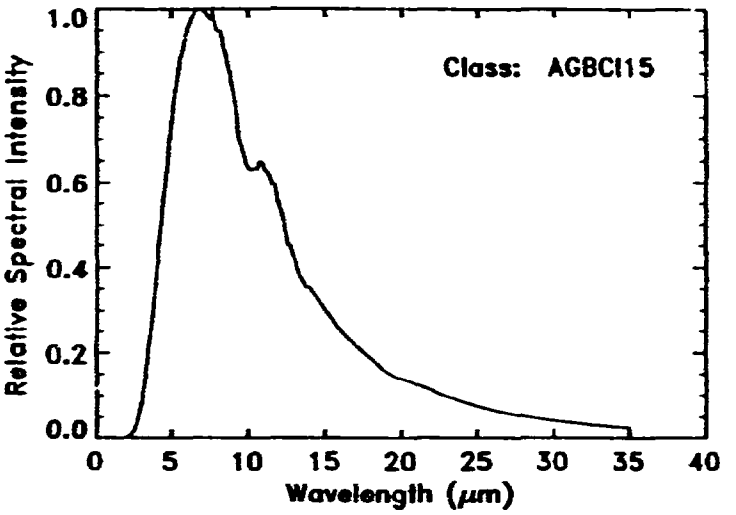
Class: AGBCI15
Relative Spectral Intensity
Wavelength (μm)
0.0
0.2
0.4
0.6
0.8
1.0
0
5
10
15
20
25
30
35
40

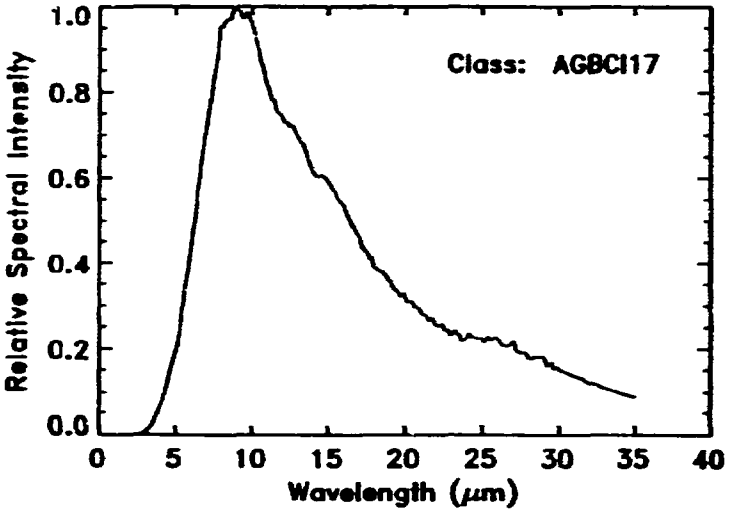
Class: AGBCI17
Relative Spectral Intensity
Wavelength (μm)
0.0
0.2
0.4
0.6
0.8
1.0
0
5
10
15
20
25
30
35
40

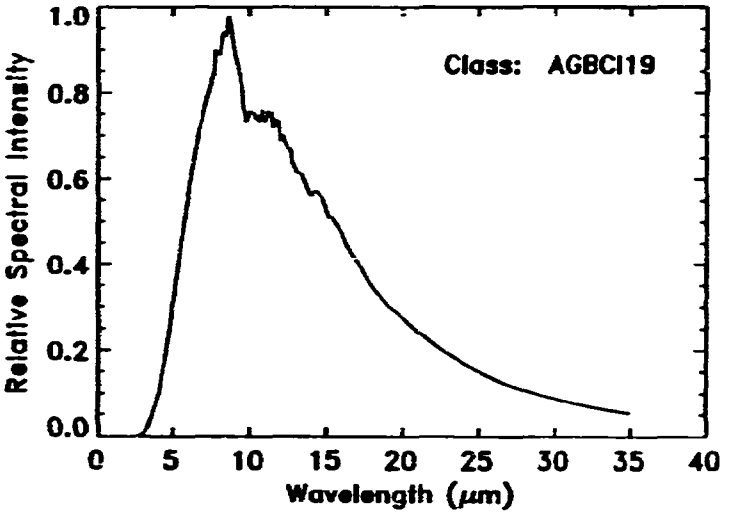
Class: AGBCI19
Relative Spectral Intensity
Wavelength (μm)
0.0
0.2
0.4
0.6
0.8
1.0
0
5
10
15
20
25
30
35
40

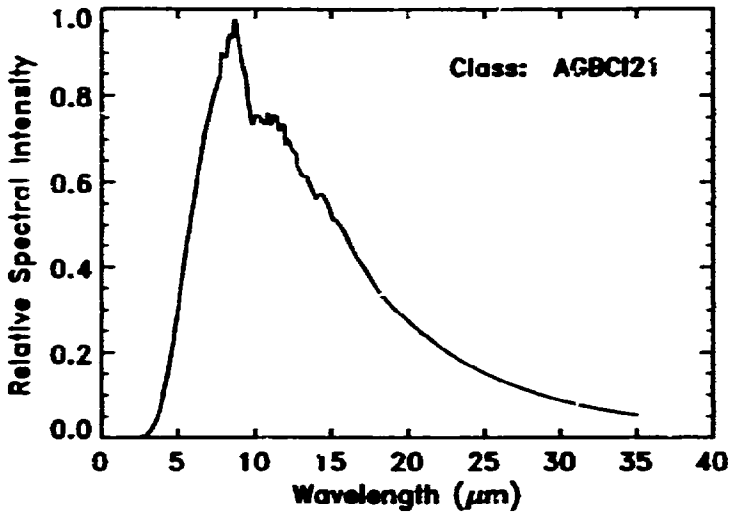
Class: AGBCI21
Relative Spectral Intensity
Wavelength (μm)
0.0
0.2
0.4
0.6
0.8
1.0
0
5
10
15
20
25
30
35
40

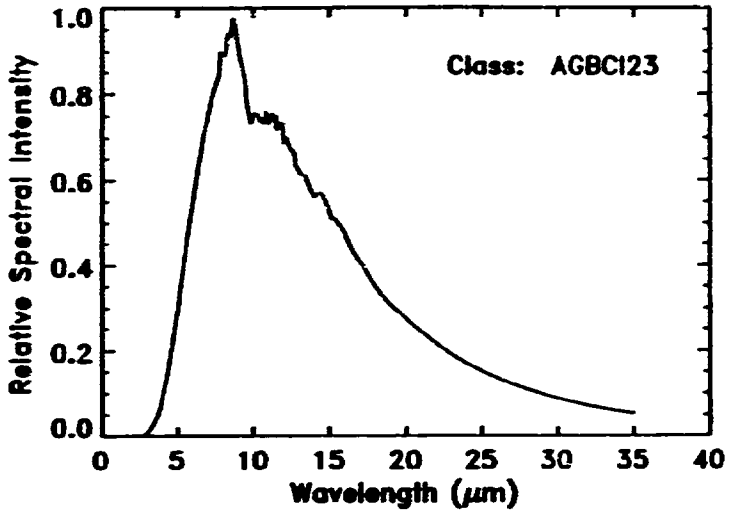
Class: AGBCI23
Relative Spectral Intensity
Wavelength (μm)
0.0
0.2
0.4
0.6
0.8
1.0
0
5
10
15
20
25
30
35
40

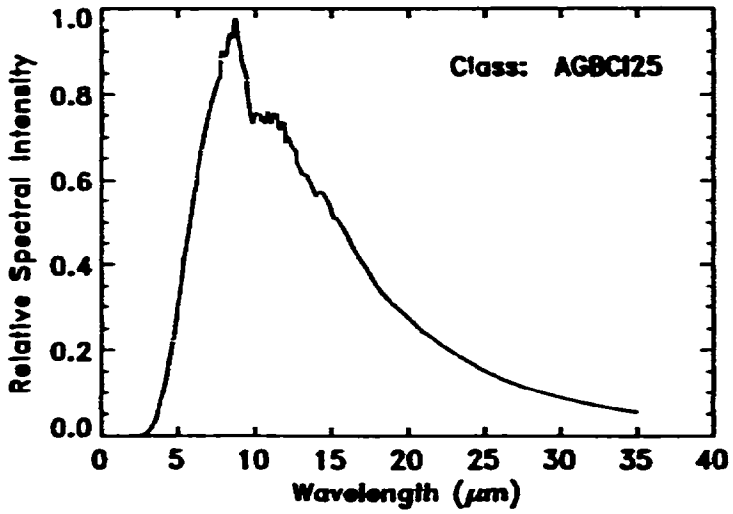
Class: AGBCI25
Relative Spectral Intensity
Wavelength (μm)
0.0
0.2
0.4
0.6
0.8
1.0
0
5
10
15
20
25
30
35
40

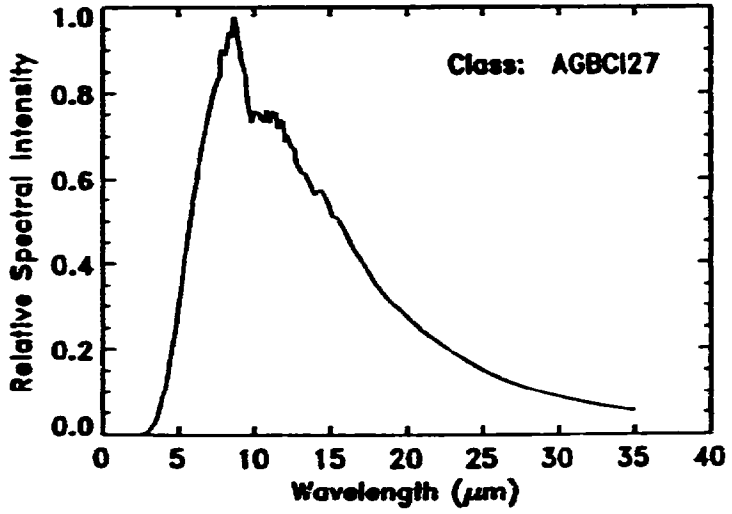
Class: AGBCI27
Relative Spectral Intensity
Wavelength (μm)
0.0
0.2
0.4
0.6
0.8
1.0
0
5
10
15
20
25
30
35
40

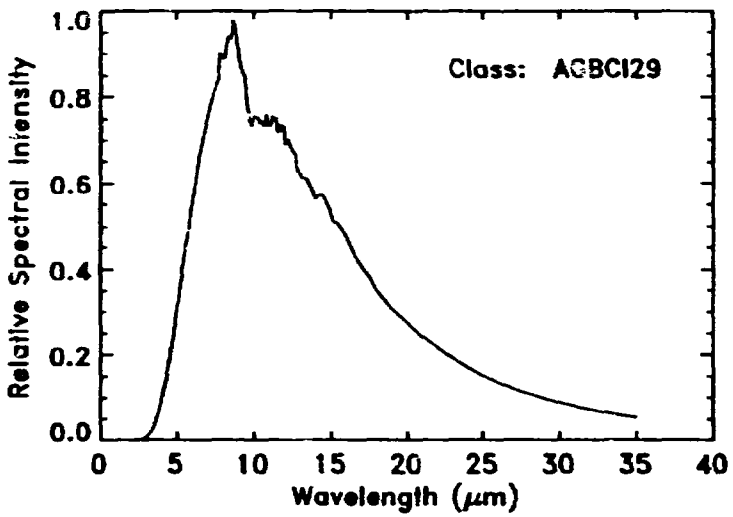
Class: AGBCI29
Relative Spectral Intensity
Wavelength (μm)
0.0
0.2
0.4
0.6
0.8
1.0
0
5
10
15
20
25
30
35
40

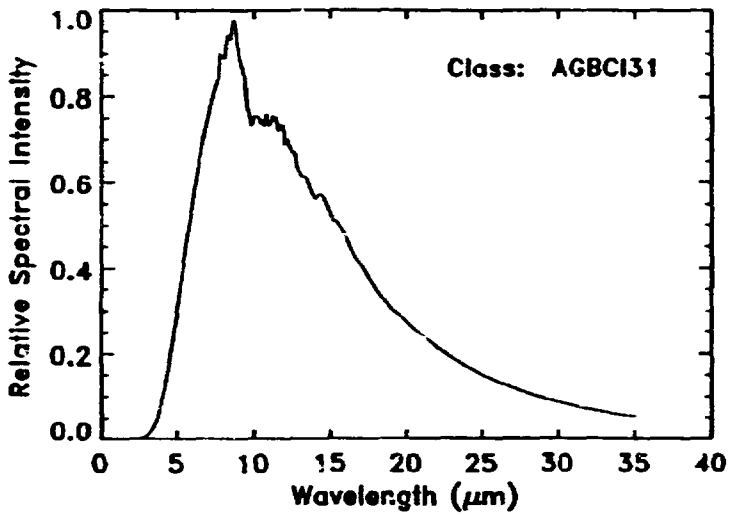
Class: AGBCI31
Relative Spectral Intensity
Wavelength (μm)
0.0
0.2
0.4
0.6
0.8
1.0
0
5
10
15
20
25
30
35
40

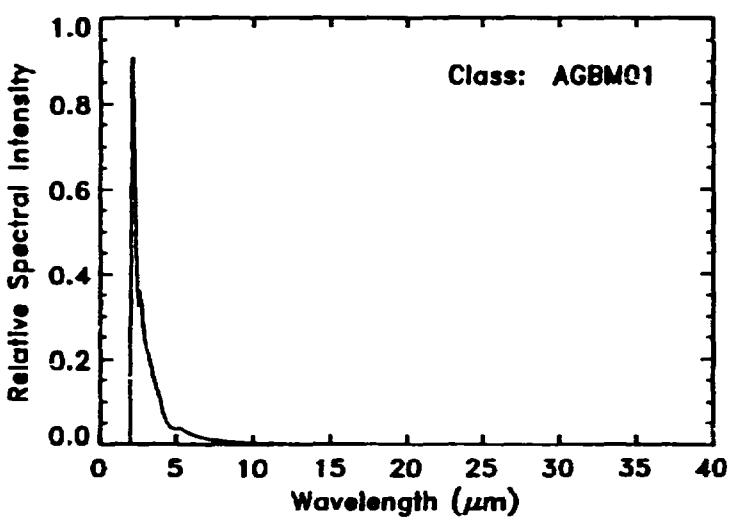
Class: AGBM01
Relative Spectral Intensity
Wavelength (μm)
0.0
0.2
0.4
0.6
0.8
1.0
0
5
10
15
20
25
30
35
40

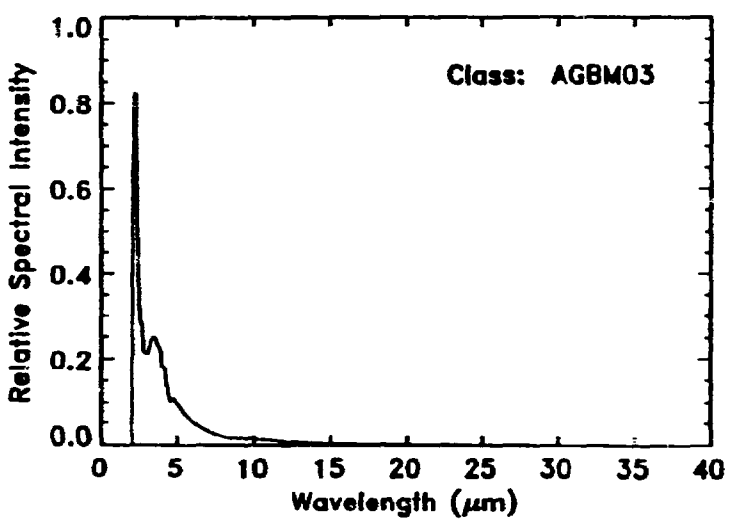
Class: AGBM03
Relative Spectral Intensity
Wavelength (μm)
0.0
0.2
0.4
0.6
0.8
1.0
0
5
10
15
20
25
30
35
40

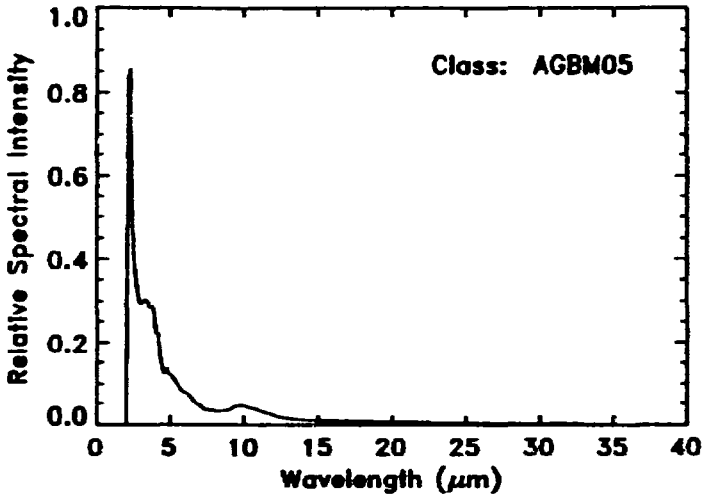
Class: AGBM05
Relative Spectral Intensity
Wavelength (μm)
1.0
0.8
0.6
0.4
0.2
0.0
0 5 10 15 20 25 30 35 40

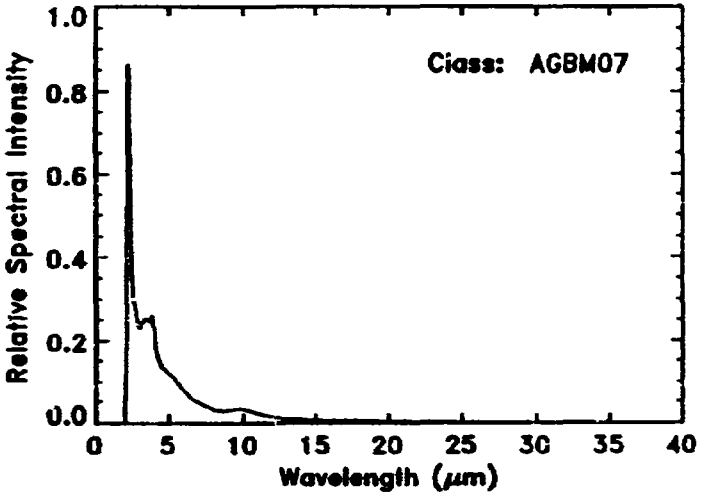
Class: AGBM07
Relative Spectral Intensity
Wavelength (μm)
1.0
0.8
0.6
0.4
0.2
0.0
0 5 10 15 20 25 30 35 40

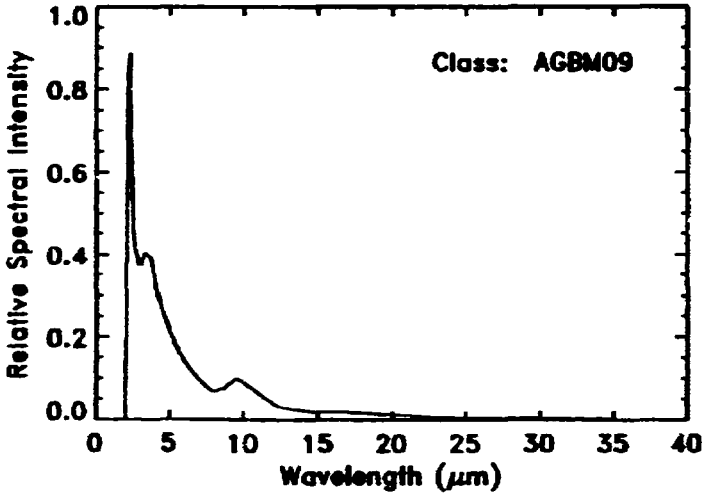
Class: AGBM09
Relative Spectral Intensity
Wavelength (μm)
1.0
0.8
0.6
0.4
0.2
0.0
0 5 10 15 20 25 30 35 40

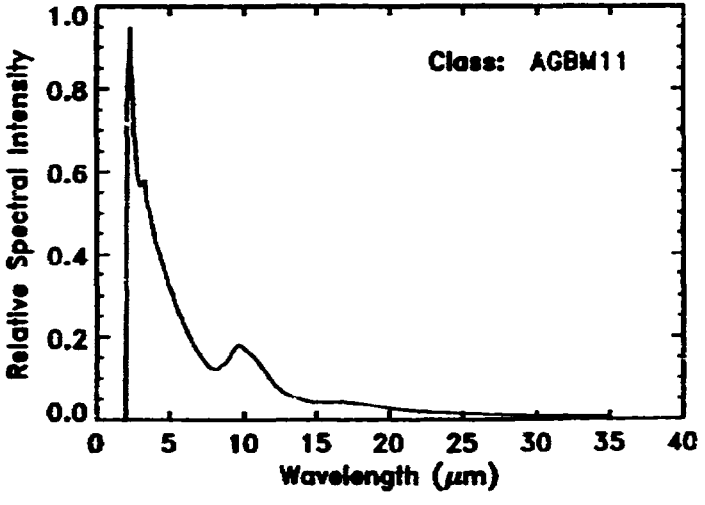
Class: AGBM11
Relative Spectral Intensity
Wavelength (μm)
1.0
0.8
0.6
0.4
0.2
0.0
0 5 10 15 20 25 30 35 40

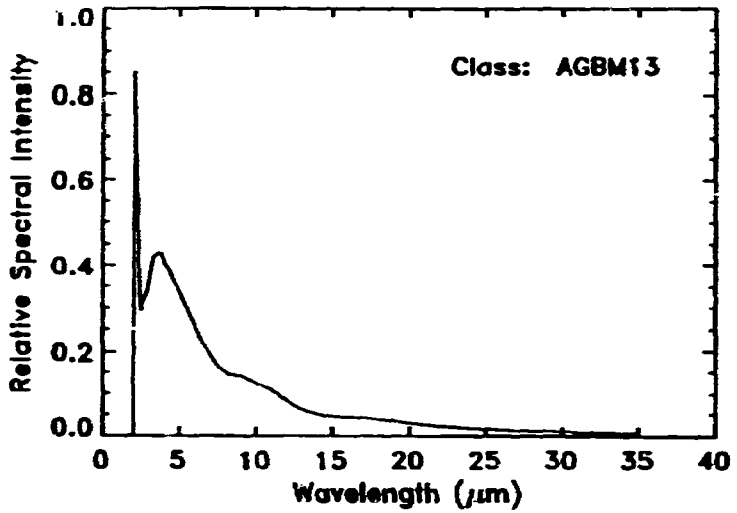
Class: AGBM13
Relative Spectral Intensity
Wavelength (μm)
0.0
0.2
0.4
0.6
0.8
1.0
0
5
10
15
20
25
30
35
40

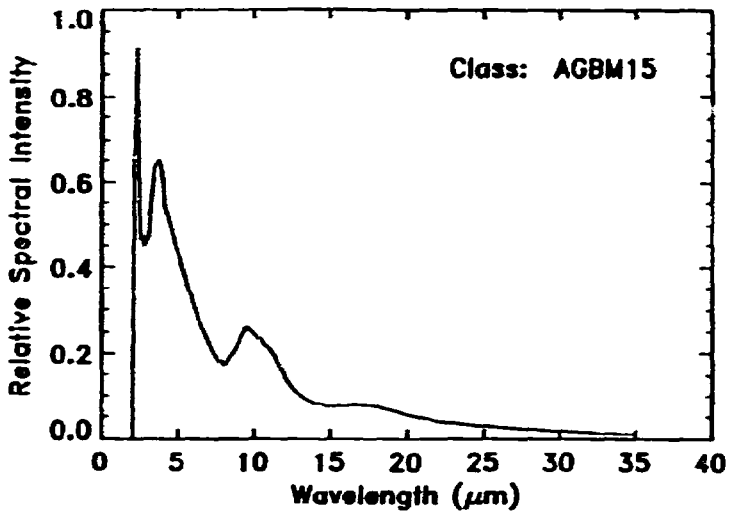
Class: AGBM15
Relative Spectral Intensity
Wavelength (μm)
0.0
0.2
0.4
0.6
0.8
1.0
0
5
10
15
20
25
30
35
40

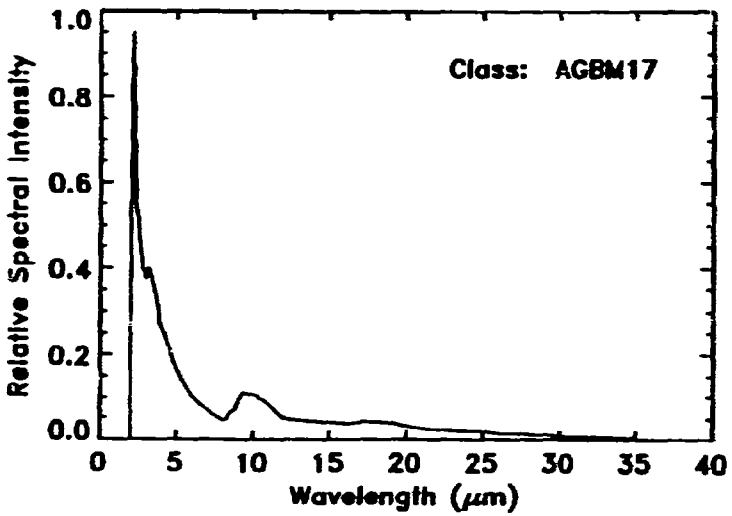
Class: AGBM17
Relative Spectral Intensity
Wavelength (μm)
0.0
0.2
0.4
0.6
0.8
1.0
0
5
10
15
20
25
30
35
40

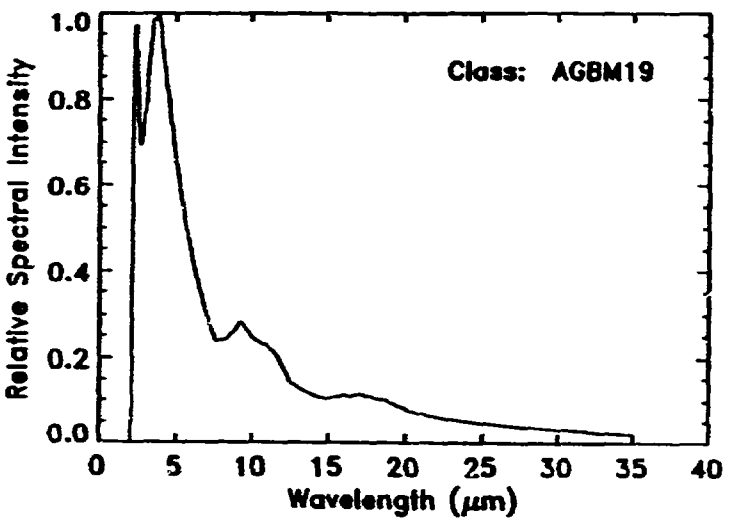
Class: AGBM19
Relative Spectral Intensity
Wavelength (μm)
0.0
0.2
0.4
0.6
0.8
1.0
0
5
10
15
20
25
30
35
40

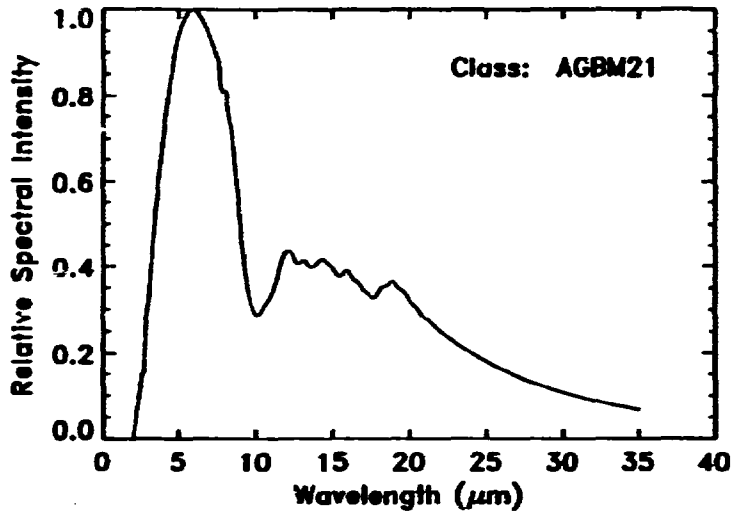
Class: AGBM21
Relative Spectral Intensity
Wavelength (μm)
0.0
0.2
0.4
0.6
0.8
1.0
0
5
10
15
20
25
30
35
40

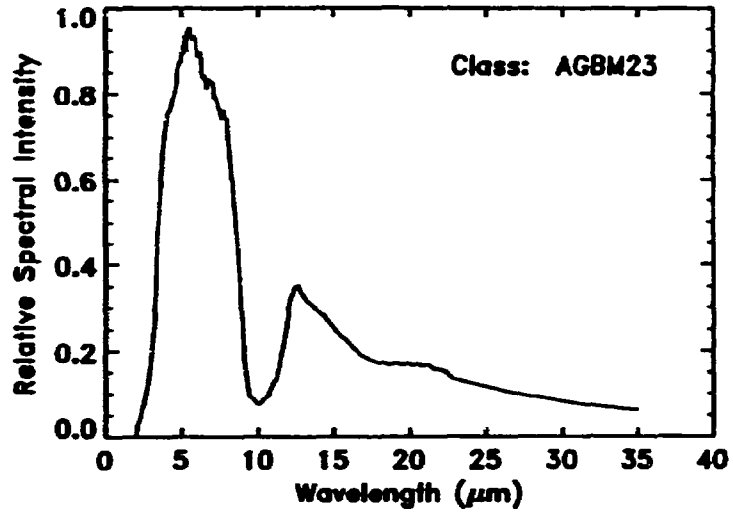
Class: AGBM23
Relative Spectral Intensity
Wavelength (μm)
0.0
0.2
0.4
0.6
0.8
1.0
0
5
10
15
20
25
30
35
40

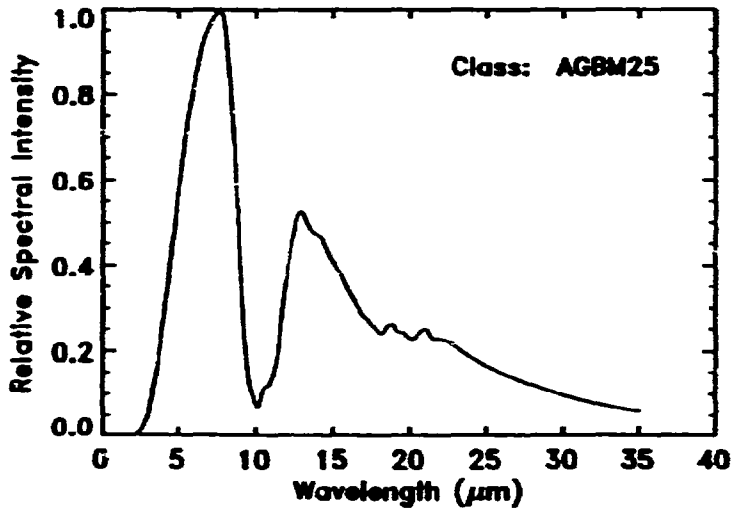
Class: AGBM25
Relative Spectral Intensity
Wavelength (μm)
0.0
0.2
0.4
0.6
0.8
1.0
0
5
10
15
20
25
30
35
40

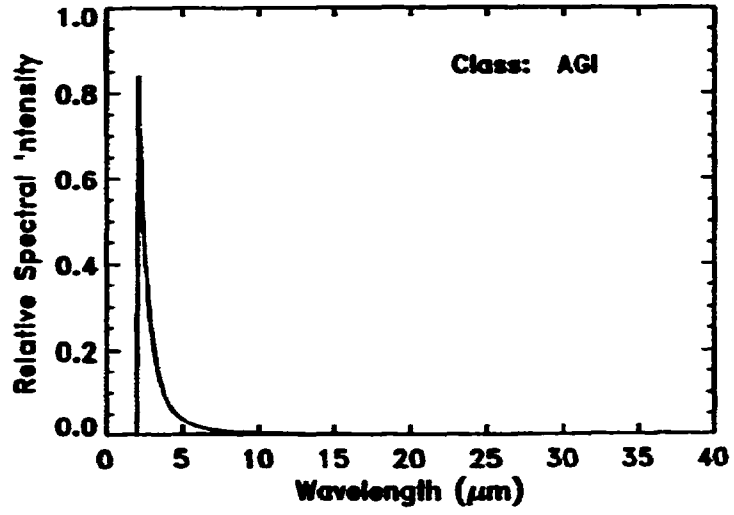
Class: AGI
Relative Spectral Intensity
Wavelength (μm)
0.0
0.2
0.4
0.6
0.8
1.0
0
5
10
15
20
25
30
35
40

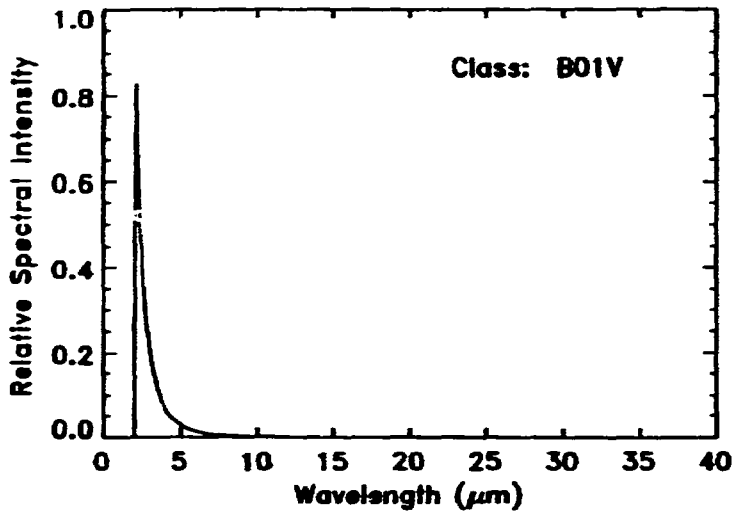
Class: B01V
Relative Spectral Intensity
Wavelength (μm)
1.0
0.8
0.6
0.4
0.2
0.0
0
5
10
15
20
25
30
35
40

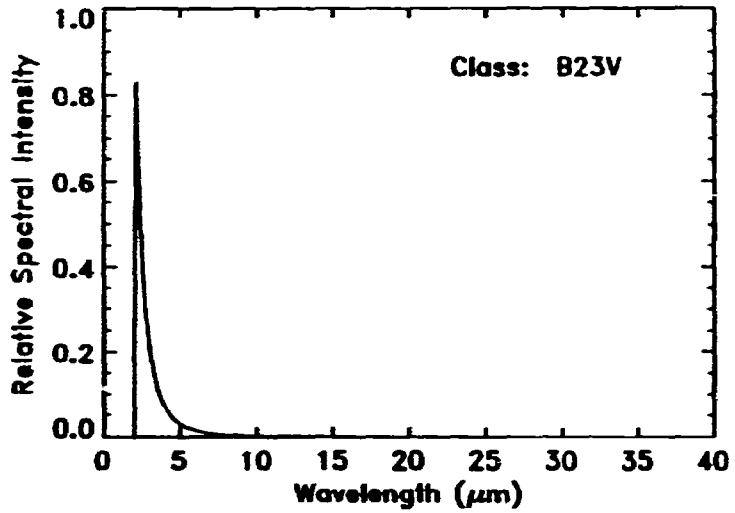
Class: B23V
Relative Spectral Intensity
Wavelength (μm)
1.0
0.8
0.6
0.4
0.2
0.0
0
5
10
15
20
25
30
35
40

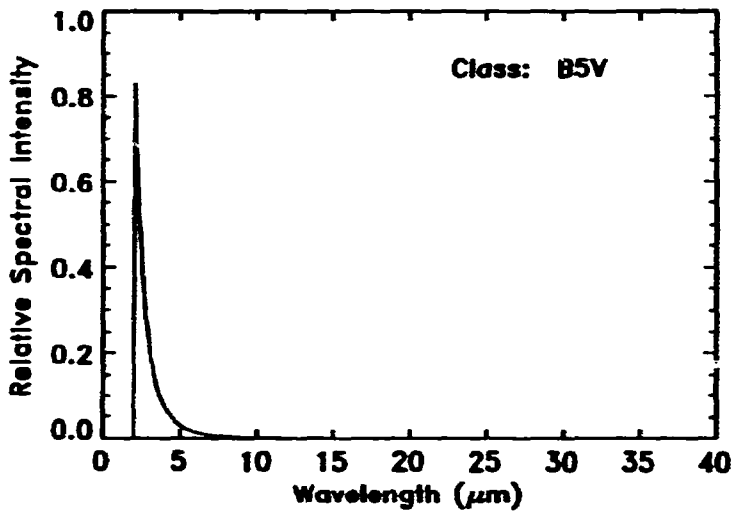
Class: B5V
Relative Spectral Intensity
Wavelength (μm)
1.0
0.8
0.6
0.4
0.2
0.0
0
5
10
15
20
25
30
35
40

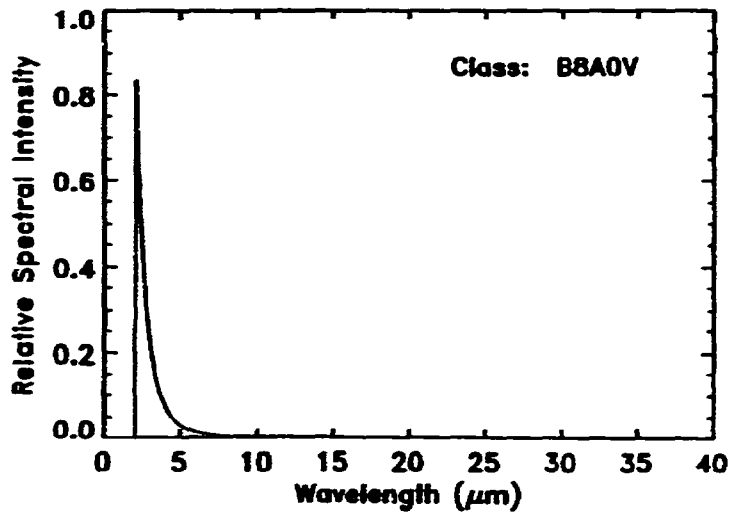
Class: B8A0V
Relative Spectral Intensity
Wavelength (μm)
1.0
0.8
0.6
0.4
0.2
0.0
0
5
10
15
20
25
30
35
40

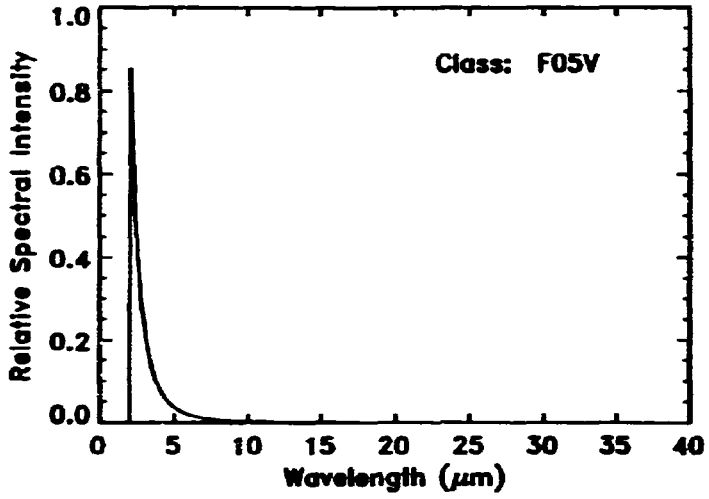
Class: F05V
Relative Spectral Intensity
1.0
0.8
0.6
0.4
0.2
0.0
0
5
10
15
20
25
30
35
40
Wavelength (μm)

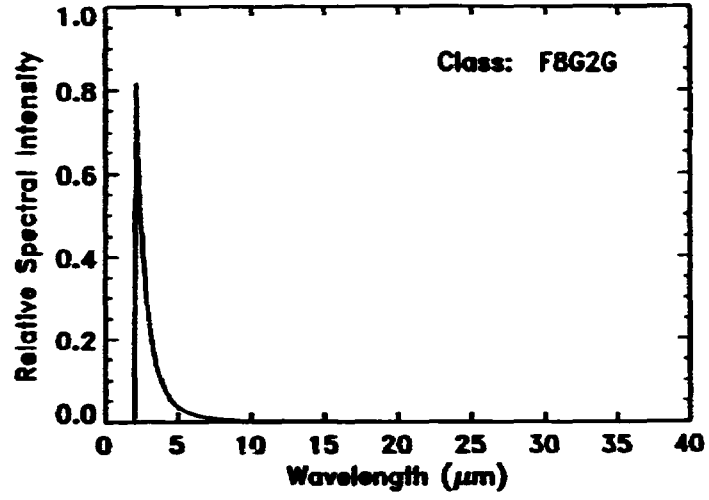
Class: F8G2G
Relative Spectral Intensity
1.0
0.8
0.6
0.4
0.2
0.0
0
5
10
15
20
25
30
35
40
Wavelength (μm)

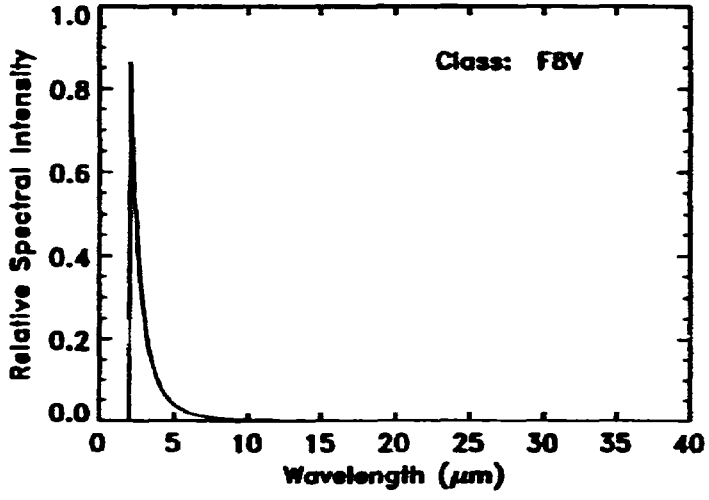
Class: F8V
Relative Spectral Intensity
1.0
0.8
0.6
0.4
0.2
0.0
0
5
10
15
20
25
30
35
40
Wavelength (μm)

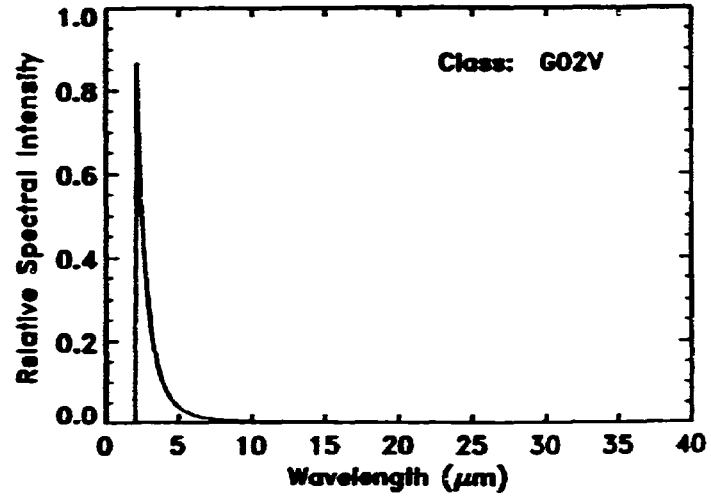
Class: G02V
Relative Spectral Intensity
1.0
0.8
0.6
0.4
0.2
0.0
0
5
10
15
20
25
30
35
40
Wavelength (μm)

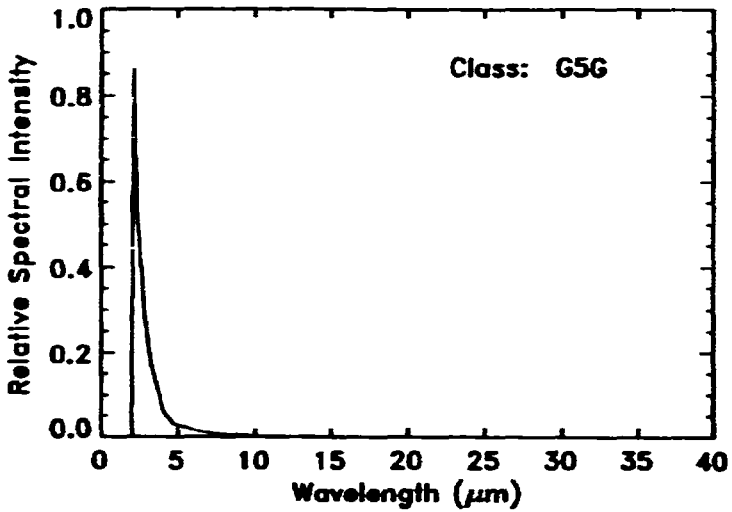
Class: G5G
Relative Spectral Intensity
Wavelength (μm)
1.0
0.8
0.6
0.4
0.2
0.0
0
5
10
15
20
25
30
35
40

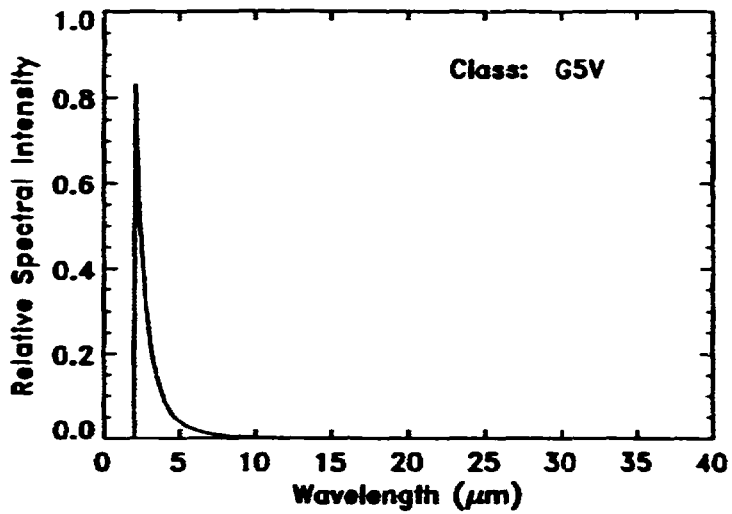
Class: G5V
Relative Spectral Intensity
Wavelength (μm)
1.0
0.8
0.6
0.4
0.2
0.0
0
5
10
15
20
25
30
35
40

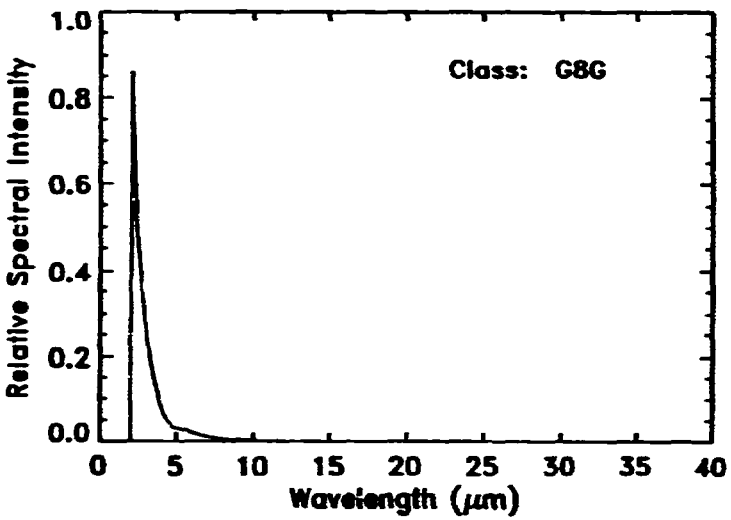
Class: G8G
Relative Spectral Intensity
Wavelength (μm)
1.0
0.8
0.6
0.4
0.2
0.0
0
5
10
15
20
25
30
35
40

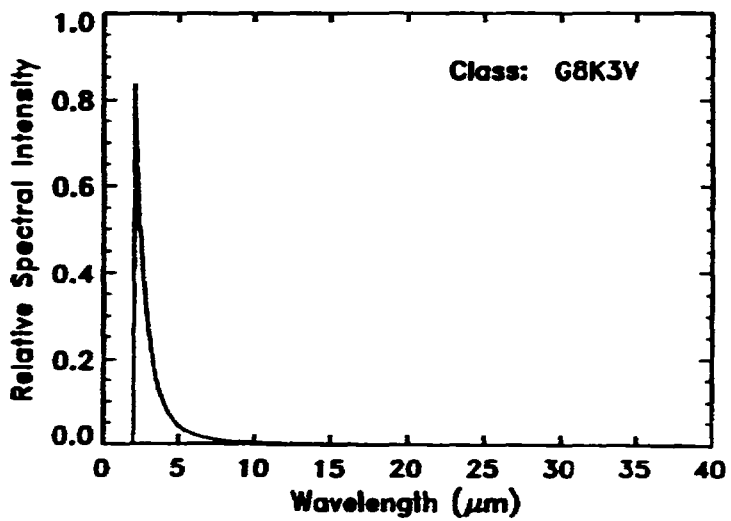
Class: G8K3V
Relative Spectral Intensity
Wavelength (μm)
1.0
0.8
0.6
0.4
0.2
0.0
0
5
10
15
20
25
30
35
40

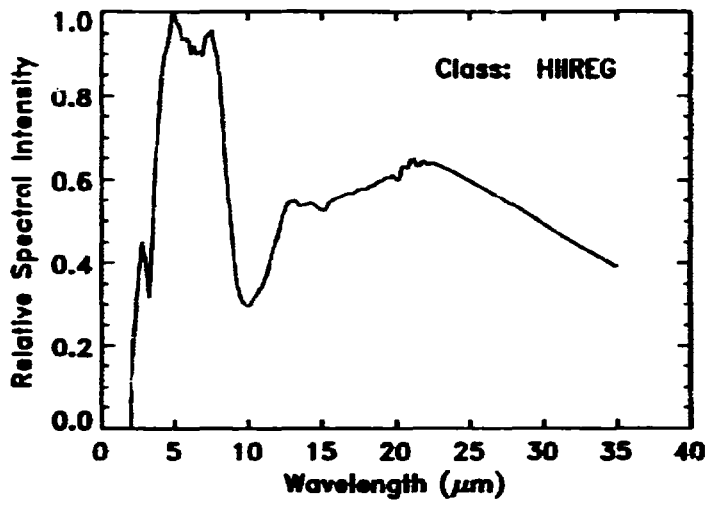
Class: HHREG
Relative Spectral Intensity
Wavelength (μm)
1.0
0.8
0.6
0.4
0.2
0.0
0
5
10
15
20
25
30
35
40

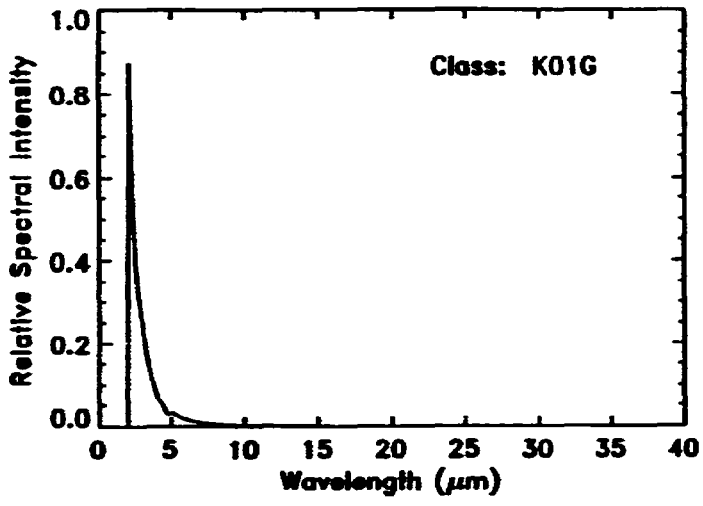
Class: K01G
Relative Spectral Intensity
Wavelength (μm)
1.0
0.8
0.6
0.4
0.2
0.0
0
5
10
15
20
25
30
35
40

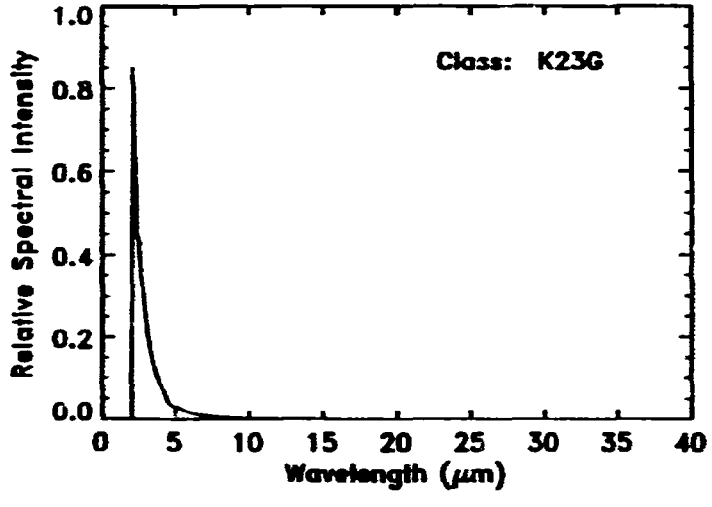
Class: K23G
Relative Spectral Intensity
Wavelength (μm)
1.0
0.8
0.6
0.4
0.2
0.0
0
5
10
15
20
25
30
35
40

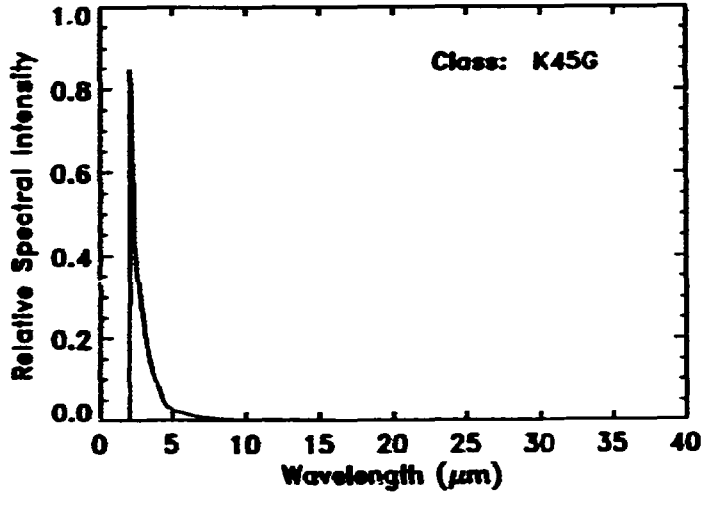
Class: K45G
Relative Spectral Intensity
Wavelength (μm)
1.0
0.8
0.6
0.4
0.2
0.0
0
5
10
15
20
25
30
35
40

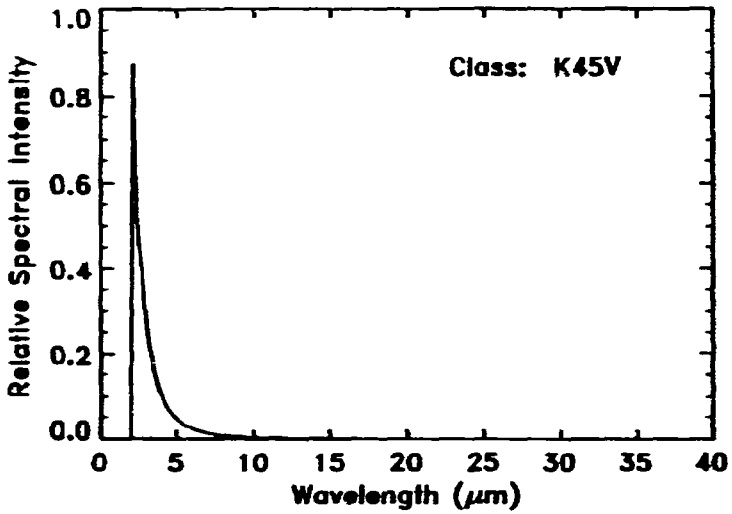
Class: K45V
Relative Spectral Intensity
1.0
0.8
0.6
0.4
0.2
0.0
0
5
10
15
20
25
30
35
40
Wavelength (μm)

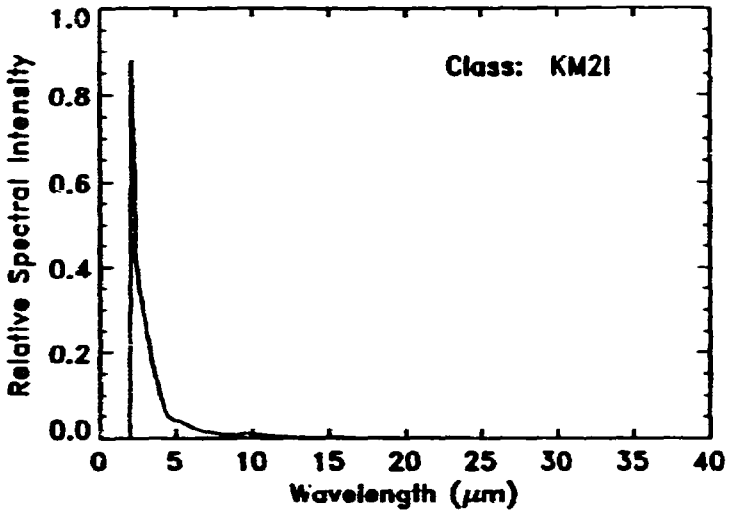
Class: KM2I
Relative Spectral Intensity
1.0
0.8
0.6
0.4
0.2
0.0
0
5
10
15
20
25
30
35
40
Wavelength (μm)

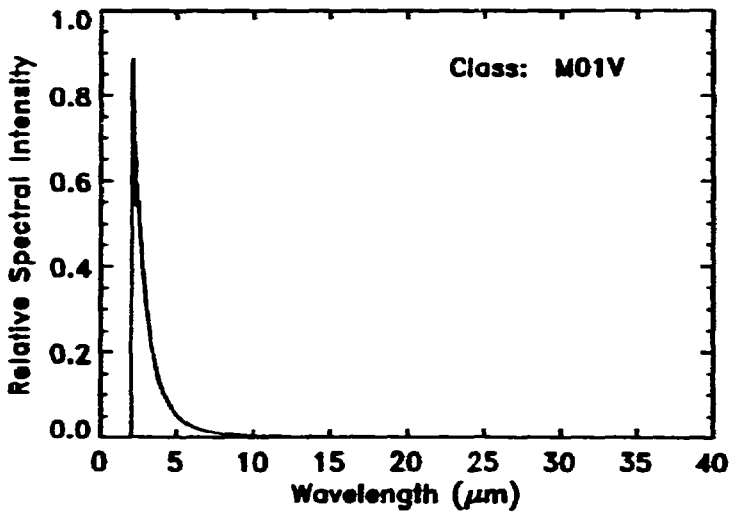
Class: M01V
Relative Spectral Intensity
1.0
0.8
0.6
0.4
0.2
0.0
0
5
10
15
20
25
30
35
40
Wavelength (μm)

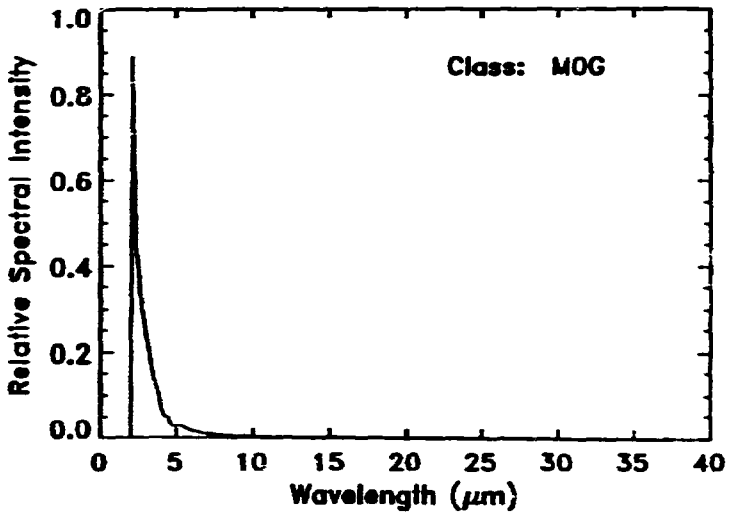
Class: M0G
Relative Spectral Intensity
1.0
0.8
0.6
0.4
0.2
0.0
0
5
10
15
20
25
30
35
40
Wavelength (μm)

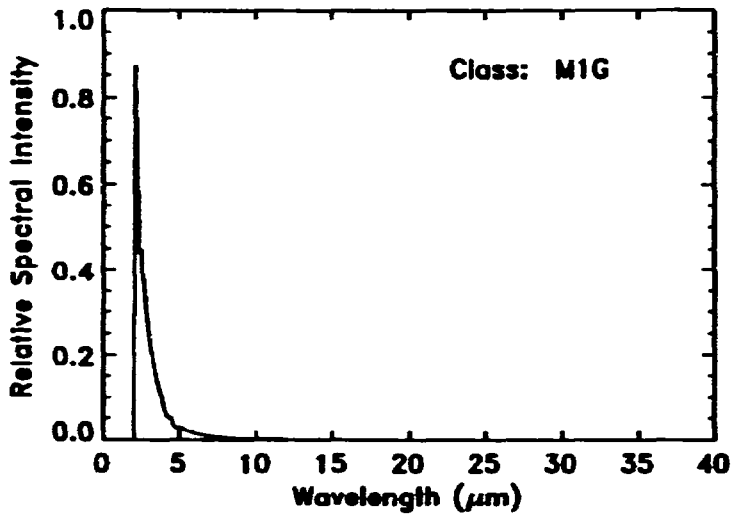
Class: M1G
Relative Spectral Intensity
1.0
0.8
0.6
0.4
0.2
0.0
0 5 10 15 20 25 30 35 40
Wavelength (μm)

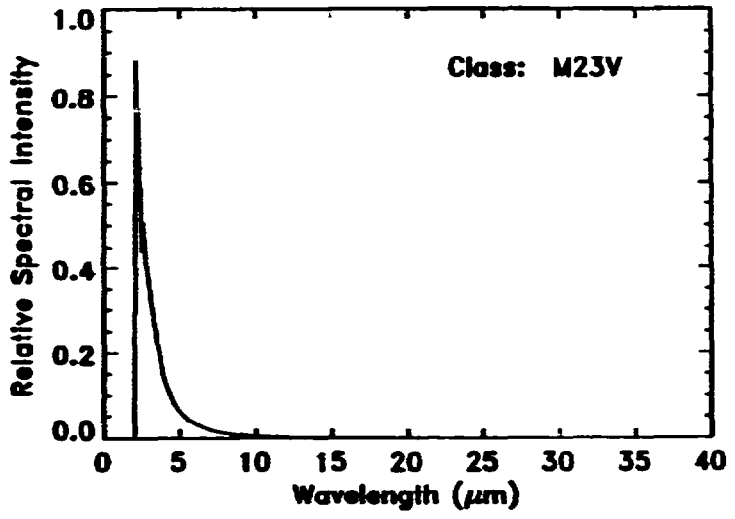
Class: M2.5V
Relative Spectral Intensity
1.0
0.8
0.6
0.4
0.2
0.0
0 5 10 15 20 25 30 35 40
Wavelength (μm)

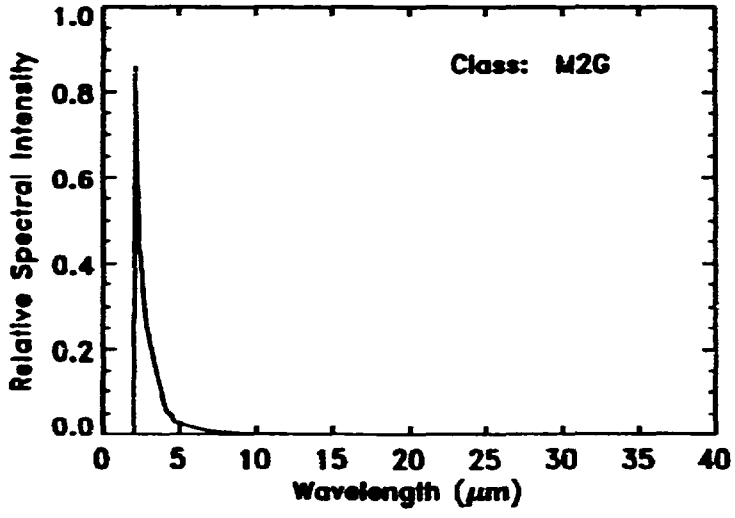
Class: M2G
Relative Spectral Intensity
1.0
0.8
0.6
0.4
0.2
0.0
0 5 10 15 20 25 30 35 40
Wavelength (μm)

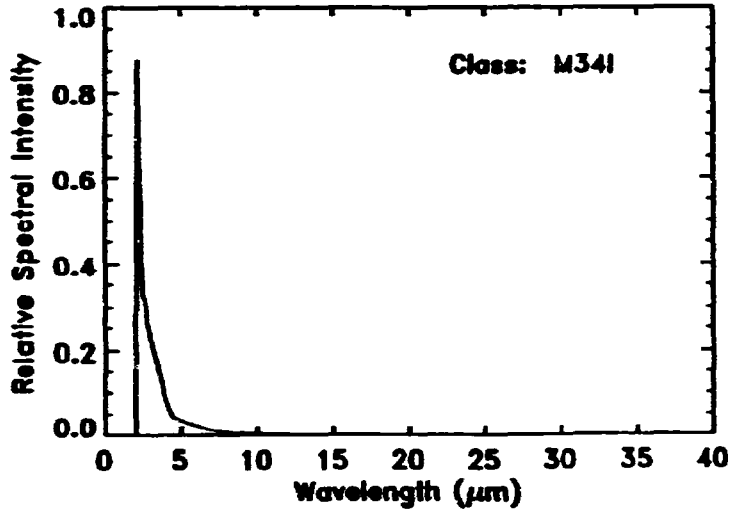
Class: M3.5I
Relative Spectral Intensity
1.0
0.8
0.6
0.4
0.2
0.0
0 5 10 15 20 25 30 35 40
Wavelength (μm)

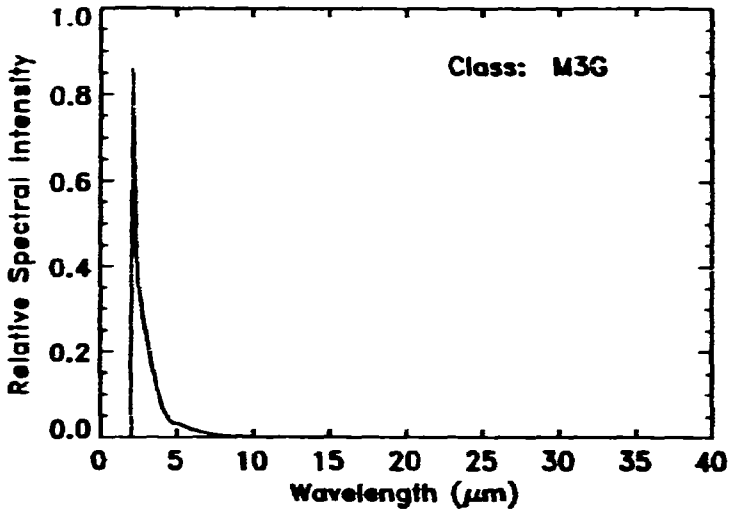
Class: M3G
Relative Spectral Intensity
1.0
0.8
0.6
0.4
0.2
0.0
0
5
10
15
20
25
30
35
40
Wavelength (μm)

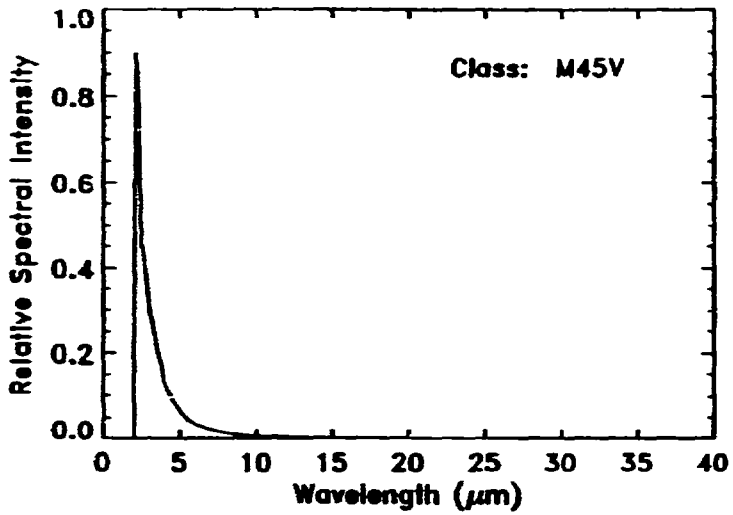
Class: M45V
Relative Spectral Intensity
1.0
0.8
0.6
0.4
0.2
0.0
0
5
10
15
20
25
30
35
40
Wavelength (μm)

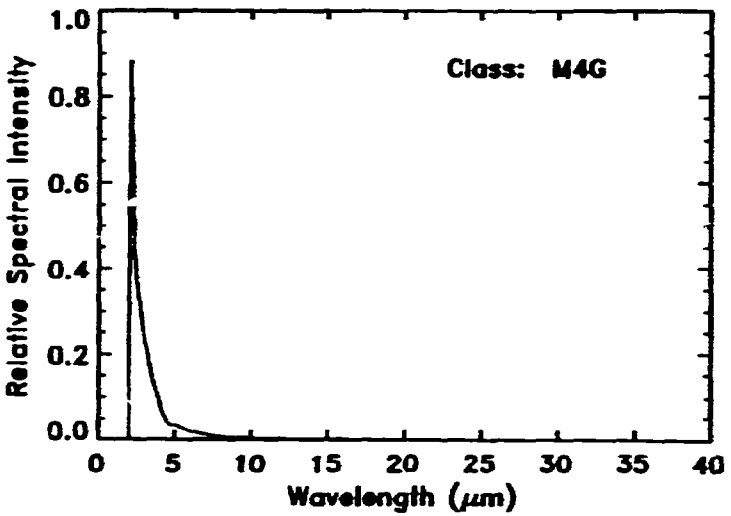
Class: M4G
Relative Spectral Intensity
1.0
0.8
0.6
0.4
0.2
0.0
0
5
10
15
20
25
30
35
40
Wavelength (μm)

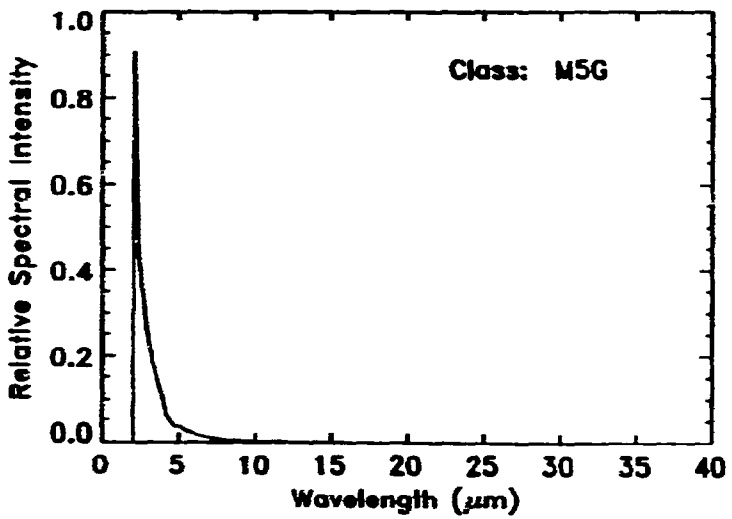
Class: M5G
Relative Spectral Intensity
1.0
0.8
0.6
0.4
0.2
0.0
0
5
10
15
20
25
30
35
40
Wavelength (μm)

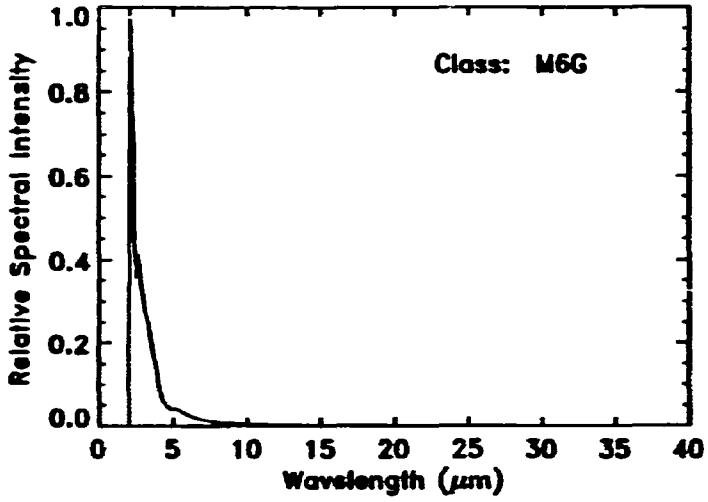
Class: M6G
Relative Spectral Intensity
1.0
0.8
0.6
0.4
0.2
0.0
0 5 10 15 20 25 30 35 40
Wavelength (μm)

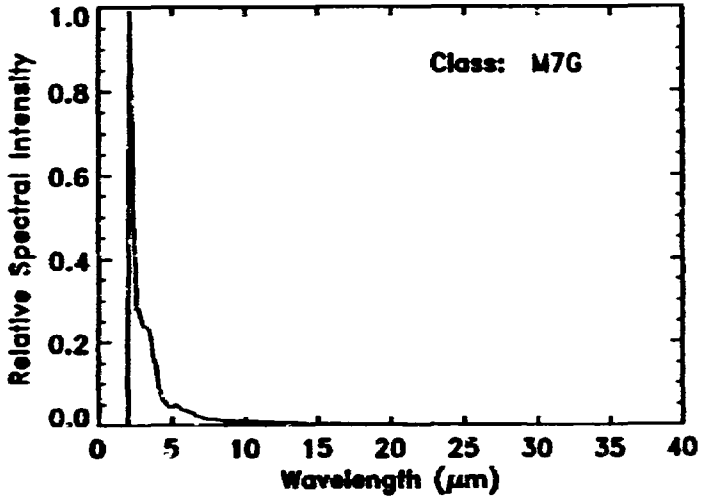
Class: M7G
Relative Spectral Intensity
1.0
0.8
0.6
0.4
0.2
0.0
0 5 10 15 20 25 30 35 40
Wavelength (μm)

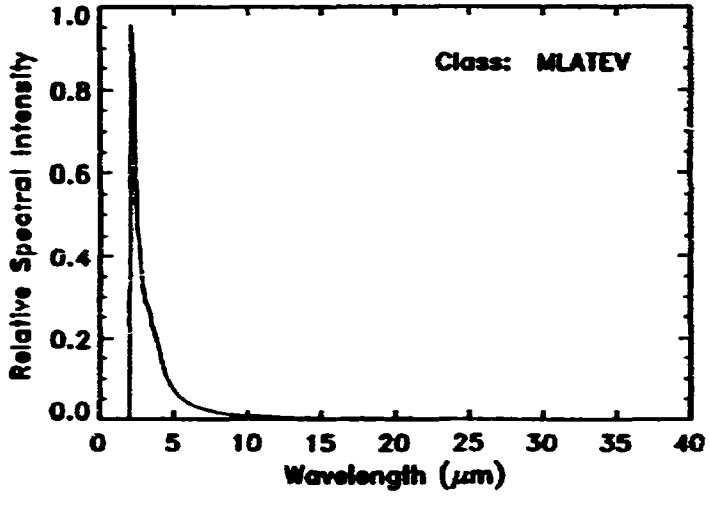
Class: MLATEV
Relative Spectral Intensity
1.0
0.8
0.6
0.4
0.2
0.0
0 5 10 15 20 25 30 35 40
Wavelength (μm)

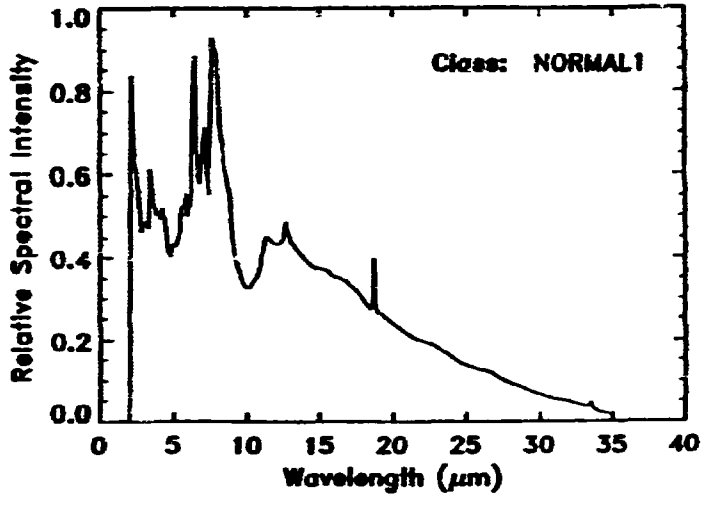
Class: NORMAL1
Relative Spectral Intensity
1.0
0.8
0.6
0.4
0.2
0.0
0 5 10 15 20 25 30 35 40
Wavelength (μm)

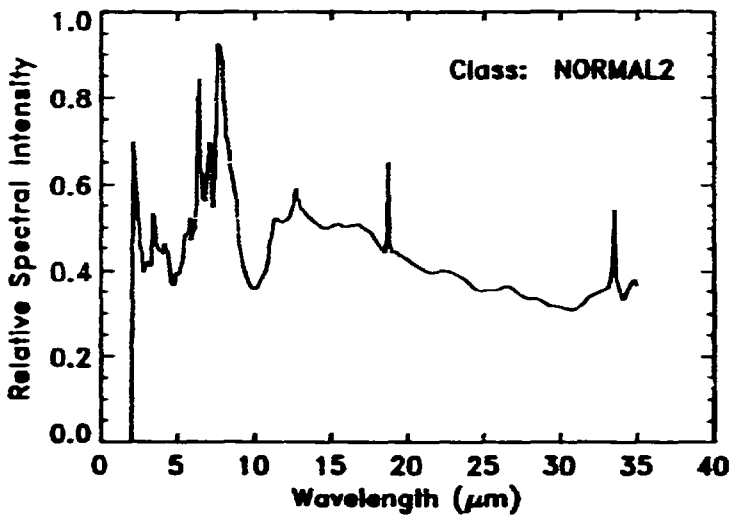
Class: NORMAL2
Relative Spectral Intensity
Wavelength (μm)
0.0
0.2
0.4
0.6
0.8
1.0
0
5
10
15
20
25
30
35
40

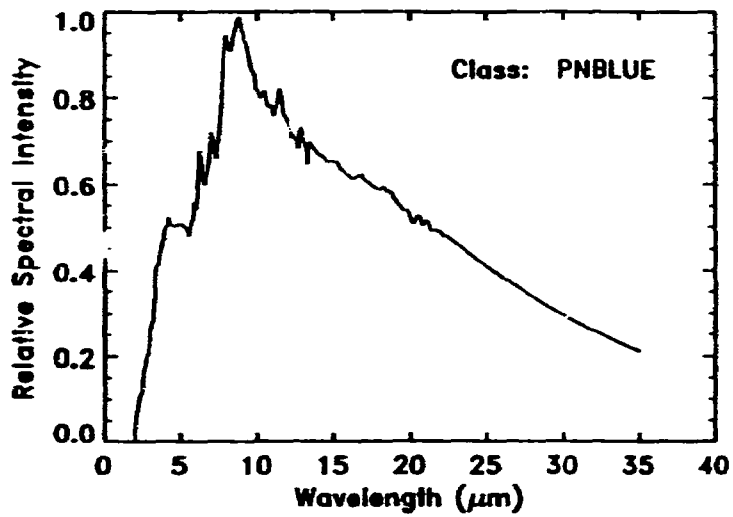
Class: PNBLUE
Relative Spectral Intensity
Wavelength (μm)
0.0
0.2
0.4
0.6
0.8
1.0
0
5
10
15
20
25
30
35
40

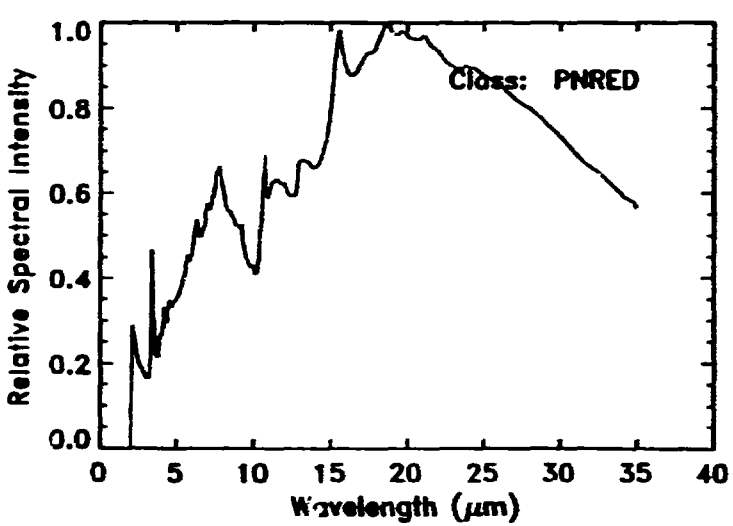
Class: PNRED
Relative Spectral Intensity
Wavelength (μm)
0.0
0.2
0.4
0.6
0.8
1.0
0
5
10
15
20
25
30
35
40

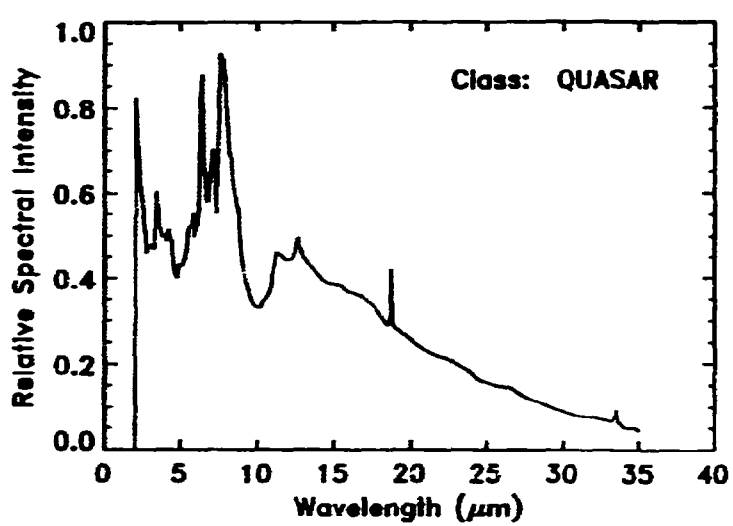
Class: QUASAR
Relative Spectral Intensity
Wavelength (μm)
0.0
0.2
0.4
0.6
0.8
1.0
0
5
10
15
20
25
30
35
40

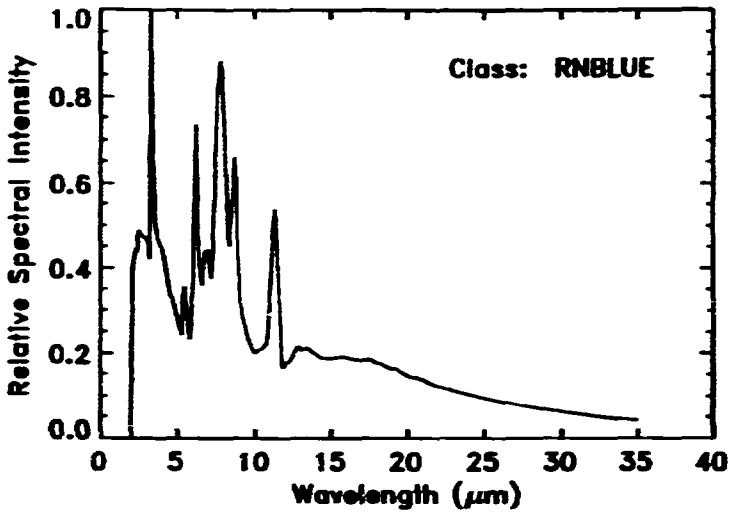
Class: RNBLUE
Relative Spectral Intensity
Wavelength (μm)
0.0
0.2
0.4
0.6
0.8
1.0
0
5
10
15
20
25
30
35
40

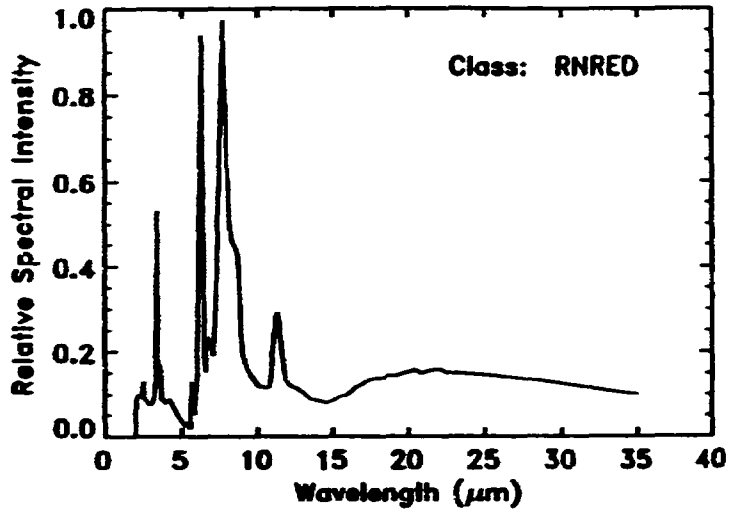
Class: RNRED
Relative Spectral Intensity
Wavelength (μm)
0.0
0.2
0.4
0.6
0.8
1.0
0
5
10
15
20
25
30
35
40

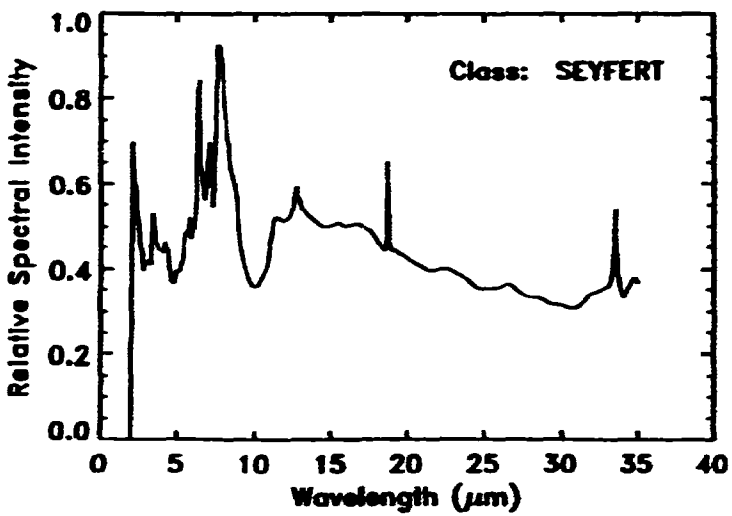
Class: SEYFERT
Relative Spectral Intensity
Wavelength (μm)
0.0
0.2
0.4
0.6
0.8
1.0
0
5
10
15
20
25
30
35
40

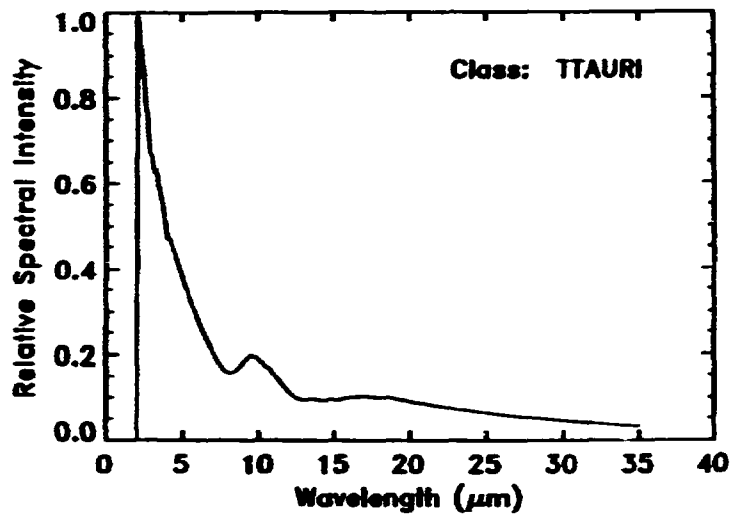
Class: TTAURI
Relative Spectral Intensity
Wavelength (μm)
0.0
0.2
0.4
0.6
0.8
1.0
0
5
10
15
20
25
30
35
40

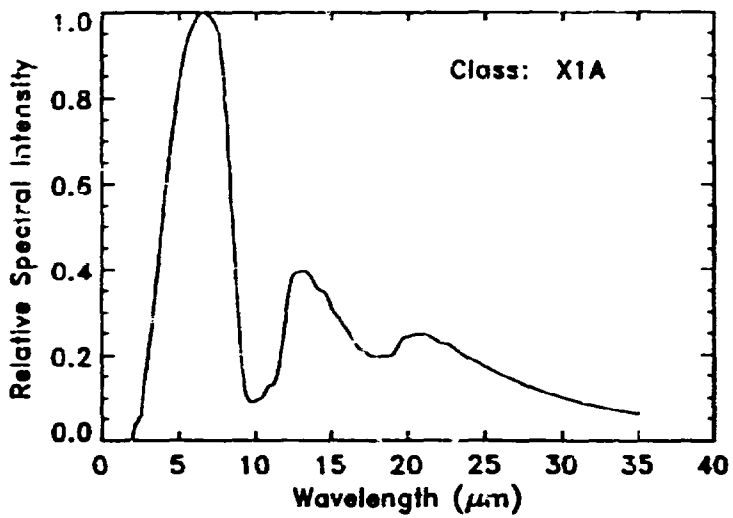
Class: X1A
Relative Spectral Intensity
Wavelength (μm)
1.0
0.8
0.6
0.4
0.2
0.0
0
5
10
15
20
25
30
35
40

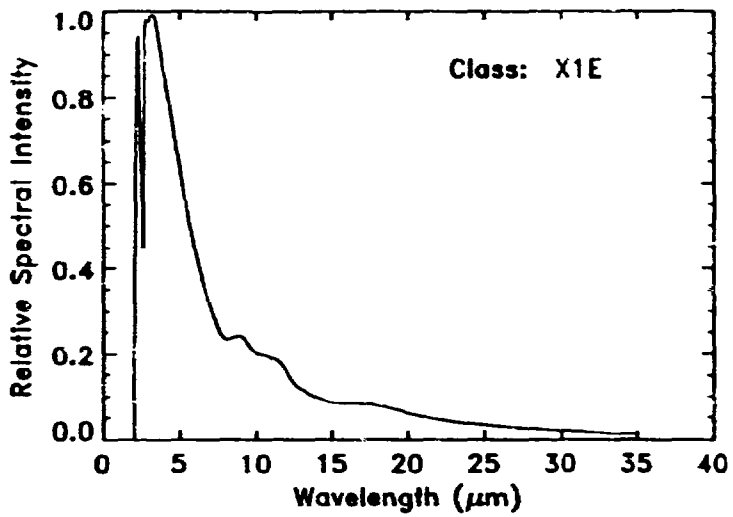
Class: X1E
Relative Spectral Intensity
Wavelength (μm)
1.0
0.8
0.6
0.4
0.2
0.0
0
5
10
15
20
25
30
35
40

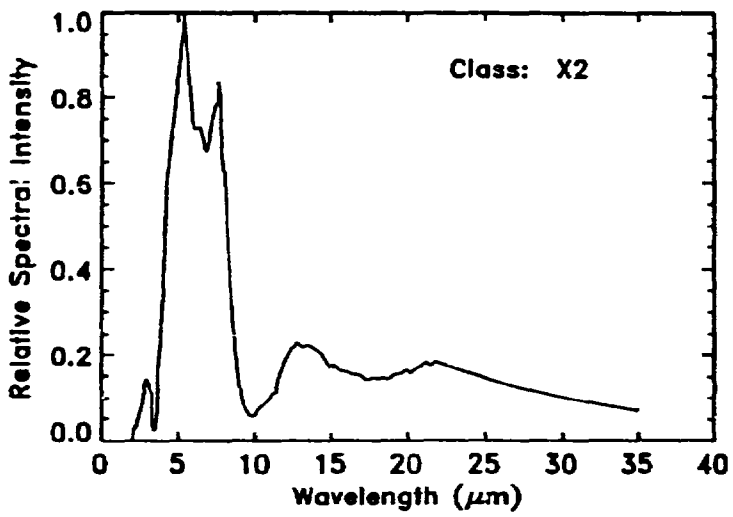
Class: X2
Relative Spectral Intensity
Wavelength (μm)
1.0
0.8
0.6
0.4
0.2
0.0
0
5
10
15
20
25
30
35
40

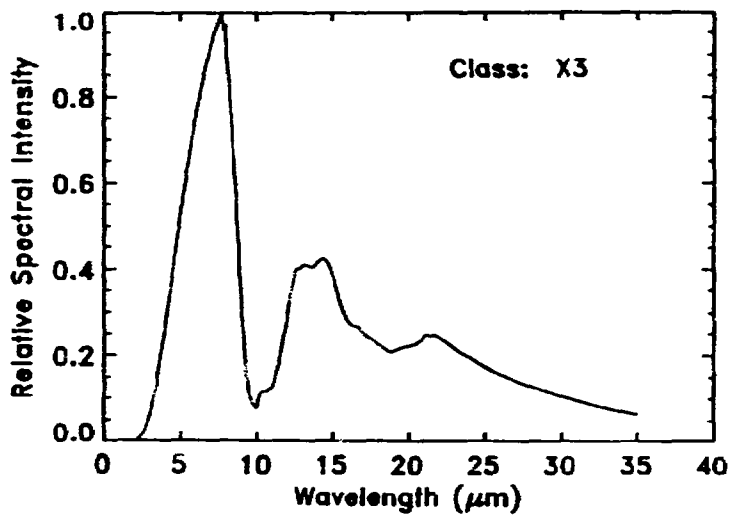
Class: X3
Relative Spectral Intensity
Wavelength (μm)
1.0
0.8
0.6
0.4
0.2
0.0
0
5
10
15
20
25
30
35
40

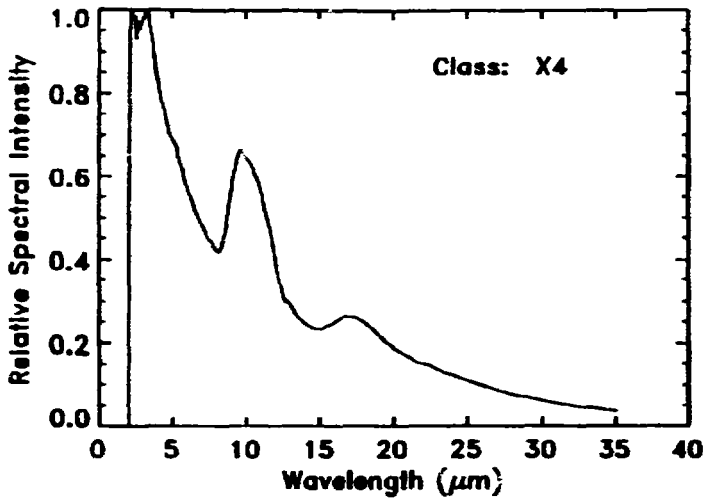
Class: X4
Relative Spectral Intensity
Wavelength (μm)
1.0
0.8
0.6
0.4
0.2
0.0
0
5
10
15
20
25
30
35
40

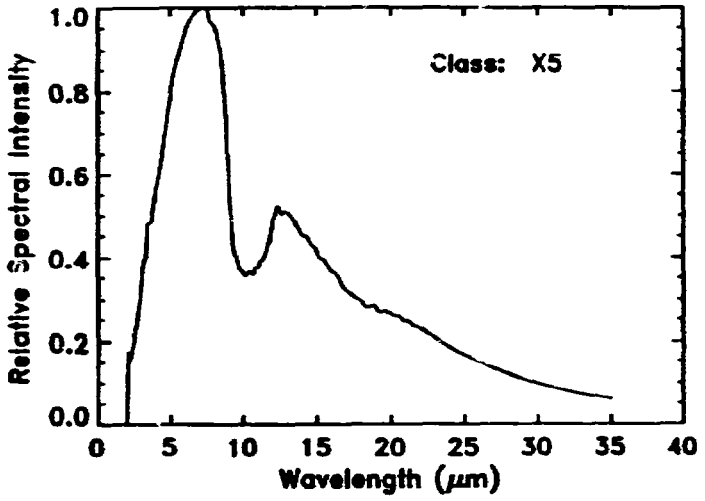
Class: X5
Relative Spectral Intensity
Wavelength (μm)
1.0
0.8
0.6
0.4
0.2
0.0
0
5
10
15
20
25
30
35
40

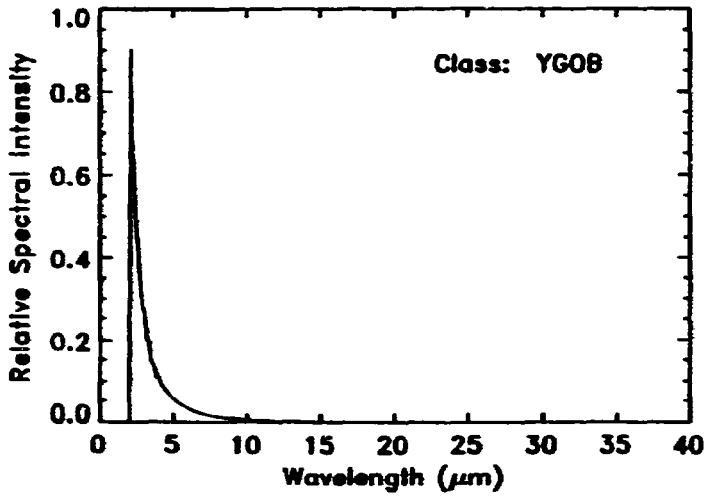
Class: YGOB
Relative Spectral Intensity
Wavelength (μm)
1.0
0.8
0.6
0.4
0.2
0.0
0
5
10
15
20
25
30
35
40

3.4 A STRATEGY FOR CBSD USAGE OF THE SKY SOFTWARE

CBSD requirements imply a magnitude limit of approximately 15 for 12μm point source emission (the IRAS Band 1 instrumental sensitivity limit was about magnitude 6). Because SKY internally computes the number of point sources per ¼-magnitude interval, it is convenient to consider SKY as a descriptor of the distribution of different brightness classes of sources, as well as different spectral classes

It was determined that CBSD requirements would be well met by sub-dividing the total magnitude range into magnitude bins, each of which has a width of one magnitude. Initially, 17 SKY bins were defined, which included point sources ranging from an upper limit of magnitude -1 down to a lower limit of magnitude 15. Each bin was centered at a half-magnitude, so, for example, the bin of dimmest stars contains stars ranging from magnitude 14 down to magnitude 15. (*At the brighter end, all point sources brighter than magnitude -1 were initially binned together. As will be discussed further on, the most recent version of the CBSD point source scene generator makes use of IRAS PSC data for sources with 12μm IRAS brightnesses greater than magnitude 0.*)

> **Phenomenologically, the net effect of this binning process is that the galactic point source background is to be described as being made up of 1479 different types of point sources: 87 spectral classes, each with 17 possible brightness sub-classes.**

Conceptually, it is possible to consider generating a galactic point source scene by first employing SKY to specify the point source densities for all 1479 point source types. For each LOS, one could then straightforwardly compute the integrated IR emission from all source types and brightnesses (at any wavelength by making use of the spectral characteristics of each of the 87 classes).

For a "typical" 512×512 pixel scene, 262,144 invocations of SKY would be required. However, even on a fast SUN SPARCstation, each SKY execution requires about 10 seconds of CPU time. Therefore,the total CPU time required for only the SKY calculations would be >700 hours !

There are a number of different means one can employ to reduce that execution time. Any such method would exploit the fact that the 1479 point source spatial distribution functions are smoothly varying, and, furthermore, vary rapidly only in the neighborhood of the galactic plane.

For any given region of space, one could eventually formulate a sub-sampling scheme, so that some relatively few invocations of SKY would generate sufficient point source density information to satisfy the point source scene generation requirements for that region of space. Similarly, it should be possible to develop **one** globally applicable sub-sampling scheme which could be called upon to drive scene generation for any region of space.

After much experimentation, and consideration of several alternatives, it was determined that CBSD requirements would best be met via an architecture which would employ a sparsely sampled point source distribution function data base generated from SKY calculations. In addition to pre-defining one globally applicable sparse sampling scheme, this has another major advantage. Once such a data base is generated from SKY calculations, an unlimited variety of CBSD point source scenes can be generated without any further SKY calculations.

To support development of a highly general form of that architecture, a point source density map (PSDM) approach was carefully designed. A principal PSDM objective was to condense the essence of each SKY point source distribution function down to a small and easily manageable digital data form.

An essential consideration was that each such digital map would reasonably replicate a corresponding SKY distribution function, so that simple and fast bi-linear interpolation could be employed to calculate point source densities at any point in the sky. An additional concern was that each such digital map also be as small as possible, so that computer I/O time associated with handing a large number of PSDMs, in the course of CBSD scene generation, would be acceptably low. Clearly, this indicated that a non-uniform sampling scheme would be required, so that the distribution functions would be sampled with satisfactory finesse in and near the galactic plane without being unnecessarily over-sampled in regions away from the plane.

The design process for this non-uniform sampling scheme was intensively experimental and iterative. Overall, >10,000 runs of the SKY code were analyzed and employed to test various tentative sparse sampling schema. The chief objective of the design process was:

> **find the sparsest sampling pattern which (for all classes) generally results in no more than 3× density differences between nearest neighbors (in galactic coordinate space) in the discretely sampled distribution functions.**

The rationale for the 3× criterion was the following: bi-linear interpolation between discretely sampled exponential-like and/or gaussian-like functions will result in average interpolation errors not exceeding 10% if the functions are generally sampled at least as frequently as their 3× points. Approximation errors on the order of 10% in the luminosity functions are felt to be acceptable for CBSD purposes.

Figure 3.4-1 illustrates the PSDM sampling grid currently in use within the CBSD program. The SKY point source distribution functions are discretely sampled at all the intersection points on this grid. There are 31 galactic latitudes and 29 galactic longitudes at which the distributions are sampled. From the Figure, it is easy to see that the sampling is significantly more dense along the galactic plane than it is far off the plane. In addition, the longitudinal sample spacing is more dense in the inner plane so that the center, its bulge, etc. will be adequately sampled. (*Note that the space is clearly over-sampled at high latitudes. However, to simplify the*

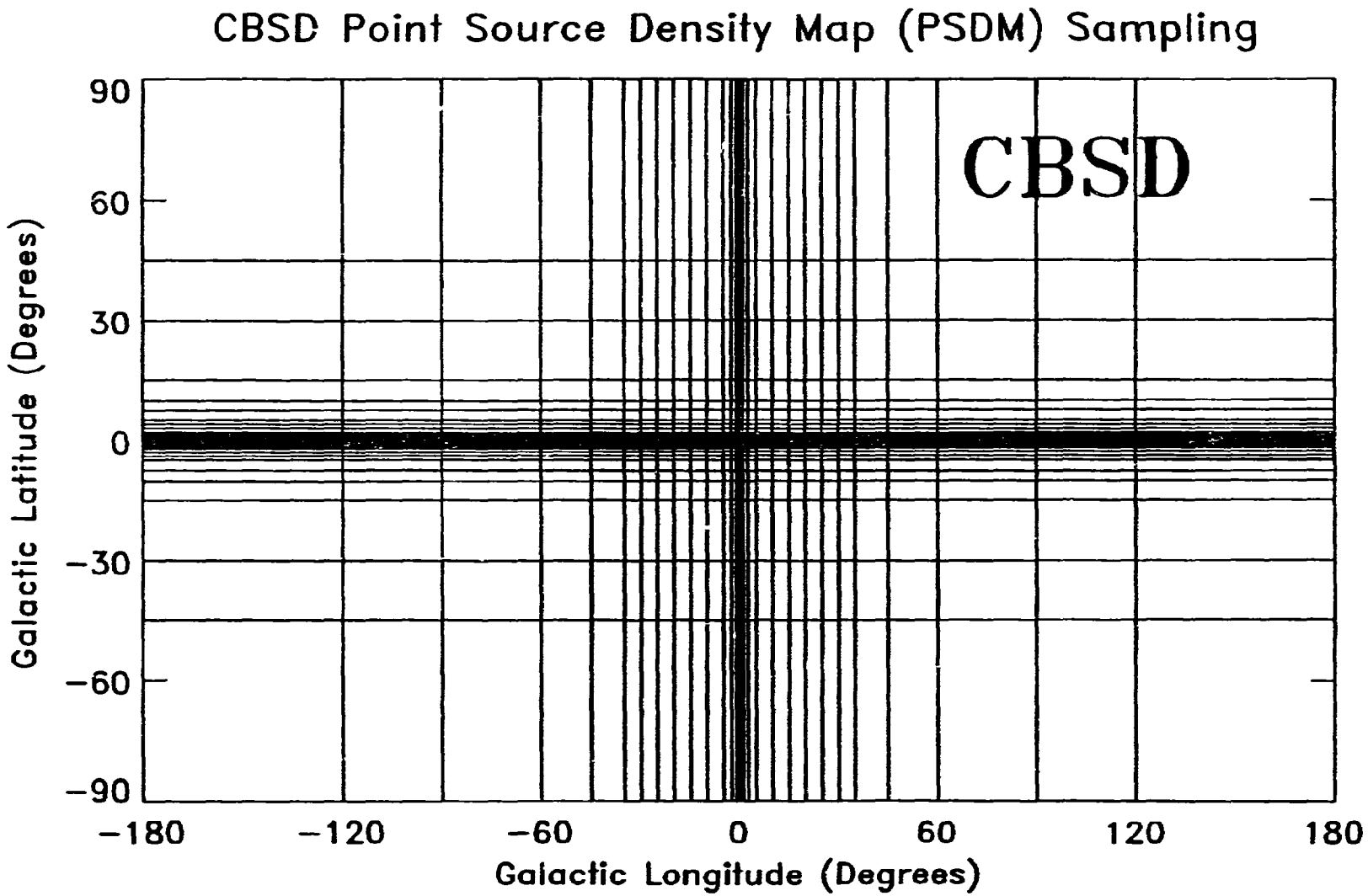
CBSD Point Source Density Map (PSDM) Sampling
CBSD
90
60
30
0
-30
-60
-90
Galactic Latitude (Degrees)
-180
-120
-60
0
60
120
180
Galactic Longitude (Degrees)

computations which will be driven by this sampling, it is convenient to have samples at the same set of longitude points for each latitude.) Because of the density of the in-plane sampling, it is impossible to resolve the lines on this plot very close to the plane. The actual coordinates of the grid nodes are:

Galactic Latitude:

$0°, \pm 0.2°, \pm 0.4°, \pm 0.7°, \pm 1°, \pm 1½°, \pm 2°, \pm 3°, \pm 4°, \pm 5°, \pm 7½°, \pm 10°, \pm 15°, \pm 30°, \pm 45°, \pm 90°$

Galactic Longitude:

$0°, \pm 1°, \pm 2½°, \pm 5°, \pm 10°, \pm 15°, \pm 20°, \pm 25°, \pm 30°, \pm 35°, \pm 45°, \pm 60°, \pm 90°, \pm 120°, \pm 180°$

For the galactic coordinates corresponding to each of the 899 nodes, a SKY run is made to compute the distribution function values for each of the 1479 point source types. Thus, 899 runs of SKY lead to development of 1479 PSDM's.

In the digital sense, each of the 1479 PSDM's is simply a data file containing an ordered listing of 899 point source density values. To minimize the total size of the 1479 data files, the density values are logarithmically compressed and stored as 2-byte integers in binary (unformatted) form. Each file is, therefore, $2 \times 899 = 1798$ bytes in size. The complete PSDM data base for one "master" wavelength is $1479 \times 1798 = 2.65$ MBytes, a size which is easily manageable and very portable.

The character of some individual PSDM's are demonstrated by Figures 3.4-2, 3.4-3, 3.4-4, 3.4-5, and 3.4-6. Each Figure illustrates, by surface plots, the inner plane sections of the 6th and 12th magnitude PSDMs for one spectral class. All of these are for a 12μm master wavelength. The spectral class for each is given in the plot title, as is the limiting magnitude of the magnitude bin. Note that the ordinates in these are auto-scaled, and these data represent point source density distributions which range from 0.1 to 100,000 point sources per deg^2.

These Figures provide a good "feel" for what a few of the distribution functions look like, how they vary, and how they are sampled, as well as demonstrating that in almost all cases the 3× sampling criterion is well satisfied.

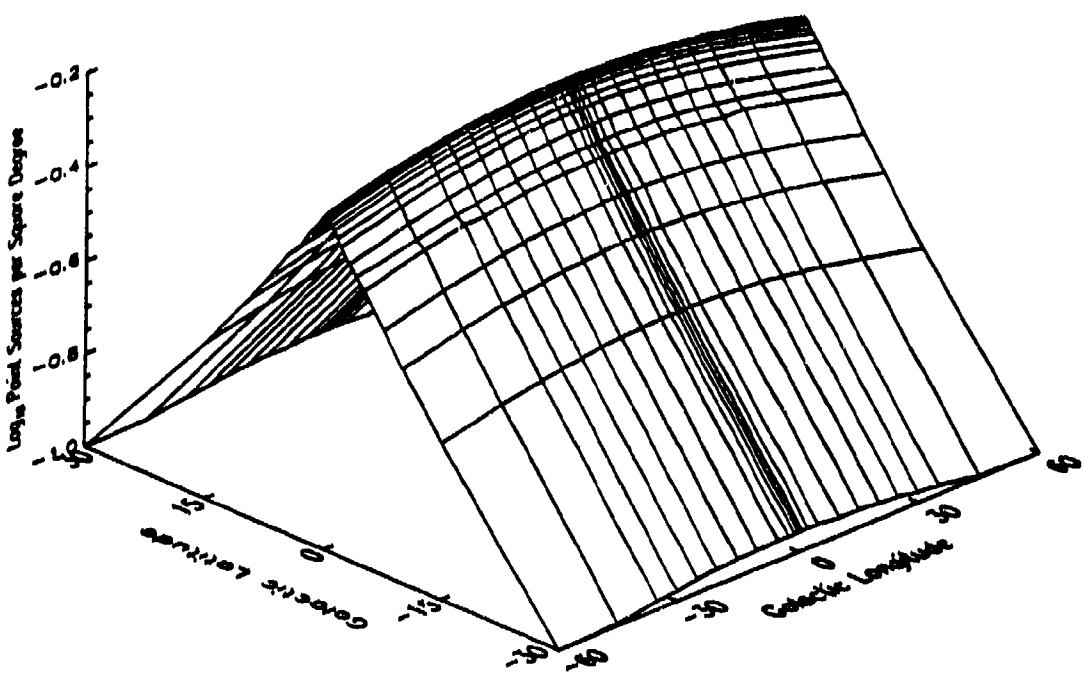

MO III 12μm Mag = 6

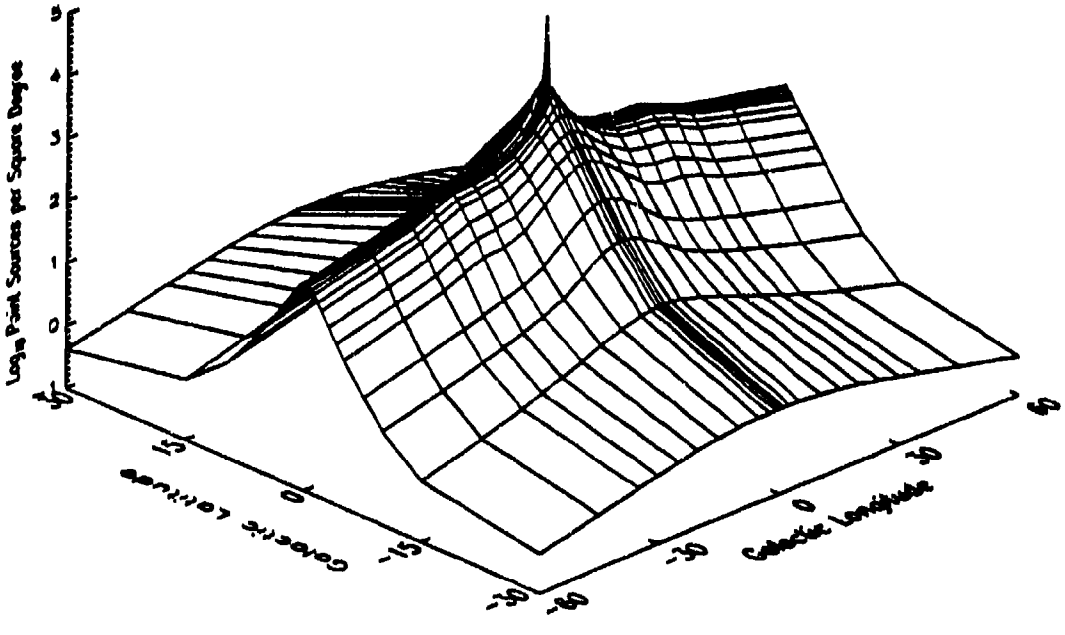

MO III 12μm Mag = 11

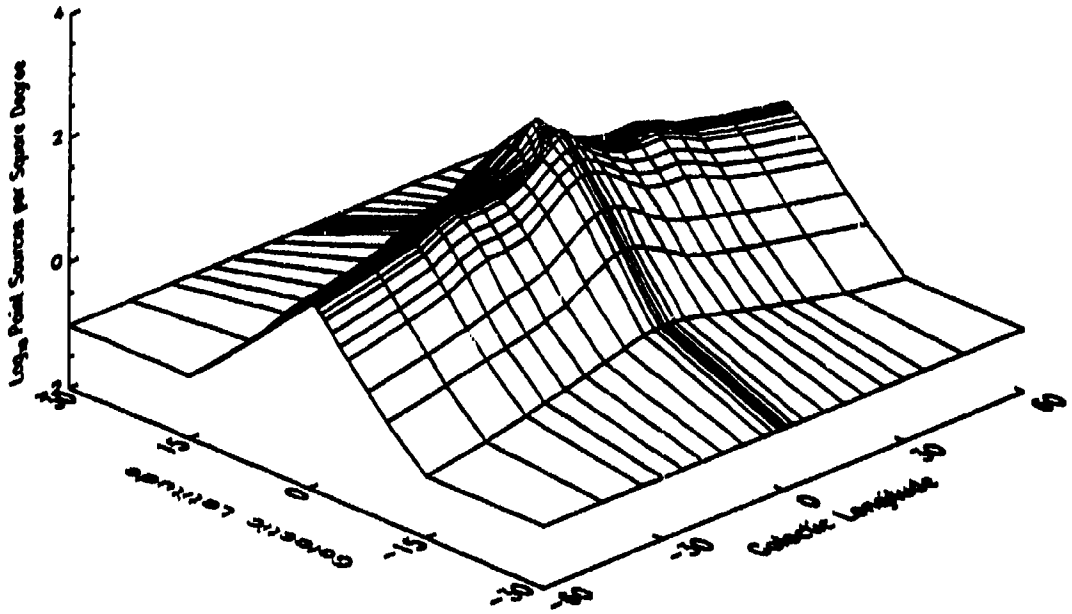

M6 III 12μm Mag = 6

28

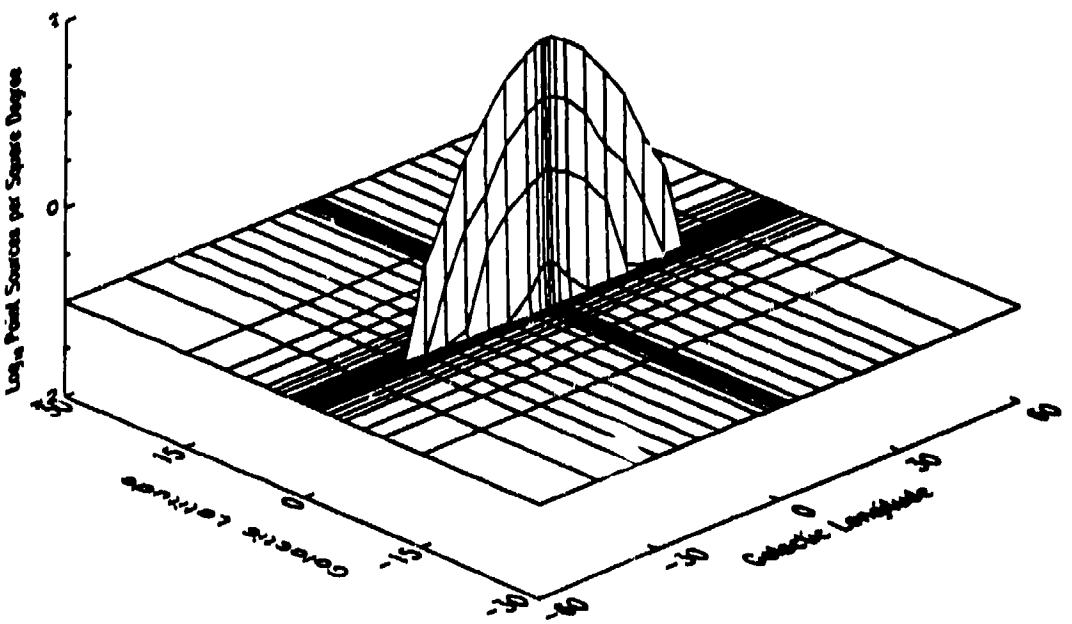

M6 III 12μm Mag = 11

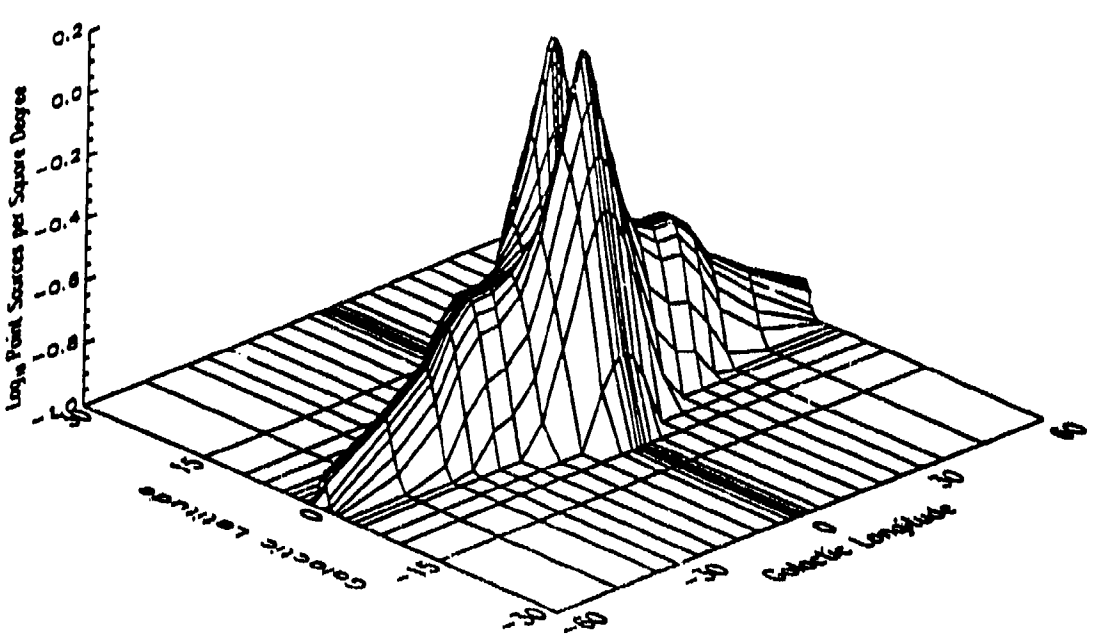

ACB M 05 12μm Mag = 6

36

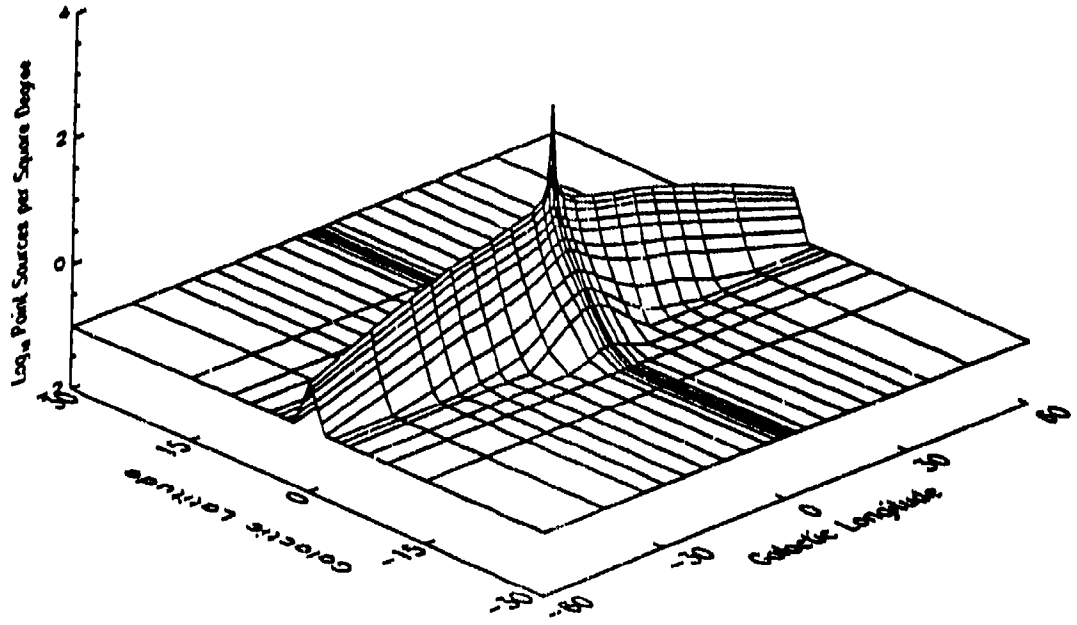

ACB M 05 12μm Mag = 11

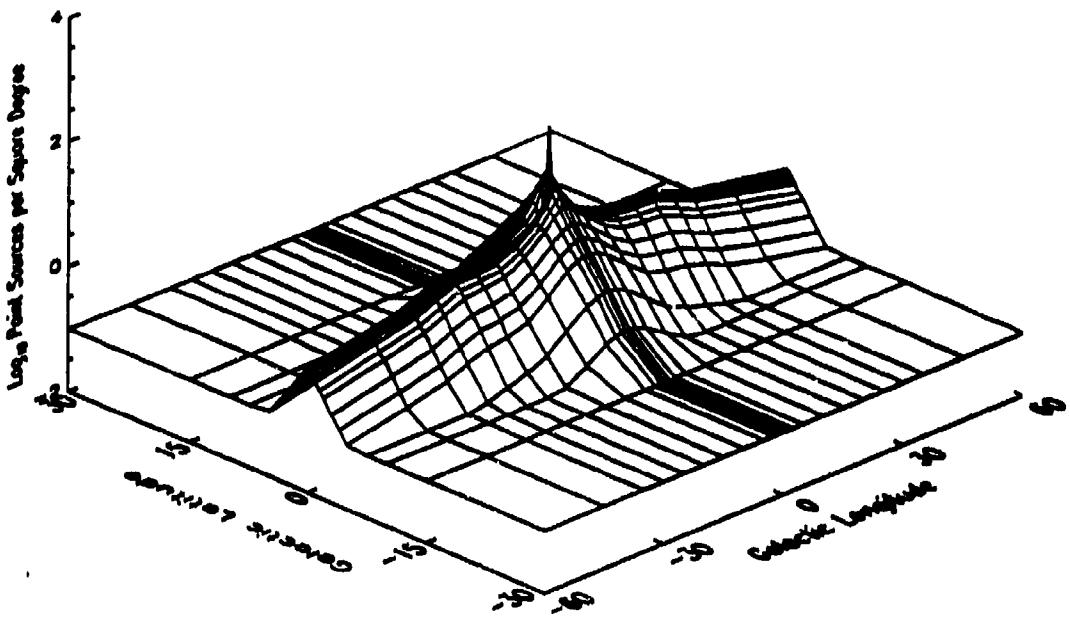

AGB M 07 12μm Mag = 6

37

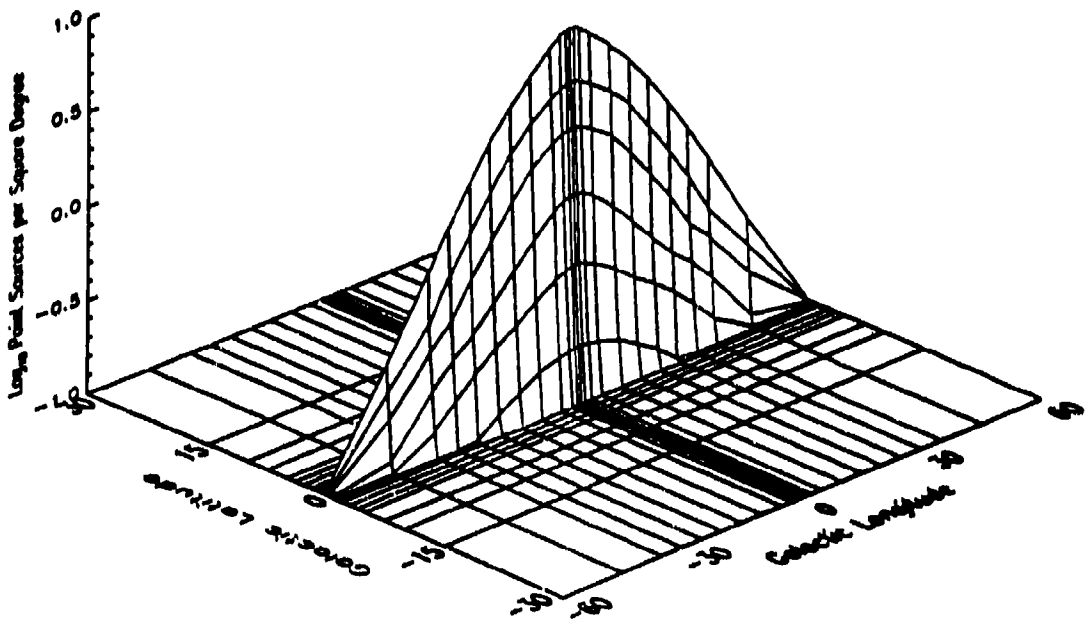

AGB M 07 12μm Mag = 11

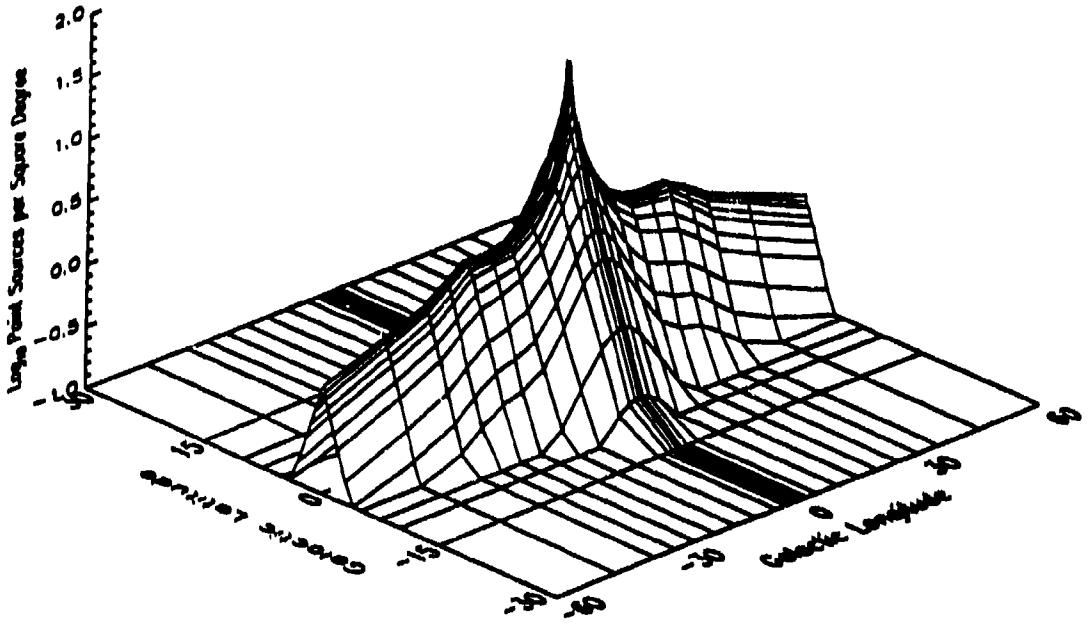

PN RED 12μm Mag = 6

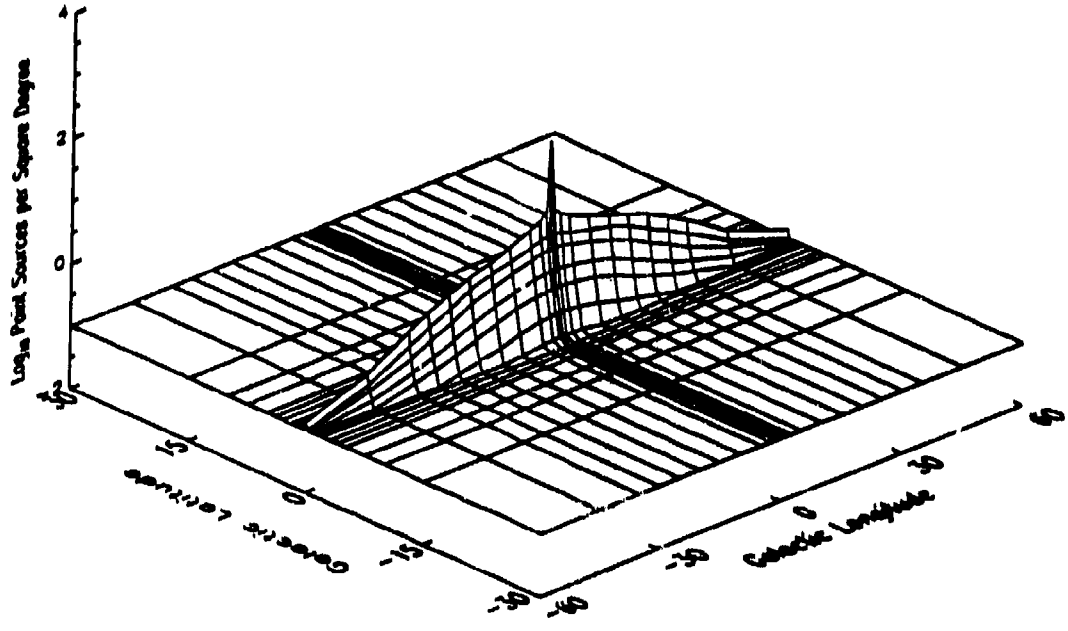

PN RED 12μm Mag = 11

3.5 POINT SOURCE SCENE GENERATION ALGORITHM & SOFTWARE

In this section, the overall architecture and the algorithms employed for actual point source scene generation are explained, and their software implementation is also described. Figure 3.5-1 provides a schematic overview of the architecture.

CBSD-modified versions of the GL-directed spectrally extended NASA/Ames SKY model, in conjunction with supplementary CBSD data base software, are employed to develop the PSDM data bases described above. Principal CBSD modifications to SKY are the:

(a) code translation into a more portable, ANSI-compliant Fortran-77; and

(b) code adaptations required so that SKY will produce magnitude-binned output rather than point source densities summed to limiting magnitudes;

(c) code conversion to double-precision to eliminate some inherent numerical "underflow" problems.

Note that the *CBSD Data Library* also includes the spectral library extracted from SKY, as well as a bright source library which will be described in the next section.

Note also that the PSDMs depicted in Figure 3.5-1 now cover only the magnitude range of 1 to 15, as opposed to the range of -1 to 15 discussed earlier as used in the initial implementation. Therefore, the PSDMs are now employed to statistically describe the distribution of $15 \times 87 = 1305$ classes of point source, and the *Bright Source* library is employed to describe point sources with 12μm brightnesses in excess of magnitude zero.

The PSDM data bases indicated by Figure 3.5-1 include PSDMs for three "master" wavelengths, 2.5, 12, and 25μm, as well as separate PSDMs for "System Bands." To fully understand the purpose for and usage of these, it is necessary to understand how the *CBSD Point Source Descriptor* module functions. However, even prior to that elaboration, some explanatory comments are appropriate.

Current CBSD thought on the requirement for usage of multiple "master" wavelengths derives primarily from the spectral character of non-AGB stellar sources. Turning back to the spectral library in Section 3.3, one can see that the spectral character of "B" class sources, for example, is well-defined only below about 10μm. Therefore, using such spectra to "spectrally transfer" magnitude-binned 12μm distribution function descriptions (i.e. PSDMs) down to 4.5μm, for example, would be prone to major errors. For at least the non-AGB stellar sources, therefore, it will be much more reliable to have a PSDM library at an SWIR wavelength, e.g. 2.5μm. On the other hand, for sources which have non-negligible 12μm spectral character, their spectra show satisfactory connectivity between their 12μm value and their values at all longer wavelengths. Therefore, it is probably not necessary to have the 25μm "master" wavelength PSDM indicated in Figure 3.5-1.

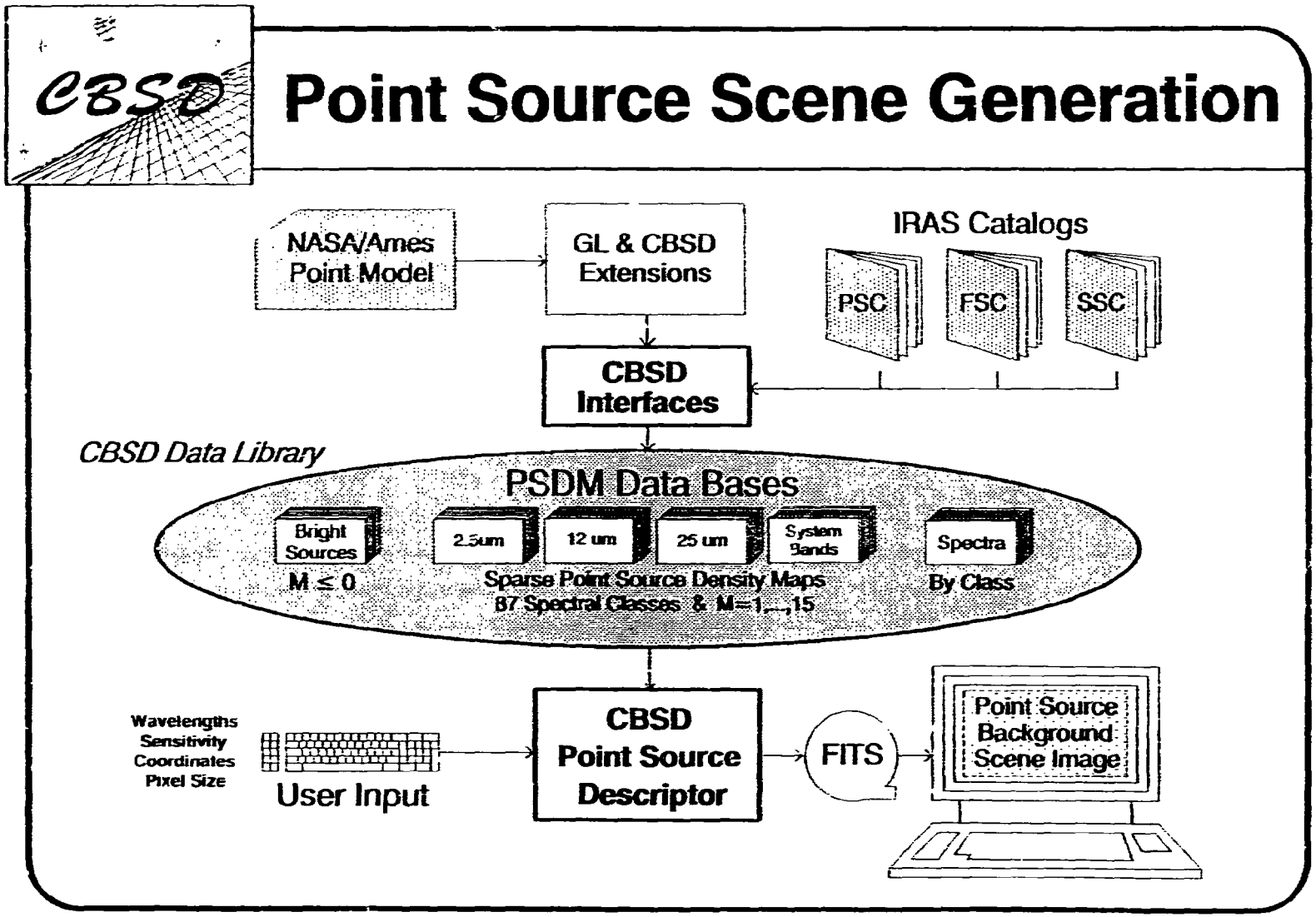
CBSD
Point Source Scene Generation
NASA/Ames Point Model
GL & CBSD Extensions
IRAS Catalogs
PSC
FSC
SSC
CBSD Interfaces
CBSD Data Library
PSDM Data Bases
Bright Sources
M ≤ 0
2.5um
12 um
25 um
System Bands
Spectra
By Class
Sparse Point Source Density Maps
87 Spectral Classes & M=1,...,15
Wavelengths
Sensitivity
Coordinates
Pixel Size
User Input
CBSD Point Source Descriptor
FITS
Point Source Background Scene Image

Actual CBSD point source background scene generation is executed by the *CBSD Point Source Descriptor* module shown near the bottom of Figure 3.5-1. Simply put, the purpose of this module is to generate images of a background scene according to a user-specified prescription. User inputs to this module are:

(a) Detection System Spectral Bandpass(es);

(b) Detection System Sensitivity Threshold;

(c) Spatial Definition of Region of Sky;

(d) System Angular IFOV (i.e. image pixel size).

Given these inputs, this module will generate one or more digital images which describes the user-specified section of the sky as a collection of discrete point sources. The generated image(s) will be in units of watt/cm^2, integrated over the user's spectral bandpass(es). The point source image(s) will be photometrically complete down to one magnitude below the user-specified sensitivity threshold(s). Each pixel in the image will be sized to the user-specified IFOV (i.e. instantaneous field of view).

Note that a critically important facet of this is that the module can generate several images of the same section of the sky, each image corresponding to a different spectral bandpass. Moreover, although statistical descriptions of the component point source classes are employed to generate the images, multi-spectral images are generated in such a manner that they are altogether spatially coherent. In other words, each of the images in a multi-spectral set will contain exactly the same discrete point sources as the other images in the set.

The sequence details of the CBSD Point Source Descriptor module's operation for generation of a single image are summarized as follows:

(a) An image array is defined. Its size in pixels is set by the user's specification of the scene size and IFOV; e.g. a $10° \times 10°$ field observed with a 1 arc-minute IFOV would require an image 600×600 pixels in size. The angular area of each pixel, A_{pix}, is determined by the user-specified IFOV; e.g. 1 arc-minute $\rightarrow A_{pix} = 2.8 \times 10^{-4}$ deg^2. Each pixel is implicitly tagged, within the program, with galactic coordinates.

(b) The *Bright Source* data base is read, and those sources which occur in the region of the sky specified by the user are placed appropriately into the image. The prescription currently used, as well as the prescription now under development, for calculating the spectral dependence of emission from the bright sources is defined in the next section.

(c) Each of the 1305 statistically-defined classes of point source is treated by the program, one at a time. Prior to full integration of the new SKY spectral library into the CBSD, the spectral characteristics of each spectral class are being described by embedded tables which define their absolute magnitudes at 2.4, 12, and 25μm; these tables are directly extracted from the SKY software. For each of the 1305 total classes, where here a class

specifies both a spectral type and a magnitude bin, the following procedure is followed:

The average in-band emission contribution from that magnitude-binned spectral class is computed and stored as a scale factor. The emission contribution is computed by:

interpolating amongst the three tables described above to find the absolute magnitude shift between the selected master wavelength and the center of the user-specified spectral bandpass;

employing the definition of the IRAS magnitude system to compute W_μ (watt/cm^2/μm) corresponding to a point source of that magnitude at the user-specified wavelengths;

convolving W_μ with the user-defined spectral bandpass to arrive at the in-band average (watt/cm^2) emission from a single point source in the class.

If the in-band emission from such a point source would be more than one magnitude beneath the system sensitivity threshold, that class is excluded from further consideration. Otherwise, the PSDM for that class is read into the program.

The 899-element PSDM is expanded from its logarithmically compressed form and scaled by the previously calculated A_{pix} so that it now defines *Point Sources per Pixel* on the previously-described PSDM grid points.

For each pixel in the image, the following procedure is then carried out for that point source class:

Simple bi-linear interpolation is employed, amongst the nearest neighbor PSDM grid points, to compute the point source density (i.e. per pixel) at each pixel location (*a small amount of stochastic character is introduced here into the bi-linear interpolation process to eliminate highly regular density contouring*);

If the point source density at a pixel, δ, is > 1, then an infrared emission contribution equivalent to NINT(δ) (i.e. nearest integer) point sources is added to that pixel;

if $\delta < 1$, then a random number, ϵ, is generated from a uniformly distributed sequence in the range $0 < \epsilon < 1$; if $\epsilon < \delta$, then emission corresponding to a single point source is added to that pixel.

(In either case of adding point source emission to a pixel, the actual numerical value of the emission to be added is randomized within the given magnitude bin, so that a completely continuous distribution of point source intensities is employed.)

It should be clear from this description that the point source scene generation is a rather exacting process. Although it employs statistical descriptions of the 1305 different point source types potentially used, it places point sources individually and with considerable care as to their individual intensities. Therefore, it should also be clear that the process described above is readily extensible to multi-spectral applications simply by "filling" multiple images simultaneously. Indeed, by carrying multiple image arrays and multiple W_μ through the above-described process in parallel, multi-spectral image generation is achieved without a large increment in total execution time for the process outlined.

For generation of three 512×512 images with different spectral prescriptions, the scene generation process described above requires about 45 minutes on a SUN SPARCstation1. At present, the software has not been highly compute-optimized.

It is believed that considerable economy can be achieved, particularly for the generation of large images, by re-organizing the process sequencing somewhat to minimize the virtual memory paging required on most machines.

The earliest mono-spectral version of this module required only about 3-5 minutes of time on the same SUN workstation. It operated by accumulating the point source density functions from all 87 spectral classes, for each magnitude bin, prior to bi-linear interpolation and distribution of discrete point sources. Effort is ongoing to achieve a similar mono-spectral adaptation of the present code so that at least a limited PC capability can be made available.

The current generation of source code for the Point Source Descriptor module is attached as an Appendix to this report.

3.6 THE BRIGHT SOURCE DATA BASE ADJUNCT

As indicated earlier, initial versions of the CBSD Point Source Background Scene Generator binned together all sources brighter than magnitude -1, and also included a bin for sources between magnitude -1 and zero magnitude.

For several reasons, this limited both the accuracy and realism of CBSD point source scenes. First, the PSC 12μm source brightnesses extend to an IRAS magnitude of -8. Therefore, using a single bin for all sources brighter than magnitude -1 undesirably limits accuracy in the photometric description of the brightest parts of a scene. However, using 7 additional bins, in order to be consistent with the rest of the PSDM treatment, would be an excessively cumbersome and inefficient means for dealing with a relatively small number of sources. Second, it was felt that adding non-statistical realism to the CBSD scenes, by preserving any asterisms made up by the bright stars, would improve the perceived quality of CBSD-generated scenes.

To address these concerns, it was decided to employ the SKY-based PSDM treatment only for sources with 12μm brightnesses less than magnitude 0 and to employ a PSC-based "mini-catalog" adjunct for sources brighter than magnitude 0.

Using 28.0 Jansky as the selection threshold, the 2503 brightest sources were extracted from the IRAS PSC. Almost all of these brightest point sources have FQUAL=3 (i.e. high-quality) PSC Band 1 fluxes. However, 64 of the brightest sources are Band 1 FQUAL=2 (moderate quality) and, somewhat surprisingly, 62 are Band 1 FQUAL=1 (lowest quality).

Figure 3.5-1 shows the distribution, in equatorial coordinates, of the selected 2503 point sources. As shown more directly by Figure 3.5-2, the heaviest concentration of the bright sources is along the galactic plane, but there is also a significant "sprinkling" of bright sources both above and below the plane. The equal area Aitoff projection in Figure 3.5-3 illustrates even more clearly the real nature of the bright point source distribution.

The most correct way to include these bright point sources in scene generation is to attach a spectral characterization to each source, so that the contribution from each source can be properly calculated for any spectral bandpass in the current CBSD 2-30μm region of operability. Indeed, individual IRAS LRS spectra exist for many of these bright sources. However, because the CBSD spectral range is broader than that of the LRS, each of the 2503 brightest IRAS PSC sources will be associated with one of the 87 SKY spectral classes. When that is done, the spectral library described in an earlier section of this chapter will be employed to give reasonable spectral character to each of the bright sources.

Until the new SKY spectral data base is fully assimilated into CBSD, an expedient approximation is being employed to spectrally describe the bright sources. The IRAS 12 and 25μm magnitudes are being used as primary descriptors of the

CBSD Point Source Scene Descriptor

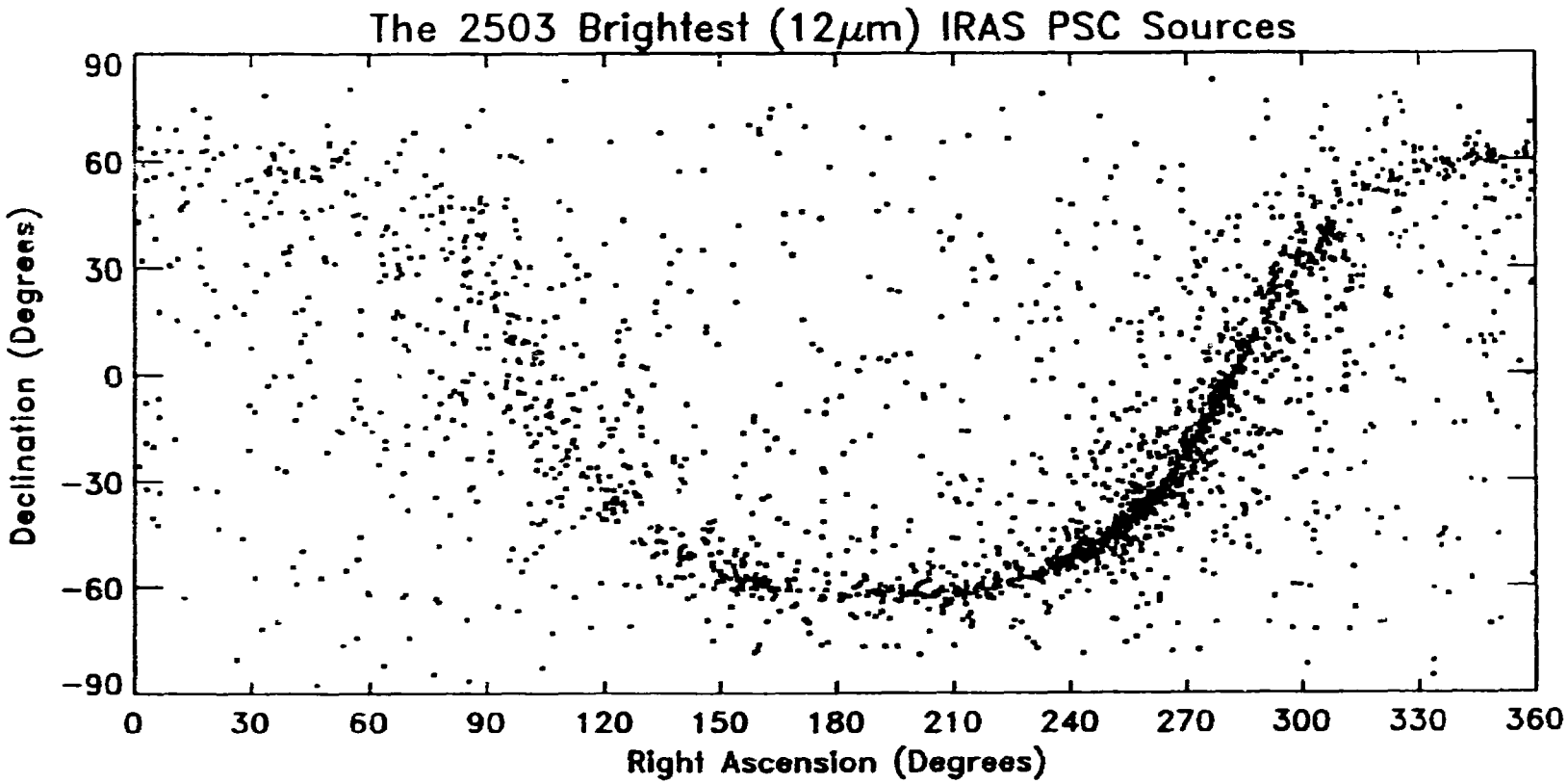

CBSD Point Source Scene Descriptor

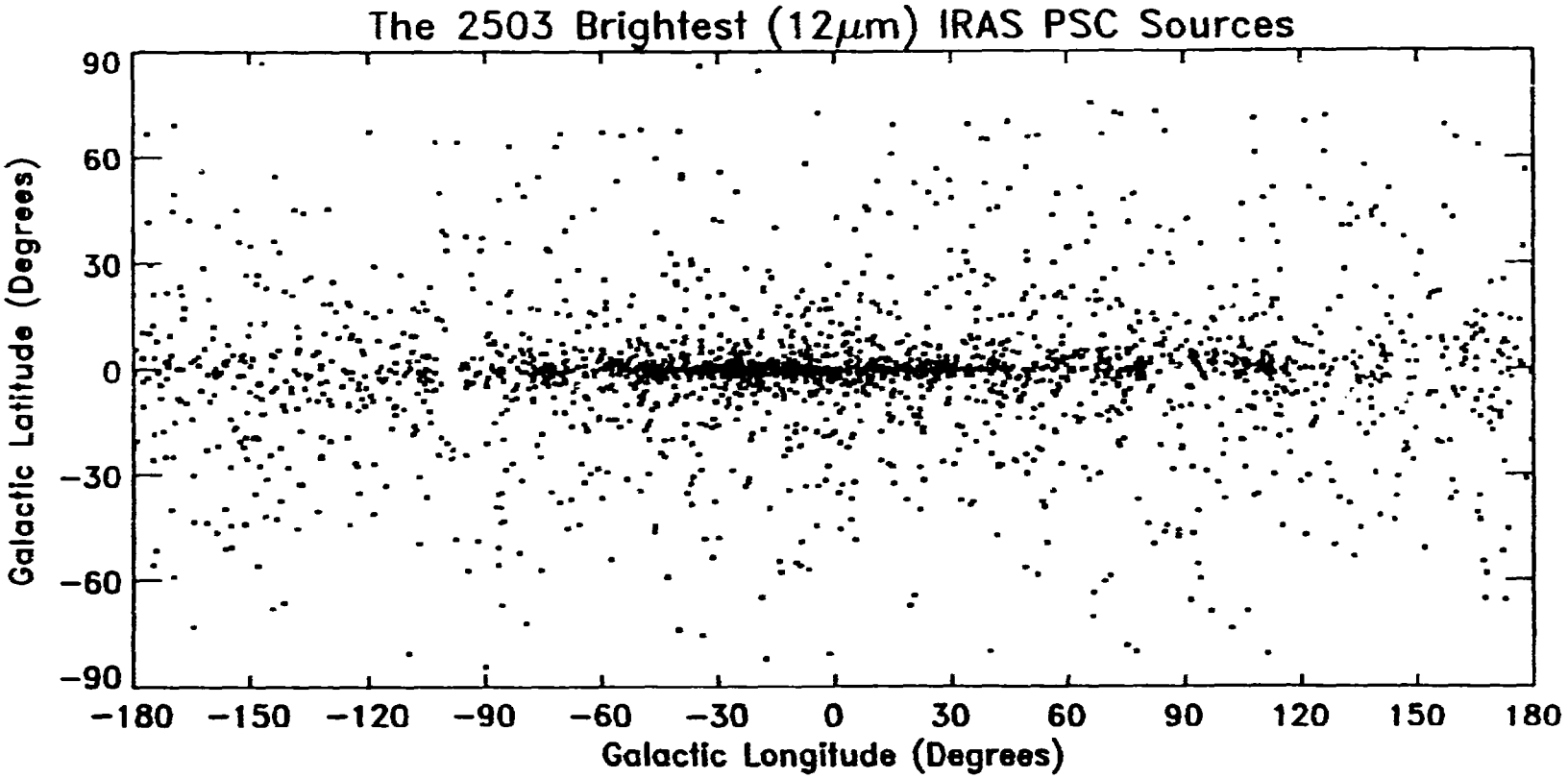

CBSD Point Source Scene Descriptor

The 2503 Brightest (12μm) IRAS PSC Sources

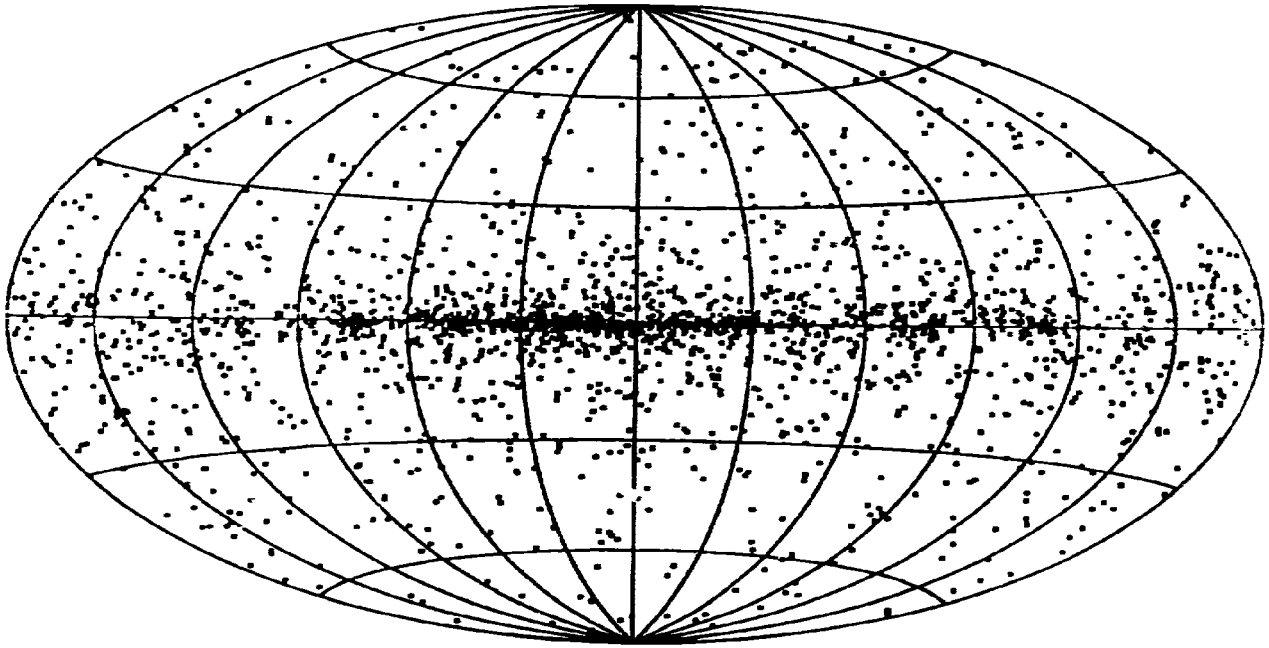

sources, and their spectral character at other wavelengths is being determined from interpolation and/or extrapolation of those two magnitudes.

This temporary approach is an error-prone approximation for determination of brightnesses below 12μm, because most of these sources have a 25μm excess due to the cooler radiation from circumstellar dust. Figure 3.5-4 shows a histogram of the 25μm excesses for these sources, clearly illustrating that fact. The average 25μm excess of these sources has been computed to be about 1.1 magnitude.

To address this weakness, MRC will supplement the IRAS 12 and 25μm magnitude data with shorter wavelength flux/magnitude data from the NASA Catalog of Infrared Observations, so that spectral character in the 2-12μm range can be interpolated rather than extrapolated. Within 4-6 months, this entire approach will be discarded and replaced with usage of the spectral library.

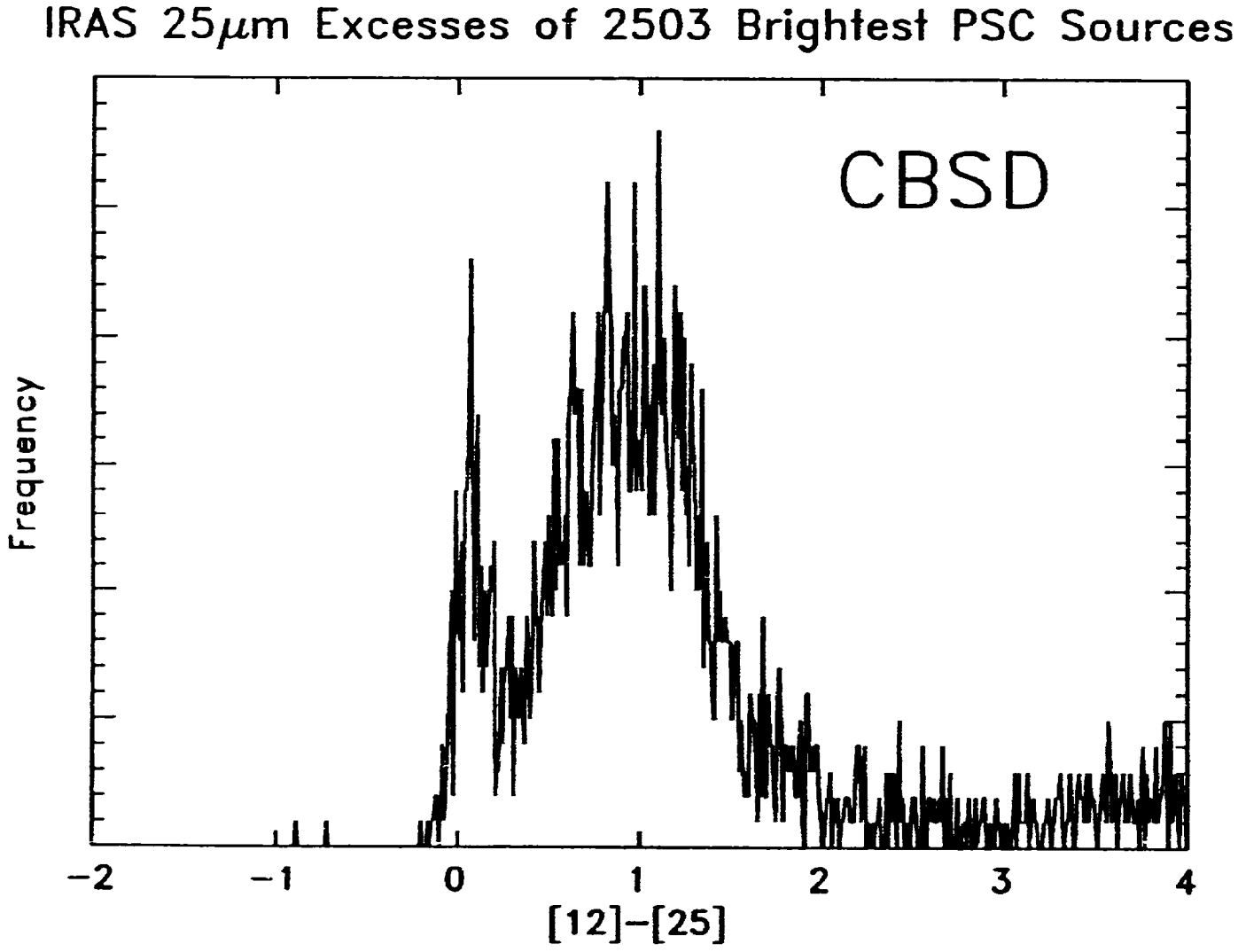
IRAS 25μm Excesses of 2503 Brightest PSC Sources
CBSD
Frequency
−2
−1
0
1
2
3
4
[12]−[25]

3.7 EXTENDED "POINT" SOURCES

As already noted, HII regions, planetary nebulae, and reflection nebulae constitute 5 of the 87 galactic "point" source classes described by the NASA/Ames SKY model. The other 82 classes are, in fact, various classes of stellar sources.

Of course, even with respect to IRAS spatial resolution, many HII regions and nebulae are spatially extended sources. CBSD scenes would clearly be more realistic if these sources were represented as spatially extended, even if the representation were as simple as a disk (or ellipsoid) with exponential, Gaussian, or Lorentzian fall-off in intensity away from the disk center. Therefore, we have begun some effort to identify a proper method for treating the HII regions and nebulae differently than stellar sources. Initially, we are attempting to use the IRAS *Small Scale Structure Catalog* (SSSC) as <u>one</u> guide to the detailed nature of the small extended sources.

First, we have extracted from the SSSC all entries which have non-zero Band 1 fluxes. There are 2001 of these, with IRAS Band 1 brightnesses ranging from magnitude 7 down to magnitude 4. Figure 3.7-1 illustrates the equatorial distribution of these sources and Figure 3.7-2 illustrates their distribution in galactic coordinates. Clearly, these sources are concentrated in the galactic plane, but there is a reasonable "sprinkling" of them off the plane as well.

Figure 3.7-3 illustrates the size distribution of these SSSC sources, as a function of brightness. From this Figure, one can also see that the vast majority of these sources are below an IRAS Band 1 magnitude of -1, and almost all are smaller than 10 arc-minutes in size. Some further processing/analysis of this SSSC data set can probably lead to a reasonable and simple size versus brightness relationship for use in CBSD scene generation. However, as may be apparent from this Figure, it is not obvious that these data can reliably be extrapolated to yield useful size-brightness relationships below magnitude 4.

To compare the phenomenological content of SKY (for HII regions and nebulae), to the SSSC, CBSD all-sky data was generated from only HII regions and nebulae and only down to a 12μm limiting magnitude of 4. This scene generation yielded 1603 spatially extended sources, comparing rather well with the 2001 sources listed in the SSSC. Figure 3.7-4 illustrates the distribution of these sources in galactic coordinate space. Comparing this Figure with Figure 3.7-2, it can easily be seen that the SKY/CBSD distribution is much more concentrated along the galactic plane than is the SSSC. In addition, the SKY/CBSD distribution is very heavily concentrated in the "inner plane," i.e. within $\ell = \pm 60°$.

Over the next few months, MRC will be conferring with the NASA/Ames SKY group and also with IPAC scientists, prior to making final decisions on the best method(s) for employing, within CBSD, the SKY and SSSC data on these classes of spatially extended sources.

CBSD Point Source Scene Descriptor

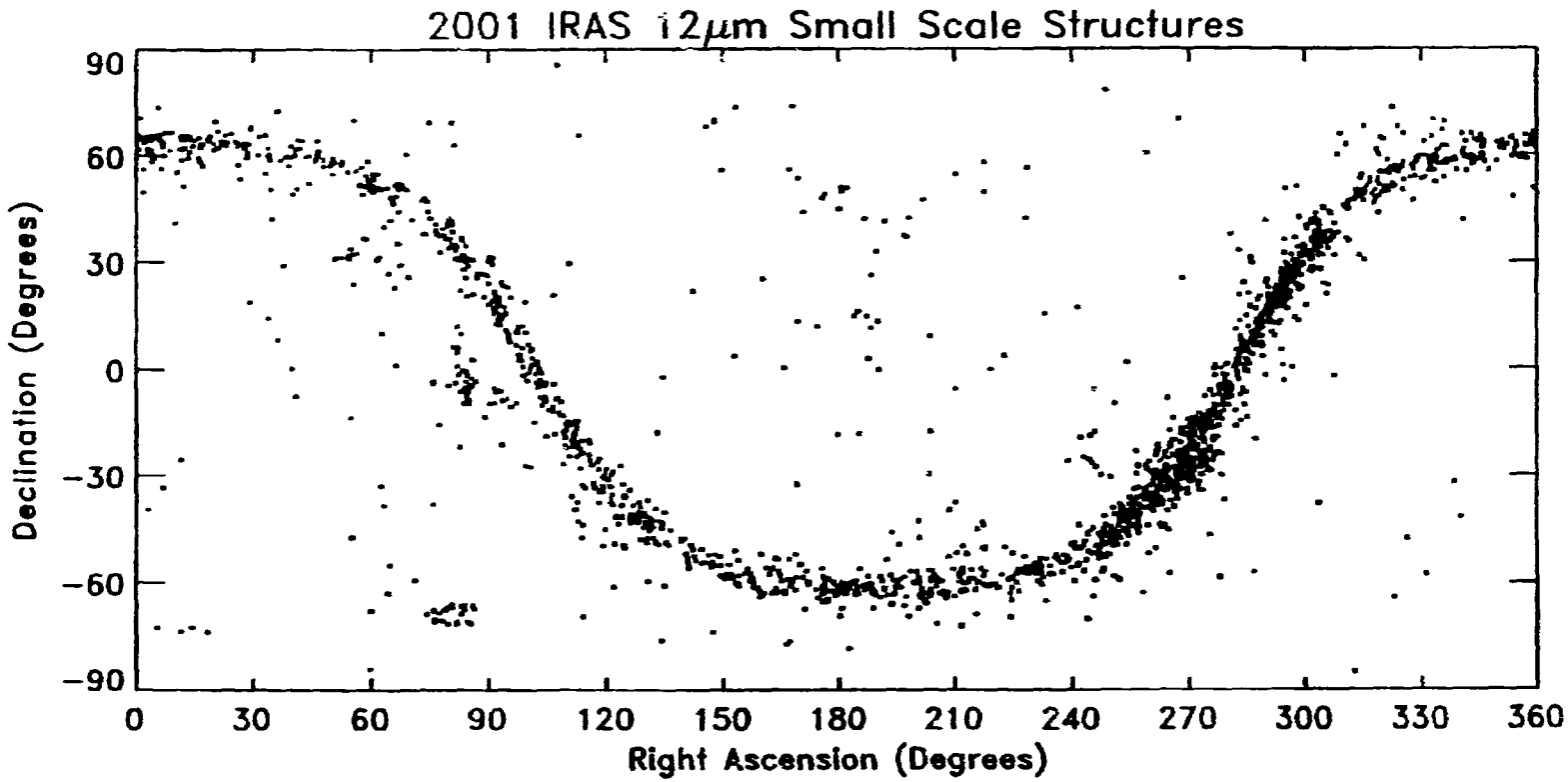

CBSD Point Source Scene Descriptor

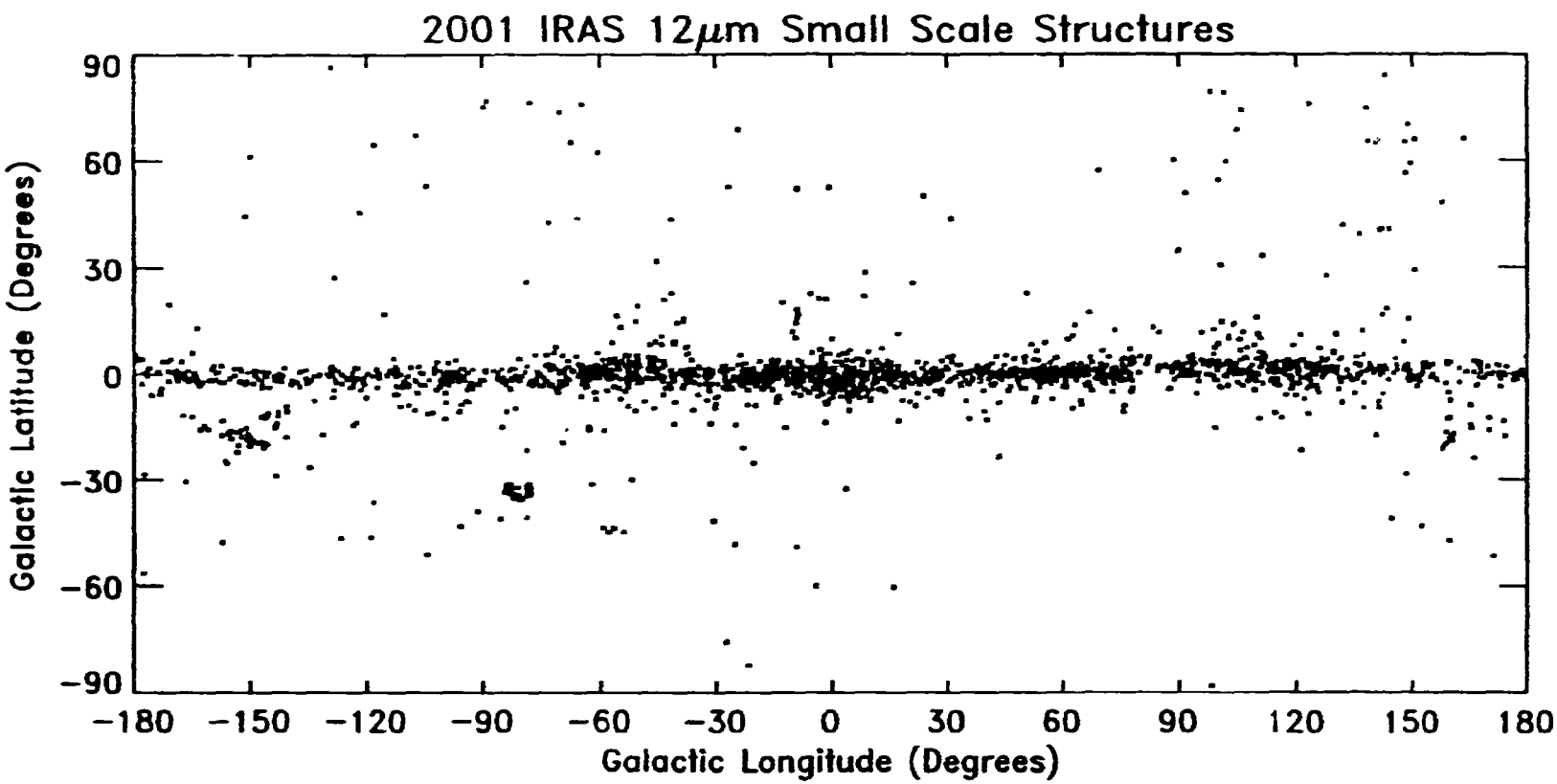

CBSD Point Source Scene Descriptor

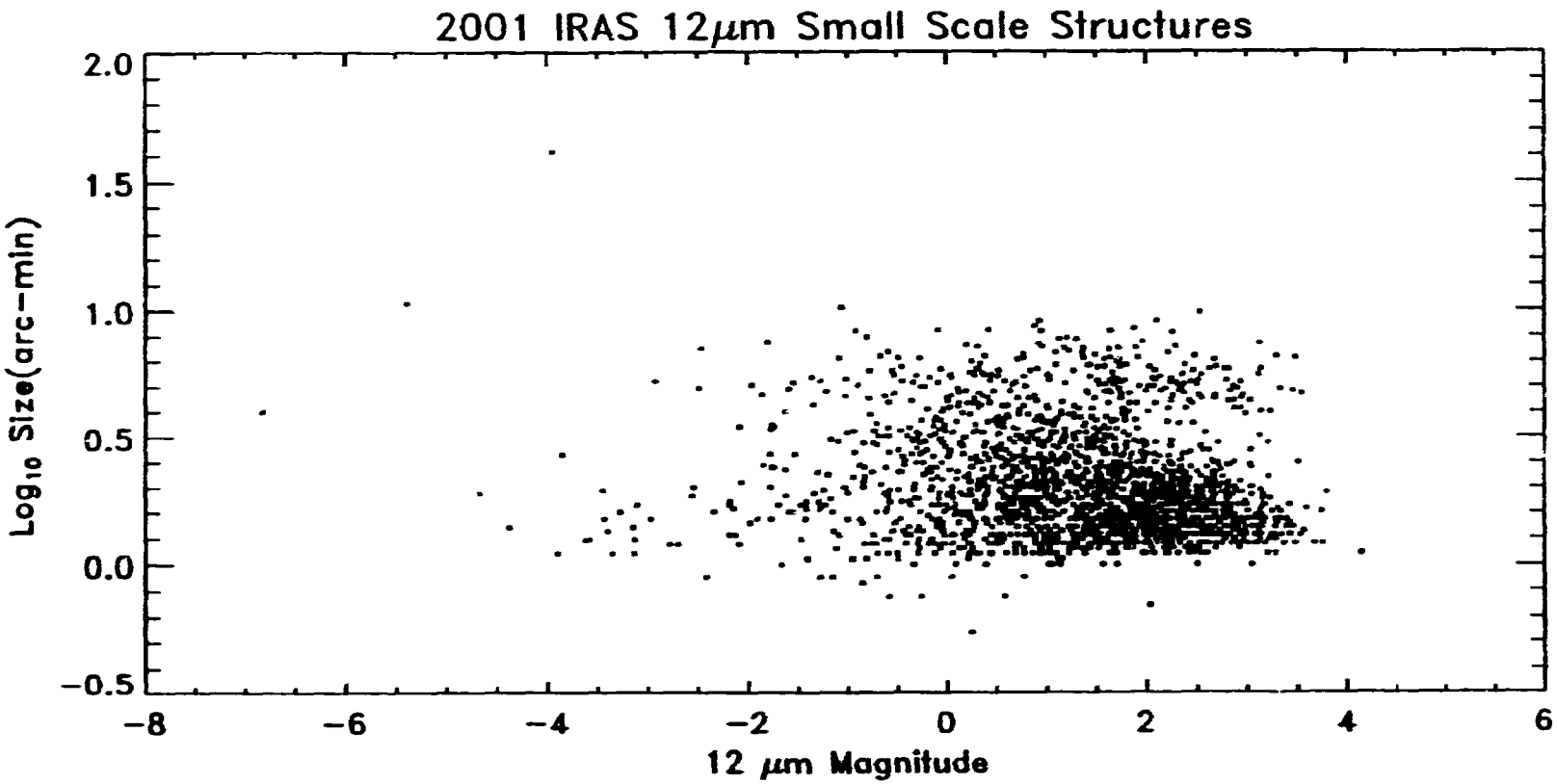

CBSD Point Source Scene Descriptor

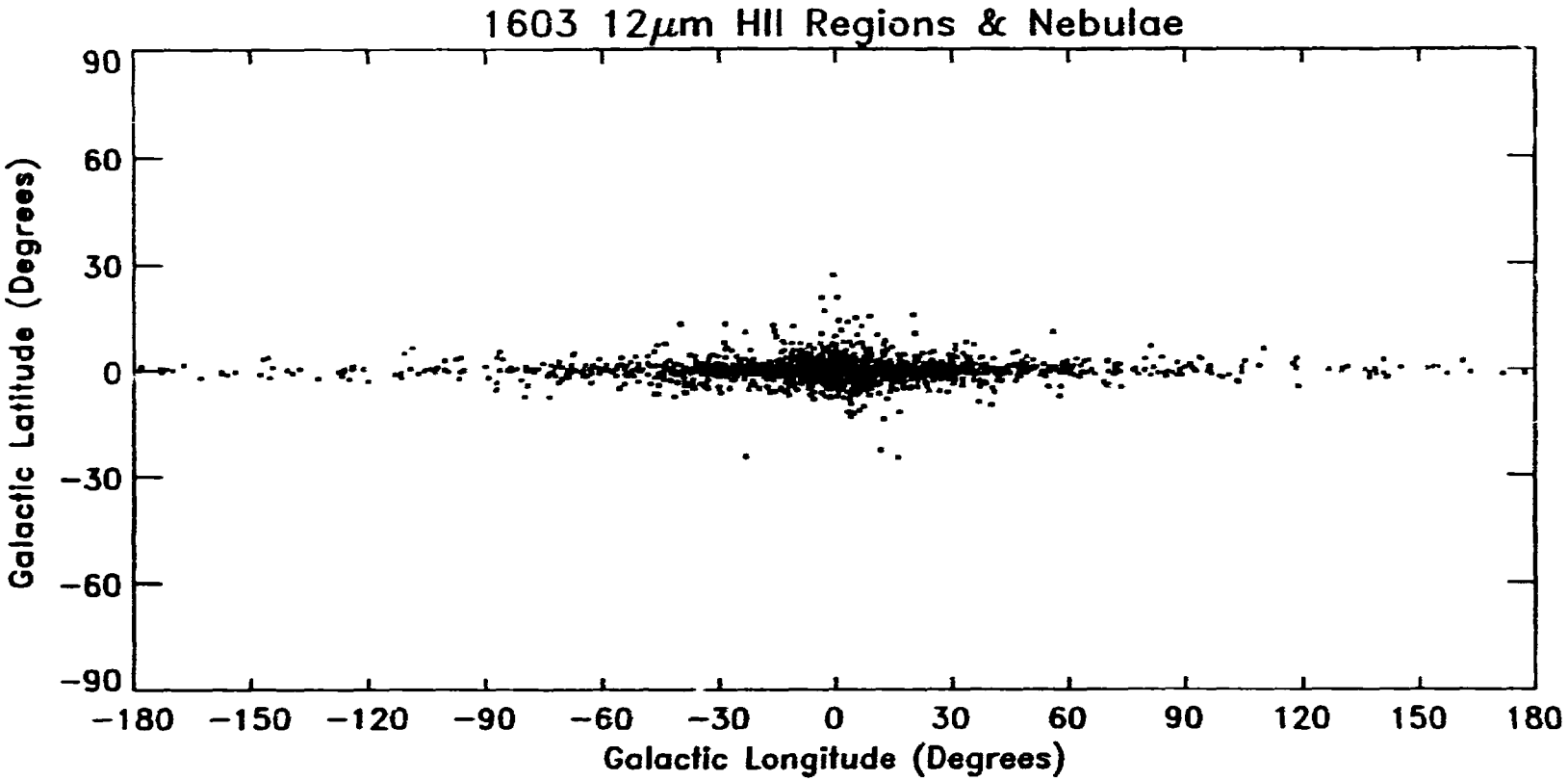

APPENDIX 3-1

User Guide for NASA/Ames SKY Version 3

POINT SOURCE MODEL OF THE MID-INFRARED SKY: VERSION 3

This program is designed to model the point source sky in the mid-infrared. It has been compared with the IRAS 12 and 25 μm observations, and, by using a library of complete 2.0–35.00μm low-resolution spectra, we have expanded the wavelength coverage of the model so that it can operate through any arbitrary filter lying entirely within this wavelength.

The model consists of two broad components:

1. GALACTIC

The Galactic section of the program is within the main body of the program. The Galaxy is assumed to be made up of 5 components:

- An exponential disk, comprising both young and old populations, exponential in both the R and z directions, and truncated at a distance R_{max}. The disk is axisymmetric. All types of star are assumed to have the same radial scale length; younger, more massive stars are assumed to have smaller scale heights than the older stars.
- Spiral arms—these represent the non-axisymmetric disk component—they are assumed to consist of young, massive stars. A four arm logarithmic spiral has been used to represent the arms.
- Molecular Ring—this is an axisymmetric disk-like component introduced to represent an over-density of IRAS sources coincident with the molecular ring. A Gaussian function, peaking at R_{ring} has been used to represent this component.
- Bulge—an axisymmetric, moderately flattened component, concentrated in the region within $\sim 0.25R_0$ of the Galactic center. This has been represented by $\rho = \rho_0 x^{-1.8} \exp(-x^3)$, where $x = \sqrt{r^2 + k^2 z^2}/R_B$, k is the axial ratio, and R_B is the "bulge radius". The bulge is assumed to consist only of old stars, but the bulge does contain high metallicity stars, meaning that high infrared luminosities can occur in AGB stars.
- Halo—an axisymmetric, slightly flattened diffuse component, considered to be made up of old metal poor stars. This is the component described by the de Vaucouleurs $r^{\frac{1}{4}}$ law. Because of the complex nature of the deprojection of this law, the density has been calculated by means of a lookup table `HALO.DAT`.

Extinction is included at all relevant wavelengths and the dust causing the extinction is assumed to have a distribution exponential in both R and z, with an extinction of 0.08 mag kpc^{-1} at K in the solar neighborhood. The following are some of the general parameters that have been used:

- $R_0 = 8.5$ kpc —the Galactocentric distance
- $R_{max} = 15.0$ kpc —the disk truncation distance
- $R_{ring} = 0.45R_0$ —the ring radius
- $R_B = 2.0$ kpc —the bulge "radius"
- $R_e = 2.8$ kpc —the halo effective radius
- $h = 3.5$ kpc —the disk scale length
- $\rho_{\rm halo} = 0.002\rho_{\rm disk}$ in the solar neighborhood
- $[12] = 4.034 - 2.5\log_{10}(S_{12})$ —definition of the 12 μm magnitude
- $[25] = 2.444 - 2.5\log_{10}(S_{25})$ —definition of the 25 μm magnitude
- $[60] = 0.490 - 2.5\log_{10}(S_{60})$ —definition of the 60 μm magnitude
- note that these magnitudes are color corrected as for a hot (10000 K) star, and S_λ is an IRAS PSC flux expressed as a flux density in Janskys by assuming that $\lambda F_\lambda = const.$

The Galactic section of the program works by assuming that the Galaxy consists of ntype different types of source. [In this version of the program, ntype = 87.] Each type of source is represented by an absolute magnitude, a dispersion in absolute magnitude, a local density, and a scale height. There are also corresponding numerical "masks", describing whether each type of source is present in a particular component.

The basic algorithm that has been used consists of looking along a ray, starting at the sun, and stepping along the ray until the "edge" of the Galaxy is reached. At each step, the volume (assuming an area of 1 square degree) is calculated, and the contribution from each component calculated and added to count buffers. To facilitate looking at extended areas, an option is included which instructs the program to look at a grid of areas specified by the user. An example of this will be given later. This is desirable for comparison with IRAS data since in general, an area of much larger than 1 square degree must be used. At each point along each ray, the total line-of-sight extinction is calculated and the apparent brightness of each source diminished by the appropriate amount.

2. EXTRAGALACTIC

The extragalactic point source sky has been modeled by assuming that the galaxies are homogeneously distributed. This part of the calculation is performed in the subroutine GALAXIES.FOR. The calculation starts by assuming a 60 μm luminosity function of the form given by Soifer *et al.* [*Ap. J.*, 320, 238]. This luminosity function has been split into four components (blue galaxies, red galaxies, seyferts and quasars) and corresponding [12]−[25] and [25]−[60] colors and standard deviations in color determined, along with a representative complete spectrum for each of these four classes of galaxy. The 12 and 25 μm luminosity functions (and if necessary the luminosity function through an arbitrary filter) are then simply calculated by transforming the 60 μm luminosity function.

The calculation is again performed by integrating along a ray. Since the galaxies are assumed to be homogeneously distributed, only one ray is ever necessary, and the result is scaled to the appropriate area passed from the main program. At each step along the ray, the contribution from each magnitude interval of the luminosity function is calculated, and added to the count buffers. The integration through space includes cosmological effects (but no evolution) and the following assumptions have been made: cosmological constant $\Lambda_0 = 0$; $\Omega_0 = 1$; Hubble constant $H_0 = 75$ km s^{-1}Mpc^{-1}. The result is not sensitive to choice of Ω_0 unless magnitudes very much fainter than IRAS are used. The integration starts at redshift $z = 5 \times 10^{-6}$ (i.e. $D = 20$ kpc) and stops at $z = 5.0$.

There is still controversy about luminosity evolution of galaxies. Further, the near-infrared colors of galaxies are not yet fully-determined; therefore, the model is designed not to permit calculation of the extragalactic contribution for broadband wavelengths shortward of 12 μm, nor for custom filters with effective wavelengths less than 5.0 μm.

NON-STANDARD FILTERS

Filters with non-standard bandpasses within the 2.0–35.0 μm wavelength scale are dealt with as follows. Firstly, the user must have a file with the transmission at each of the nwav wavelengths [note that nwav=331.] Such a file can be produced with the auxiliary program INTLRS.FOR, an example of the use of which will be given later. The main program, when asked to process a non-standard filter, calls the subroutine SPECIAL.FOR. This subroutine takes as input from the main program an array of absolute 12 μm magnitudes. There are ntype magnitudes in this array. The subroutine

then obtains the characteristic spectrum for each of the ntype sources from the auxiliary file LIBRARY.DAT for the Galactic sources, or GALAXY_LIBRARY.DAT for the extragalactic sources. The subroutine then calibrates each of the nwav spectra to F_λ units (W m^{-2} μm^{-1}), based on the input absolute magnitude. It then integrates the flux through the specified bandpass. For convenience, an effective wavelength for the filter is determined (assuming $\lambda F_\lambda = const$) and a corresponding magnitude scale defined. The subroutine returns an array of "magnitudes" through the special filter, along with the new transformation back to in-band flux. In the final output, the user always has the option of either in-band flux or magnitude. Throughout the integrations along the line-of-sight, magnitudes are always used.

Note that INTLRS.FOR resides in a different subdirectory from the main programs SKY.FOR and SPECIAL.FOR. Consequently, after running INTLRS.FOR to generate the customized response file, be sure to move this file to the upper level directory, [.model].

DETAILS OF THE DIRECTORIES AND FILES

The following files are supplied:

SKY.FOR	the main program
SKY.EXE	executable form of SKY
SPECIAL.FOR	the subroutine which deals with the non-standard filters
GALAXIES.FOR	the subroutine which performs the galaxy integration
BREAKDOWN.DAT	the breakdown of extragalactic sources into the 4 types
LINK.COM	a command file to compile and link the program
SETUP.COM	command file to setup logical names
INTLRS.FOR	program to define user's filter at the nwav wavelengths
INTLRS.EXE	executable form of INTLRS
LIBRARY.DAT	galactic source spectral library
GALAXY_LIBRARY.DAT	extragalactic source spectral library
LIBRARY.FOR	program which creates *LIBRARY.DAT
LIBRARY.EXE	executable form of LIBRARY
*.AVE	91 spectra used by LIBRARY.FOR
EXTINCT.DAT	representation of interstellar extinction from 2.0–35.0 μm
HALO.DAT	lookup table for the $r^{\frac{1}{4}}$ law
TABLE.FOR	program that creates HALO.DAT
TABLE.EXE	executable form of TABLE
POLINT.FOR	subroutine called by TABLE
QROMB.FOR	subroutine called by POLINT
MAKE.COM	a command file to compile and link the programs to create the halo lookup table
TRAPZD.FOR	subroutine called by POLINT
LUMA.FOR	standalone subsection of SKY.FOR for Galactic sources
LUMA.EXE	executable form of LUMA
GALZA.FOR	standalone form of GALAXIES.FOR for extragalactic so urces
GALZA.EXE	executable form of GALZA
EXPLAIN.TEX	this file (actually in LATEX)

The organization of directories (with sizes in VAX blocks) in account USER is as follows:

Directory [USER.MODEL]

```
EXPLAIN.TEX;1  53/54
GALAXY.DIR;1   1/3
LINK.COM;1     2/3
LRS.DIR;1      1/1
LUMA.EXE;1     165/165
LUMA.FOR;1     115/117
NORM.DIR;1     1/3
SETUP.COM;1    1/3
SKY.EXE;1      167/168
SKY.FOR;1      117/117
SPECIAL.FOR;1  19/21
```

Directory [USER.MODEL.GALAXY]

```
BREAKDOWN.DAT;1  17/18
GALAXIES.FOR;1   26/27
GALZA.EXE;1      132/132
GALZA.FOR;1      45/45
```

Directory [USER.MODEL.NORM]

```
HALO.DAT;1     4/6
MAKE.COM;1     1/6
POLINT.FOR;1   2/6
QROMB.FOR;1    1/6
TABLE.EXE;1    11/12
TABLE.FOR;1    3/6
TRAPZD.FOR;1   1/6
```

Directory [USER.MODEL.LRS]

EXTINCT.DAT;1	6/6
GALAXY_LIBRARY.DAT;1	11/12
INTLRS.EXE;1	12/12
INTLRS.FOR;1	15/15
LIB.DIR;1	7/9
LIBRARY.DAT;1	226/228

Total of 7 files, 291/300 blocks.

Directory [USER.MODEL.LRS.LIB]

A25V.AVE;1	6/6	AGBC01.AVE;1	6/6	AGBC03.AVE;1	6/6
AGBC05.AVE;1	6/6	AGBC07.AVE;1	6/6	AGBC09.AVE;1	6/6
AGBC11.AVE;1	6/6	AGBC13.AVE;1	6/6	AGBC15.AVE;1	6/6
AGBC17.AVE;1	6/6	AGBC19.AVE;1	6/6	AGBC21.AVE;1	6/6
AGBC23.AVE;1	6/6	AGBC25.AVE;1	6/6	AGBCI01.AVE;1	6/6
AGBCI03.AVE;1	6/6	AGBCI05.AVE;1	6/6	AGBCI07.AVE;1	6/6
AGBCI09.AVE;1	6/6	AGBCI11.AVE;1	6/6	AGBCI13.AVE;1	6/6
AGBCI15.AVE;1	6/6	AGBCI17.AVE;1	6/6	AGBCI19.AVE;1	6/6
AGBCI21.AVE;1	6/6	AGBCI23.AVE;1	6/6	AGBCI25.AVE;1	6/6
AGBCI27.AVE;1	6/6	AGBCI29.AVE;1	6/6	AGBCI31.AVE;1	6/6
AGBM01.AVE;1	6/6	AGBM03.AVE;1	6/6	AGBM05.AVE;1	6/6
AGBM07.AVE;1	6/6	AGBM09.AVE;1	6/6	AGBM11.AVE;1	6/6
AGBM13.AVE;1	6/6	AGBM15.AVE;1	6/6	AGBM17.AVE;1	6/6
AGBM19.AVE;1	6/6	AGBM21.AVE;1	6/6	AGBM23.AVE;1	6/6
AGBM25.AVE;1	6/6	AGI.AVE;1	6/6	B01V.AVE;1	6/6
B23V.AVE;1	6/6	B5V.AVE;1	6/6	B8A0V.AVE;1	6/6
F05V.AVE;1	6/6	F8G2G.AVE;1	6/6	F8V.AVE;1	6/6
G02V.AVE;1	6/6	G5G.AVE;1	6/6	G5V.AVE;1	6/6
G8G.AVE;1	6/6	G8K3V.AVE;1	6/6	HIIREG.AVE;1	6/6
K01G.AVE;1	6/6	K23G.AVE;1	6/6	K45G.AVE;1	6/6
K45V.AVE;1	6/6	KM2I.AVE;1	6/6	LIBRARY.EXE;1	9/9
LIBRARY.FOR;1	6/6	M01V.AVE;1	6/6	M0G.AVE;1	6/6
M1G.AVE;1	6/6	M23V.AVE;1	6/6	M2G.AVE;1	6/6
M34I.AVE;1	6/6	M3G.AVE;1	6/6	M45V.AVE;1	6/6
M4G.AVE;1	6/6	M5G.AVE;1	6/6	M6G.AVE;1	6/6
M7G.AVE;1	6/6	MLATEV.AVE;1	6/6	NORMAL1.AVE;1	6/6
NORMAL2.AVE;1	6/6	PNBLUE.AVE;1	6/6	PNRED.AVE;1	6/6
QUASAR.AVE;1	6/6	RNBLUE.AVE;1	6/6	RNRED.AVE;1	6/6
SEYFERT.AVE;1	6/6	TTAURI.AVE;1	6/6	X1A.AVE;1	6/6
X1E.AVE;1	6/6	X2.AVE;1	6/6	X3.AVE;1	6/6
X4.AVE;1	6/6	X5.AVE;1	6/6	YG0B.AVE;1	6/6

For a VAX running the VMS operating system, simply mimicking this directory and file structure will result in a clone of the new version of the Model at the user's VAX site. This same structure and organization is now established in the IRAF account on the AFGL VAX machine.

Note that the executable is linked with the MONGO87 plotting package. The executable provided will work in a limited manner (for example using device=3 for a Tektronix); if the site where the program is to be installed has MONGO87, it is recommended that the executable be relinked—otherwise, the last part of the subroutine MONGOPLOT within SKY.FOR could be modified to make use of the locally preferred plotting package. Change the calling directory in which your own MONGO87 resides in the routine LINK.COM.

RUNNING THE PROGRAM

The following are examples of the use of SKY.EXE.

```
$ set default disk:[user.model]
$ @setup
$ r sky
Integrate over area?  N          (case of a small area)
Enter galactic latitude:  30          (in degrees)
Enter galactic longitude:  30          (in degrees)
Enter passband - 1=B, 2=V, 3=J, 4=H, 5=K, 6=2.4um, 7=12um, 8=25um, 9=other:  7
Should the y-axis be cumulative?  - <cr>=y:  Y
Should the x-axis show magnitudes?  - <cr>=y:  Y
Enter device number (3 = Tektronix, 6 = Sun Window, 12 = Falco, -5 = LaserWriter (portrait),-6
= LaserWriter (landscape), 0 = quit):  0
output files SKY.LOG and SKY.OUT have been created
$ r sky
Integrate over area?  Y          (case of a large area)
Enter limits of galactic latitude:  60 90
Enter limits of galactic longitude:  0 180
Enter incremental steps in lat and long:  5 30          be sensible here!  Enter passband
- 1=B, 2=V, 3=J, 4=H, 5=K, 6=2.4um, 7=12um, 8=25um, 9=other:  7
Should the y-axis be cumulative?  - <cr>=y:
Should the x-axis show magnitudes?  - <cr>=y:
Enter device number (3 = Tektronix, 6 = Sun Window, 12 = Falco, -5 = LaserWriter (portrait),-6
= LaserWriter (landscape), 0 = quit):  -6
output files SKY.LOG and SKY.OUT have been created
Do you wish to plot observed points?  - <cr>=y:
to compare model to existing data in that area
Enter name of file containing the data:  FILE.EXT
plot is now made
More plotting?  - <cr>=y, a=change axes:  A
Should the y-axis be cumulative?  - <cr>=y:  N          use differential
Should the x-axis show magnitudes?  - <cr>=y:  N          want flux
Enter device number (3 = Tektronix, 6 = Sun Window, 12 = Falco, -5 = LaserWriter (portrait),-6
= LaserWriter (landscape), 0 = quit):  3
extra output file SKY.OUT (differential/flux) is created
Do you wish to plot observed points?  - <cr>=y:  N
plot is now made
More plotting?  - <cr>=y, a=change axes:  N
$ r sky
Integrate over area?  N          (use of a non-standard filter)
Enter galactic latitude:  30
Enter galactic longitude:  30
Enter passband - 1=B, 2=V, 3=J, 4=H, 5=K, 6=2.4um, 7=12um, 8=25um, 9=other:  9
Enter name of file containing system response.  The file must contain
331 values matching the spectral wavelengths:  [.LRS]FILTER.DAT
```

```
Should the y-axis be cumulative?  - <cr>=y:
Should the x-axis show magnitudes?  - <cr>=y:  N
Enter device number (3 = Tektronix, 6 = Sun Window, 12 = Falco, -5 = LaserWriter (portrait),-6
= LaserWriter (landscape), 0 = quit):  -6
output files SKY.LOG and SKY.OUT have been created
```

The output file SKY.LOG has a detailed listing of the contribution from each type of source at a range of magnitudes. The file SKY.OUT contains the magnitude/log flux in the first column and the log number (cumulative/differential) in the second, depending upon the response to the prompts when running the program. The lower portion of SKY.LOG includes the surface brightness output: a table of cumulative flux and equivalent cumulative magnitude vs. x-axis magnitude for the zone area calculated; and a second pair of columns detailing the same quantities but now per square degree.

The contents of the two columns of SKY.OUT are summarized in the table below:

	MAGNITUDE	FLUX
CUMULATIVE	mag / $\log_{10} N$	$\log_{10}$ *Flux* (Wm^{-2}) / $\log_{10} N$
DIFFERENTIAL	mag / $\log_{10} N$ (mag^{-1})	$\log_{10}$ *Flux* (Wm^{-2}) / $\log_{10} N$ (dex^{-1})

INTLRS.EXE is self documenting, and should not cause any problems when executed.

SKY.EXE takes approximately 6–8 CPU seconds per ray on a VAX 8600 computer. This CPU time varies with direction; longer times are required for directions close to the Galactic center. In addition, the extragalactic component, which is calculated once each time the program is run, takes approximately 22 CPU seconds.

LUMA.EXE is a subsection of SKY.EXE for calculating the Galactic components only. This will probably be useful for studying fields close to the Galactic plane, where the extragalactic contribution will be relatively insignificant.

GALZA.EXE is a standalone form of the subroutine GALAXIES.FOR which calculates the extragalactic component. This subroutine assumes that the Galactic absorption is zero. For any region away from the plane, this assumption is valid. However, more caution is required in the plane. For example, there is expected to be over 1 mag of extinction between us and the Galactic Center at 12 μm. The amount of extinction decreases rapidly with latitude. The extinction is the reason that GALZA and LUMA were merged to form SKY. Note that the usage of GALZA and LUMA is similar to SKY .

Note that SKY and LUMA require input in Galactic coordinates. These are defined (by the IAU) as:

$$\sin b = \sin\delta\cos 62.6^\circ - \cos\delta\sin(\alpha - 282.25^\circ)\sin 62.6^\circ, \quad (1)$$

$$\cos b\sin(l - 33^\circ) = \cos\delta\sin(\alpha - 282.25^\circ)\cos 62.6^\circ + \sin\delta\sin 62.6^\circ, \quad (2)$$

$$\cos b\cos(l - 33^\circ) = \cos\delta\cos(\alpha - 282.25^\circ), \quad (3)$$

where l is the galactic longitude, b is the galactic latitude, and α and δ are the right ascension and declination respectively, for equinox 1950.0.

HOW WELL DOES THE MODEL WORK?

A detailed discussion of the model's performance at 12 and 25 μm, across the entire sky, is included in the paper by Wainscoat et al. (1990, shortly to be submitted to The Astrophysical Journal). We can plausibly attribute the deficient predictions of the model to one or more of the following causes:

- Our representation of the spiral arms as both homogeneously populated and symmetrically distributed about the plane of the Galaxy is overly simplistic.
- Accurate color characterization of the metal-rich stars of the bulge is still problematic.
- The extragalactic sky is also not homogeneous, although the effects of clustering are at a much lower level than the former two causes.

APPENDIX 3-2

CBSD Point Source Scene Generation Software
FORTRAN Code Listing

```
********************************** CBPSIMG5 ***********************************
*                                                                             *
*                    Code Author: John P. Kennealy, MRC/Nashua                *
*                                                                             *
*   (Interim) Version 3.5 of CBSD Point Source Scene Descriptor Image Module   *
*                                                                             *
* CBPSIMG# will generate images (watt/cm^2) for up to three user-specified    *
* wavelength bandpasses. CBPSIMG# is an expedient version to make spatially    *
* coherent multi-spectral capability available as soon as possible (i.e.      *
* without the final NASA/Ames extended spectral data base).  CBPSIMG# uses    *
* a linear interpolation between absolute magnitudes of the three master      *
* wavelengths (2.4, 12, and 25 um) to compute watt/cm^2/um at the center      *
* of the user-specified band and multiplies this by the spectral bandwidth    *
* to produce the final images in watt/cm^2.                                   *
*                                                                             *
* Beginning with v3.50, CBPSIMG uses a data base extracted from the IRAS PSC  *
* to describe point sources with magnitudes > or = 0.  This data base (PSCO)  *
* includes the descriptions of 2503 bright IRAS Band 1 & Band 2 sources.      *
*                                                                             *
* This multi-spectral implementation is a transitional adaptation of the     *
* most recent CBSD monochromatic version. Consequently, the architecture     *
* is far from optimal with respect to either speed or address space for the   *
* spatially coherent multi-spectral applications.                             *
*                                                                             *
*  CBPSIMG# requires the CBSD PSDM (Point Source Density Map) data bases, as  *
*  well as data files "clist2" and "PSDMmaxes," and (beginning with v3.50)    *
*  the PSC bright point data base file "pscbrt_g.mag"                         *
*                                                                             *
* !!!!!!!!!!!!!!!!!!!!!!!!!!!!!!!!!!!!!!!!!!!!!!!!!!!!!!!!!!!!!!!!!!!!!!!! *
* !!!!   NOTE THAT THE FULL PATH NAME OF THE DIRECTORY CONTAINING THE   !!!! *
* !!!!   PSDM DATA BASE MUST BE IN THE STATEMENT DEFINING "FullPath"    !!!! *
* !!!!!!!!!!!!!!!!!!!!!!!!!!!!!!!!!!!!!!!!!!!!!!!!!!!!!!!!!!!!!!!!!!!!!!!! *
*                                                                             *
********************************** CBPSIMG4 ***********************************
*                                                                             *
*  Version 3.48 Adds Small Amount of Stochastic Character to the Use of the   *
*    Point Source Density Functions to Help in Reducing Image "Contouring"    *
*                                                                             *
********************************** CBPSIMG4 ***********************************
*                                                                             *
*  Version 3.49 Modifies Definition of PSDmin, Accounting for Small Pixels    *
*    Corrected Ordering of Lon,Lat in DNTO4 Calculation, 9/20/90, (via JimG)  *
*                                                                             *
********************************** CBPSIMG5 ***********************************
*                                                                             *
*  Version 3.50 Introduces Usage of IRAS/PSC Sources for > 12um Magnitude 0   *
*                                                                             *
********************************** CBPSIMG5 ***********************************
*                                                                             *
*  Version 3.51 Offers User an Option of Defining Region in R.A. and Dec, but *
*  the Ouput Images Are Still Generated as Galactic Coordinate Projections    *
*                                                                             *
********************************** CBPSIMG5 ***********************************
*                                                                             *
*  Version 3.52 Supports Generation of Up to 10 Different Output Image Sets   *
*     Generates a "Log" File, IM352.#.B.L, for each Scene Generation          *
*     Permits Single Column, Single Row, or Single Point Runs                 *
*                                                                             *
********************************** CBPSIMG5 ***********************************

      program CBPSIMG5

*     This is CBSD Point Source Scene Descriptor Version
      parameter (Versn=3.52)
*     Maximum Linear Image Size is
      parameter (MaxSize=1024)
*     Maximum Number of User Wavelength Bands Simultaneously Treated is
      parameter (MaxB=3)
*     The Reference Temperature for the IRAS Magnitude System is
      parameter (Tref=10000.)
*     The Number of IRAS PSC Entries in the Bright Source Data Base is
      parameter (NBrite=2503)
```

```
      integer*2     MMag(30),IDNTB(29,31)
      integer*2     PSDMmax(87,-1:15),MagLim(MaxB)
      integer*4     NLat,Nlon,Ntp

      real*4        TbLat(31),TbLon(29)
      real*4        M2p4(87),M12p(87),M25p(87)
      real*4        W1(MaxB),W2(MaxB),WC(MaxB),DW(MaxB)
      real*4        Thr(MaxB),FOMag(MaxB),fm1(MaxB),fm2(MaxB),fmb(MaxB)
      real*4        PSFlx(MaxB,87)
      real*4        DNTB(87,29,31),DNTO(29,31)

      character*10  DumName,OutName(MaxB+1)
      character*15  MapName,TmpName
      character*33  FullPath

      logical       TooSmall(87),Finished,UseBrite,Already

*  The FlxU arrays are the (w/cm^2) images at user-specified wavelengths

      real*4        FlxU(MaxB,MaxSize,MaxSize)

*************************************************************************
* For the 87 Different Point Source Spectral Classes Included:

*  Absolute 2.4um Magnitudes are, from NASA/Ames SKYv2
      DATA M2p4/
     +   -2.92, -1.32, -0.52,  0.34,  1.33,
     +    1.87,  2.73,  3.15,  3.52,  4.18,
     +    4.54,  5.04,  5.51,  6.49,  7.49,
     +    0.41, -0.05, -0.52, -0.72, -1.55,
     +   -2.97, -3.97, -4.22, -4.57, -5.02,
     +   -5.82, -5.86, -7.66, -8.65, -4.69,
     +   -6.99, -9.30,-10.73,
     +   -4.38, -4.85, -5.39, -6.86, -7.82,
     +   -8.63, -9.30, -9.21, -8.65, -7.93,
     +   -7.68, -7.28, -6.80,
     +   -7.41, -7.41, -7.45, -7.64, -8.01,
     +   -8.19, -8.32, -8.43, -8.62, -8.67,
     +   -8.76, -8.68, -8.83,
     +   -5.81, -6.22, -6.09, -7.25, -8.65,
     +   -8.81, -9.21,-10.01, -8.16, -6.00,
     +   -6.34, -6.68, -7.02, -7.36, -7.70, -8.04,
     +   -9.71, -2.80, -7.15, -3.71,-11.30,-12.38,
     +   -4.37, -1.72, -0.10, -0.10, -1.47,  1.74/

*  Absolute 12.um Magnitudes are, from NASA/Ames SKYv2
      DATA M12p/
     +   -2.80, -1.27, -0.50,  0.27,  1.31,
     +    1.99,  2.73,  3.23,  3.58,  4.15,
     +    4.97,  5.04,  5.82,  6.70,  7.25,
     +    0.92,  0.00, -0.59, -0.78, -1.53,
     +   -3.20, -4.30, -4.67, -5.08, -5.56,
     +   -6.28, -6.93, -8.56,-10.23, -4.64,
     +   -7.29,-10.37,-11.50,
     +   -4.64, -5.51, -6.60, -8.36, -9.69,
     +  -10.90,-12.32,-13.32,-13.81,-14.03,
     +  -14.18,-14.28,-14.30,
     +   -8.55, -8.57, -8.79, -8.67, -9.04,
     +   -9.19, -9.32, -9.43, -9.62, -9.77,
     +   -9.86, -9.78, -9.93,
     +   -8.92, -9.12, -9.69,-10.09,-11.49,
     +  -11.81,-12.21,-13.01,-11.16, -9.00,
     +   -9.34, -9.68,-10.02,-10.36,-10.70,-11.04,
     +  -14.31,-14.40,-15.35,-16.31,-16.80,-16.98,
     +  -11.00, -8.35, -4.05, -4.54, -8.50, -1.86/
```

```
*  Absolute 25.um Magnitudes are, from NASA/Ames SKYv2
      DATA M25p/
     +   -3.30,  [illegible].77,  [illegible].00,  0.27,  1.31,
     +    [illegible],  [illegible],  [illegible],  [illegible],  [illegible].10,
     +    [illegible],  [illegible],  [illegible],  [illegible],  [illegible].05,
     +    [illegible],  [illegible],  [illegible],  [illegible],  [illegible].79,
     +    [illegible],  [illegible],  [illegible],  [illegible],  [illegible],
     +    [illegible],  [illegible],  [illegible],  [illegible],  [illegible],
     +   -7.29,-10.47,-11.70,
     +   -4.74, -5.81, -7.10, -9.06,-10.59,
     +  -12.00,-13.62,-14.82,-15.51,-15.93,
     +  -16.28,-16.58,-16.80,
     +   -8.65, -8.87, -9.29, -9.37, -9.94,
     +  -10.29,-10.62,-10.93,-11.32,-11.67,
     +  -11.96,-12.08,-12.43,
     +   -9.02, -9.42,-10.19,-10.79,-12.39,
     +  -12.91,-13.51,-14.51,-12.86,-10.90,
     +  -11.44,-11.98,-12.52,-13.06,-13.60,-14.14,
     +  -15.82,-16.55,-17.75,-18.80,-17.77,-18.88,
     +  -12.96,-12.06, -5.92, -7.65,-12.26, -3.81/

      Ntp=0

*************************************************************************
      write(*,'(a/a,f4.2/a/)')
     +' ***************************************************************',
     +'        CBSD Point Source Scene Descriptor, Version ',Versn,
     +' ***************************************************************'
*************************************************************************

* Get the Problem Description From the User, Starting with Wave Band(s)
7     write(*,'(a,i1,a)')
     +  ' How Many Wavelength Bands (Maximum of ',MaxB,'):  '
      read(*,*) NumB
      if(NumB.gt.MaxB) then
        write(*,'(a,i1,a)') ' Hey, Wild Man, no more than ',MaxB,' !!'
        go to 7
       endif

      write(*,'(a)') ' BAND DEFINITIONS:'
      do 25 NB=1,NumB
9       write(*,'(a,i1,a)')
     +    '  Band ',NB,': WVmin(um), WVmax(um), Threshold(w/cm^2): ?'
        read(*,*) W1(NB),W2(NB),Thr(NB)
        if(W1(NB).ge.W2(NB)) then
          write(*,*) '   Silly Band Description, Try That One Again ...'
          go to 9
         endif

*       The Spectral Bandpass is
        DW(NB)=W2(NB)-W1(NB)
*       The Band Center is
        WC(NB)=W1(NB)+0.5*DW(NB)

        if(WC(NB).lt.2.4) then
          write(*,*) '   Band Center Must be >2.4um !! Try It Again ...'
          go to 9
         endif
        if(WC(NB).gt.25.) then
          write(*,*) '   Band Center Must be <25um !!  Try It Again ...'
          go to 9
         endif

        ArgE=14388.3/(WC(NB)*Tref)
        FDen=exp(ArgE)-1.
        FNum=11910.7/(WC(NB)**5)
*       The Brightness (w/cm^2/um) of Zero Absolute Magnitude is defined
*        (IPAS Explanatory Supplement Eqn VI.C.1) as:
        WOMag=1.57e-16*FNum/FDen
*       The In-Band Flux (w/cm^2) from Zero Magnitude Point Sources is
        FOmag(NB)=WOMag*DW(NB)
        SMRng=Thr(NB)/FOMag(NB)
```

```
        MagLim(NB)=1-nint(2.5*alog10(SMRng))
        write(*,*)
     +  '    ---------------------------------'
        write(*,'(a,i1,a,i3)')
     +  '    Band ',NB,' Limiting Magnitude is ',MagLim(NB)
        write(*,'(a,i1,a,1pe7.1)')
     +  '    Band ',NB,' Magnitude 0 In-Band Is ',F0Mag(NB)
        write(*,*)
     +  '    ---------------------------------'

*  The interpolation formula to be used for each band & spectral class is
*    AMag = Mag + fm1(NB)*(M2p4(Klass)-M12p(Klass))
*               + fm2(NB)*(M25p(Klass)-M12p(Klass))
*    where
        if(WC(NB).le.12.) then
          fm1(NB) = (12.-WC(NB))/(12.-2.4)
          fm2(NB) = 0.0
         else
          fm1(NB) = 0.0
          fm2(NB) = (WC(NB)-12.)/(25.-12.)
         endif

25      continue

*************************************************************************
* Now Get the User's Spatial Specification of the Scene (Image)
      write(*,'(/a)')
     +          ' Scene Definition May Be in Equatorial (R.A. & Dec)'
      write(*,*) '   or Galactic (GLon & GLat) Coordinate System;'
      write(*,*) '     ENTER 1 for Equatorial or 2 for Galactic:'
      read(*,*) ICtype
27    if(ICtype.eq.1) then
        write(*,*) ' RAmin, RAmax, DecMin, DecMax Should be in Degrees.'
        write(*,*) ' DLAM is Differential Lat/Lon (IFOV) in Arc-Minutes'
        write(*,*) ' ENTER RAmin, RAmax, DecMin, DecMax, DLAM : '
        read(*,*)    RAmin, RAmax, DecMin, DecMax, DLAM
        if((RAmin.gt.RAmax).or.(RAmin.lt.0.).or.
     +   (RAmax.gt.360.)) then
           write(*,'('' Silly R.A. Input  -  try again !'')')
           go to 27
         endif
        if((DecMin.gt.DecMax).or.(DecMin.lt.-90.).or.
     +     (DecMax.gt.90.)) then
             write(*,'('' Silly Declination Input  -  try again !'')')
             go to 27
         endif
*       Now Find the Galactic Coordinate Limits
        d2r=3.141593/180.
        r2d=180./3.141593
        rmrad192=d2r*(-192.25)
        s27=sin(d2r*27.4)
        c27=cos(d2r*27.4)
        GLatMin=90.
        GLatMax=-90.
        GLonMin=180.
        GLonMax=-180.
        do 2050 k=1,4
          if(k.eq.1) then
            ra=RAmin
            dc=DecMin
           else if (k.eq.2) then
            ra=RAmax
            dc=DecMin
           else if (k.eq.3) then
            ra=RAmin
            dc=DecMax
           else if (k.eq.4) then
            ra=RAmax
            dc=DecMax
           endif
          d=d2r*dc
          r=d2r*ra
```

```
          rm=r+rmrad192
          cdc=cos(d)
          sdc=sin(d)
          crm=cos(rm)
          srm=sin(rm)
          b=asin(cdc*[illegible])
          y=sdc*[illegible]
          x=cdc*srm*[illegible]
          rl=atan(y,[illegible])
          gb=[illegible]
          if(gb.lt.GLatMin) GLatMin=gb
          if(gb.gt.GLatMax) GLatMax=gb
          gl=33.+r2d*rl
          if(gl.gt.180.) gl=gl-360.
          if(gl.lt.GLonMin) GLonMin=gl
          if(gl.gt.GLonMax) GLonMax=gl
2050      continue
        write(*,2051) GLatMin,GLatMax,GLonMin,GLonMax
2051    format(/'The Galactic Coordinate Limits Will Be:'/
     +    '      Galactic Latitude: ',f6.1,' --> ',f6.1/
     +    '     Galactic Longitude: ',f6.1,' --> ',f6.1)
      else if(ICtype.eq.2) then
        write(*,*) ' GLatMin, GLatMax, GLonMin, GLonMax Are in Degrees.'
        write(*,*) ' DLAM is Differential Lat/Lon (IFOV) in Arc-Minutes'
        write(*,*) ' ENTER GLatMin, GLatMax, GLonMin, GLonMax, DLAM : '
        read(*,*)    GLatMin, GLatMax, GLonMin, GLonMax, DLAM
      endif
      if((GLatMin.gt.GLatMax).or.(GLatMin.lt.-90.).or.
     +  (GLatMax.gt.90.)) then
          write(*,'('' Silly latitude(s) input  -  try again !'')')
          go to 27
      endif
      if((GLonMin.gt.GLonMax).or.(GLonMin.lt.-180.).or.
     +   (GLonMax.gt.180.)) then
            write(*,'('' Silly longitude(s) input  -  try again !'')')
            go to 27
      endif
      write(*,'(/a/a/)')
     +' ***************************************************************',
     +' ***************************************************************'

* Pixel Size in Degrees and Pixel Area in deg^2
      DL=DLAM/60.
      APix=DL*DL

* Number of Pixels per Square Degree is
      PixPD=1./APix

* Initial Minimum Point Source Density of Interest = 0.01
      if((1./PixPD).lt.0.001) then
        PSDmin=0.1/PixPD
       else
        PSDmin=0.001
       endif
      LPSDmin=nint(1000.*alog10(PSDmin))

* NLat and NLon are Pixel Height and Width (in Galactic Latitude and
*  Longitude Space, Respectively) for the User-Specified Scene Image
      NLat=1+nint((GLatMax-GLatMin)/DL)
      if(NLat.gt.MaxSize) then
        write(*,'(i6,'' Latitude Pixels Are Too Many !!!'')') NLat
        go to 27
       endif
      NLon=1+nint((GLonMax-GLonMin)/DL)
      if(NLon.gt.MaxSize) then
        write(*,'(i6,'' Longitude Pixels Are Too Many !!!'')') NLon
        go to 27
       endif

      write(*,'('' Images will be: '',i4,'' cols, '',i4,'' rows'')')
     +        NLon,NLat
```

```
      KOutRecL=4*NLon
      DumName(1:3)='IM.'
      NVersn=nint(100.*Versn)
      write(DumName(4:7),'(i3,''.'')') NVersn
      do 10 n=0,9
        write(DumName(8:9),'(i1,''.'')') n
        do 5 NB=1,NumB
          OutName(NB)=DumName
          write(OutName(NB)(10:10),'(i1)') NB
          inquire(file=OutName(NB),exist=Already)
          if(Already) go to 10
5       continue
        if(Already) then
          go to 10
         else
          go to 12
         endif
10      continue
      write(*,'(//''!!!!! 10 Image Sets Already Exist !!!!!''//)')
      stop
12    do 14 NB=1,NumB
        OutName(NB)=DumName
        write(OutName(NB)(10:10),'(i1)') NB
        LUN=50+NB
        open(LUN,file=OutName(NB),access='direct',form='unformatted',
     +       recl=KOutRecl)
14      continue
      OutName(NumB+1)=DumName(1:9)//'L'
      open(50,file=OutName(NumB+1))
      write(50,'(3x,a/4x,a,f4.2/4x,a/)')
     +' ***************************************************************',
     +'        CBSD Point Source Scene Descriptor, Version ',Versn,
     +' ***************************************************************'
      write(50,'(4x,i1,a)') NumB,' Spectral Band Images'
      do 16 NB=1,NumB
        write(50,*)
     + '    ----------------------------------'
        write(50,'(a,i1,a,f4.1,a,f4.1,a,1pe8.2)')
     + '    Band ',NB,': W1=',W1(NB),' W2=',W2(NB),'  Thr=',Thr(NB)
        write(50,'(a,i1,a,i3)')
     + '    Band ',NB,' Limiting Magnitude is ',MagLim(NB)
        write(50,'(a,i1,a,1pe7.1)')
     + '    Band ',NB,' Magnitude 0 In-Band Is ',F0Mag(NB)
        write(50,*)
     + '    ----------------------------------'
16      continue
      write(50,'(/)')
      write(50,*)
     + '    GLatMin GLatMax GLonMin GLonMax   Pixel(Arc-Min)'
      write(50,*)
     + '    ------- ------- ------- -------   -------------'
      write(50,'(4x,4(f7.2,1x),5x,f7.3)')
     +       GLatMin,GLatMax,GLonMin,GLonMax,DLAM
      write(50,*)
     + '    ------- ------- ------- -------   -------------'
      write(50,'(/)')
      write(50,'(''    Images are: '',i4,'' cols, '',i4,'' rows'')')
     +       NLon,NLat
      write(50,'(/)')

      write(*,'(/a/)') '  Beginning Calculations ...'

*********************************************************************
```

```
*************************************************************************
* Read In The PSDM Coordinates List and Fill the Coordinates Tables
*  (n.b. the file "clist2" contains only the glat/glon values >=0)

      open(10,file='clist2')

      read(10,*) KLat
      do 30 NLa=KLat,(2*KLat-1)
        read(10,*) TbLat(NLa)
        NLamn=(2*KLat)-NLa
        TbLat(NLamn)=-TbLat(NLa)
30      continue
      KLat=2*KLat-1

      read(10,*) KLon
      do 35 NLo=KLon,(2*KLon-1)
        read(10,*) TbLon(NLo)
        NLomn=(2*KLon)-NLo
        TbLon(NLomn)=-TbLon(NLo)
35      continue
      KLon=2*KLon-1

      close(10)

* KLat and KLon are Now the Total Numbers of Galactic Latitudes
*  and Longitudes in the Filled Point Source Density Maps

*************************************************************************
* Read in the Array of PSDM Max Values
      open(20,file='PSDMmaxes',form='unformatted',access='direct',
     +       recl=2958)
      read(20,rec=1) PSDMmax
      close(20)

*************************************************************************
* Initialize the Flux Output Array(s)
      do 50 m=1,NLat
        do 50 l=1,NLon
          do 50 NB=1,NumB
            FlxU(1,l,m)=0.
            FlxU(2,l,m)=0.
            FlxU(3,l,m)=0.
50          continue

*************************************************************************
* First Get the PSC Bright Sources Which Are in the User-Specified Field

      NBriteU=0
      HalfDL=DL/2.0
      gbmin=GLatMin-HalfDL
      gbmax=GLatMax+HalfDL
      glmin=GLonMin-HalfDL
      glmax=GLonMax+HalfDL
      do 2100 NB=1,NumB
2100    fmb(NB)=(WC(NB)-12.)/(25.-12.)
      open(8,file='pscbrt_g.mag')
      do 2300 n=1,NBrite
        UseBrite=.false.
        read(8,'(f7.3,f8.3,2f6.1)') gb,gl,rm1,rm2
        if((gb.lt.gbmin).or.(gl.lt.glmin).or.(gl.gt.glmax)) go to 2300
        if(gb.gt.gbmax) go to 2350
        IndLat=nint(1.+(gb-GLatMin)/DL)
        IndLon=nint(1.+(gl-GLonMin)/DL)
        do 2200 NB=1,NumB
          AMag=rm1+fmb(NB)*(rm2-rm1)
          if(AMag.gt.MagLim(NB)) go to 2200
          UseBrite=.true.
          PFlux=F0Mag(NB)*(10.**(-0.4*AMag))
          FlxU(NB,IndLon,IndLat)=FlxU(NB,IndLon,IndLat)+PFlux
2200      continue
        if(UseBrite) NBriteU=NBriteU+1
2300    continue
```

```
2350  continue

      close(8)
      write(*,'(a,i10)')
     + '    IRAS/PSC Point Sources >= 12um Magnitude  0 = ',NBriteU
      write(*,*)
     + '    ------------------------------------------------------'
      write(50,'(a,i10)')
     + '    IRAS/PSC Point Sources >= 12um Magnitude  0 = ',NBriteU
      write(50,*)
     + '    ------------------------------------------------------'

*************************************************************************

*** CENTRAL MASTER WAVELENGTH ***
          Lambda=12
*********************************

      Lambda10=nint(10.*Lambda)

* Initialize the PSDM Name Template
      TmpName='PSDM_tt_mmm_www'
*                 `6 `9  `13
      if(Lambda10.ge.100) then
        write(TmpName(13:15),'(i3)') Lambda10
       else
        write(TmpName(13:15),'(''0'',i2)') Lambda10
       endif

*****  CORRECT ONLY FOR MagMax=-1 *****
*****   v3.5: MagMax=+1 Now !!!   *****
**!!! Temporarily
      MagLimx=15
*     NMag=2+MagLimX
      NMag=  MagLimX
      do 60 N=1,NMag
*        MMag(N)=-2+N
         MMag(N)=   N
60       continue
*****************************************

*************************************************************************
*************************************************************************
*  Point Source Image Generation, First Looping Over the Magnitude Bins
      do 900 NM=1,NMag
        Mag=MMag(NM)
        MapName=TmpName
        MMag10=10*MMag(NM)
        if(MMag10.lt.0) then
          write(MapName(9:11),'(i3)') MMag10
         else if(MMag10.lt.10) then
          write(MapName(9:11),'(''00'',i1)') MMag10
         else if(MMag10.lt.100) then
          write(MapName(9:11),'(''0'',i2)') MMag10
         else
          write(MapName(9:11),'(i3)') MMag10
         endif

*************************************************************************
        Finished=.true.
        do 100 Klass=1,87
          TooSmall(Klass)=.true.
          do 75 NB=1,NumB
            AMag  = Mag + fm1(NB)*(M2p4(Klass)-M12p(Klass))
     +                  + fm2(NB)*(M25p(Klass)-M12p(Klass))
            if(AMag.le.MagLim(NB)) then
              TooSmall(Klass)=.false.
              Finished=.false.
             endif
            PSFlx(NB,Klass) = F0Mag(NB)*(10.**(-0.4*AMag))
75          continue
```

```
          if(Klass.lt.10) then
            write(MapName(6:7),'(''0'',i1)') Klass
           else
            write(MapName(6:7),'(i2)') Klass
           endif

*  !!!!!!!!!!!!!!!!!!!!!!!!!!!!!!!!!!!!!!!!!!!!!!!!!!!!!!!!!!!!!!!!!!!!!!!
*  !!! The Proper PSDM Directory Name Must be Here !!!
          FullPath='/files3/PSDM.3.15/'//MapName
*  !!!!!!!!!!!!!!!!!!!!!!!!!!!!!!!!!!!!!!!!!!!!!!!!!!!!!!!!!!!!!!!!!!!!!!!

          open(30,file=FullPath,access='direct',form='unformatted',
     +      status='old',recl=1798)
          read(30,rec=1) IDNTB
          close(30)

          do 90 NLa=1,KLat
            do 85 NLo=1,KLon
            if(IDNTB(NLo,NLa).lt.LPSDmin) then
              DNTB(KLass,NLo,NLa)=0.
             else
              DNTB(Klass,NLo,NLa)=10.**(real(IDNTB(NLo,NLa))/1000.)
             endif
            DNTO(NLo,NLa)=DNTO(NLo,NLa)+DNTB(Klass,NLo,NLa)
85          continue
90        continue

100       continue

        if(Finished) go to 925

*************************************************************************
*  Loop Over Latitude & Longitude to Accumulate Flux into Image Pixels
        do 500 m=1,NLat
*         Compute a Latitude Value of the Output Image
          GLat=GLatMin+real(m-1)*DL
*         Find the Proper Latitude Table Entries to Interpolate Between
          do 200 j=1,KLat
            if((GLat.ge.TbLat(j)).and.(GLat.le.TbLat(j+1))) then
              Lat1=j
              TbLat1=TbLat(Lat1)
              Lat2=j+1
              TbLat2=TbLat(Lat2)
              go to 205
             endif
200         continue

205       Lon1=-1
          Lon2=0
          do 400 n=1,NLon
*           Compute a Longitude Value of the Output Image
            GLon=GLonMin+real(n-1)*DL
            if(Lon1.eq.-1) then
*             Find the Proper Longitude Table Entries to Interpolate Between
              do 300 k=1,KLon
                if((GLon.ge.TbLon(k)).and.(GLon.le.TbLon(k+1))) then
                  Lon1=k
                  TbLon1=TbLon(Lon1)
                  Lon2=k+1
                  TbLon2=TbLon(Lon2)
                  go to 310
                 endif
300             continue
             endif
305         if(GLon.gt.TbLon2) then
              Lon1=Lon1+1
              TbLon1=TbLon(Lon1)
             Lon2=Lon2+1
              TbLon2=TbLon(Lon2)
             endif
            if(GLon.gt.TbLon2) go to 305
```

```
*  Add a little randomness to choice of map grid points in order
*  to reduce visibility of contouring in the flux output images
310         if((Lat1.gt.1).and.(Lat1.lt.KLat)) then
              if(rand(0).lt.0.67) then
                Lat1U=Lat1
               else
                Lat1U=Lat1-1
              endif
             else
              Lat1U=Lat1
             endif
            TLat1U=TbLat(Lat1U)

            if((Lat2.gt.1).and.(Lat2.lt.KLat)) then
              if(rand(0).lt.0.67) then
                Lat2U=Lat2
               else
                Lat2U=Lat2+1
              endif
             else
              Lat2U=Lat2
             endif
            TLat2U=TbLat(Lat2U)

            if((Lon1.gt.1).and.(Lon1.lt.KLon)) then
              if(rand(0).lt.0.67) then
                Lon1U=Lon1
               else
                Lon1U=Lon1-1
              endif
             else
              Lon1U=Lon1
             endif
            TLon1U=TbLon(Lon1U)

            if((Lon2.gt.1).and.(Lon2.lt.KLon)) then
              if(rand(0).lt.0.67) then
                Lon2U=Lon2
               else
                Lon2U=Lon2+1
              endif
             else
              Lon2U=Lon2
             endif
            TLon2U=TbLon(Lon2U)

            Atot=(TLon2U-TLon1U)*(TLat2U-TLat1U)

            DNTO4 = DNTO(Lon1U,Lat1U)+DNTO(Lon1U,Lat2U)
     +             +DNTO(Lon2U,Lat1U)+DNTO(Lon2U,Lat2U)
            if(DNTO4.lt.PSDmin) go to 400

* Set Up the Factors for Bi-Linear Interpolation
            f1=GLat-TLat1U
            f2=TLat2U-GLat
            f3=GLon-TLon1U
            f4=TLon2U-Glon
            r1=f2*f3/Atot
            r2=f2*f4/Atot
            r3=f1*f4/Atot
            r4=f1*f3/Atot

*    Rough, Preliminary Implementation of Dispersion Within a Magnitude
*           FlxDsp=10.**(-0.2+0.4*rand(0))
*    Changed for Version 5.0 So, For Example, Bin M=1 Now Accounts For
*      Sources with Magnitudes <0 and >1 Rather Than for Sources With
*      Average Magnitude=1.  In Addition to Being More Appropriate for
*      Working With the PSC Data Base, This is Also More Correct Than
*      Before for Working With the SKY-Derived PSDM Data Base.
            FlxDsp=10.**(-0.4+0.4*rand(0))
```

```
            do 375 Klass=1,87
              if(TooSmall(Klass)) go to 375
              ADEN=
     +        (r1*DNTB(Klass,Lon2U,Lat1U))+(r2*DNTB(Klass,Lon1U,Lat1U))+
     +        (r3*DNTB(Klass,Lon1U,Lat2U))+(r4*DNTB(Klass,Lon2U,Lat2U))
              if(ADEN.lt.PSDmin) go to 375
              PDEN=APix*ADEN
               if(PDEN.ge.1.) then
                PDEN=nint(PDEN)
                Ntp=Ntp+PDEN
                do 350 NB=1,NumB
                  FlxU(NB,n,m)=FlxU(NB,n,m)+PDEN*FlxDap*PSFlx(NB,Klass)
350               continue
               else
                if(rand(0).gt.PDEN) go to 375
                Ntp=Ntp+1
                do 360 NB=1,NumB
                  FlxU(NB,n,m)=FlxU(NB,n,m)+FlxDap*PSFlx(NB,Klass)
360               continue
               endif
375           continue

400         continue
500       continue

          write(*,'(a,i2,a,i10)')
     +  '   CBSD/PSM Point Sources >= 12um Magnitude ',Mag,' = ',Ntp
          write(50,'(a,i2,a,i10)')
     +  '    CBSD/PSM Point Sources >= 12um Magnitude ',Mag,' = ',Ntp

          if(PSDmin.lt.1.) then
            PSDmin=PSDmin*1.58489
            LPSDmin=LPSDmin+200
           endif

900       continue
**************************************************************************
**************************************************************************

925    Ntp=NBriteU+Ntp
       write(*,*)
      +  '  ------------------------------------------------'
       write(*,'
      +('' Total Point Sources in Image(s):    '',i10)') Ntp
       write(50,*)
      +  '    ------------------------------------------------'
       write(50,'
      +('' Total Point Sources in Image(s):    '',i10)') Ntp
       close(50)

*  The FITS File Writer Has Been Temporarily Removed for Re-Writing in a Form
*    Which Accommodates Both Byte-Reversed and Non-Byte-Reversed Hardware.

       do 1000 NB=1,NumB
         LUN=50+NB
         krec=1
         do 950 m=1,NLat
           write(LUN,rec=krec) (FlxU(NB,n,m), n=1,NLon)
           krec=krec+1
950        continue
         close(LUN)
1000     continue

       stop

       end


spa%
```

4 THE CBSD ASTEROIDS, SUN, MOON, & PLANETS MODULE

4.1 INTRODUCTION

This purpose of this chapter is to assist the general user in applying the CBSD Asteroids, Moon, and Planets (CBAMP) module to generate IR celestial background scenes which include the major and minor planets, as well as the Sun and Moon. Sections 2 and 3 provide a general and detailed description of CBAMP. Section 4 contains user information for program operation. Section 5 discusses portability.

4.2 GENERAL DESCRIPTION

Program CBAMP generates an image file of asteroid and major planets, with proper positions and with relative intensity levels corresponding to predicted asteroid infrared flux densities at a specified wavelength. The Sun and Moon are also shown in the image if within the field of view. The user specifies the field of view by entering the number of pixels per degree, and also the center of the image. The time for calculation of the geocentric ephemeris is also entered by the user. A radiance map file is also generated, containing infrared flux densities of all objects except the Sun.

The asteroid database AST1989.002 contains radiometry data for all ID 1 asteroids listed in the IRAS Infrared Astronomical Satellite Asteroid and Comet Survey. The named asteroid database (ELEM1989.002) and the unnamed asteroid database (U891001.AST) were provided by Ed Tedesco, JPL, Calif. Institute of Technology.

The position, distances and phase angle of the major planets are calculated in the same manner as the asteroids. The same thermal model is also applied, using a phase integral of 1.5 for all major planets.

4.3 DETAILED DESCRIPTION

The Sun's geocentric equatorial rectangular coordinates are calculated for the time of the ephemeris, using Newcomb's method. Perturbation corrections due to gravitational influences from the Moon, Venus, Mars, Jupiter and Saturn are applied, giving a highly accurate position of the Earth-Sun.

After reading the orbital osculating elements of an asteroid, subroutine LOCATE is called. LOCATE returns the following: Minor planet's mean place; Sun-asteroid distance (radius vector); Earth-asteroid distance, and the phase angle (Sun-asteroid-Earth). Planetary aberration, ie. annual aberration and light-time correction, is applied in calculating the above elements.

The standard thermal model used to calculate the infrared flux densities was provided by Mark Sykes (University of Arizona) and has been described previously in a CBSD Topical Report. The input parameters from the database used by Sykes' algorithm are: bolometric Bond albedo, phase integral, and diameter. These parameters are available from data in the IRAS database.

4.3.1 Subroutine LOCATE

Subroutine LOCATE performs the function of calculating the geocentric ephemeris of elliptic orbits, given the following inputs:

X,Y,Z	Sun's geocentric equatorial coordinates
T1	Julian date for calculation of ephemeris
T2	Julian date for EPOCH of orbital elements
MM	Mean motion (degrees per day)
M0	Mean anomaly at T2
AP	Argument of perihelion (referred to B1950.0)
OMEGA	Longitude of ascending node (referred to B1950.0)
INCL	Inclination of orbit (referred to B1950.0)
E	Eccentricity SMA Semi-major axis (AU)
OBLIQ	Obliquity of the ecliptic (at B1950.0)

The true anomaly is derived from the eccentric anomaly which is found using the Keplerian equation. After the heliocentric coordinates of the object are calculated, they are summed with the Sun's geocentric coordinates to obtain the geocentric coordinates of the asteroid or planet. A second pass thru the above process using a modified mean anomaly, by subtracting light-time, corrects the geocentric coordinates of the object to account for planetary aberration. Right ascension, declination and phase angle are subsequently computed.

Returned parameters:

RA	Right ascension at T1
DEC	Declination at T1
RV	Sun-object distance
DR	Earth-object distance

BETA Phase angle (Sun-object-Earth)

4.3.2 Minor Planets

The IRAS asteroid database (AST1989.002) contains geometric albedo, diameter and phase integral extracted from the IRAS Asteroid and Comet Survey for all ID 1 asteroids. The named asteroid database (ELEM1989.002) is comprised of 4000 asteroids and includes all 1790 IRAS ID 1 asteroids. The unnamed asteroid database (U891001.AST) contains 9643 asteroids. The orbital elements for all asteroids are for Epoch October 1,1989.

For all IRAS asteroids, the orbital elements are extracted from the named asteroid database. If the IRAS asteroid is located within the field of view, parameter values in the IRAS asteroid database are used in the Standard Thermal Model to determine the flux density of the asteroid.

For all non-IRAS asteroids located within the field of view, an albedo must be assumed in order to calculate a diameter. From photometric parameters and orbital elements for a given asteroid, the asteroid is assigned to 1 of 8 groups of asteroids. A geometric albedo is then randomly selected for the asteroid based on an albedo histogram of the group members. (The histogram data is contained in file ALBPROB.DAT) The bolometric Bond albedo and diameter can then be estimated. The flux density is determined with the Standard Thermal Model using the above derived Bond albedo and diameter.

If the asteroid is not occulted by the Sun or Moon, a gray level that is proportional to the logarithm of the flux density is inserted in the image array. A logarithmic range is selected in order to display all asteroids. A radiance map is also generated with the flux (JY/SR) scaled to the pixel size .

4.3.3 Major Planets

The major planet database (PLAN1990.002) contains the orbital elements, geometric albedo, and radius for all the planets. This information was obtained from the Astronomical Almanac 1990. The orbital elements, thus obtained, are for Epoch August 17,1990 and are referred to the mean ecliptic and equinox of J2000.0.

In order to refer the major planets to the same equator and equinox as the asteroids, the following orbital elements are reduced from equinox J2000.0 to B1950.0.:

Inclination of orbit,
Longitude of ascending node,
Argument of the perihelion.

Then the same procedure used for the asteroids is used to obtain the planet's mean place, radius vector, distance from the Earth and phase angle. Also, the same thermal model is used to obtain the flux density. A phase integral of 1.5 is used for all major planets.

The flux density is calculated for all planets and written to the list file CBAMP.LST. An asterisk is placed before the name of each planet that appears within the field of view.

The planets which are located within the field of view are shown in the image above the first two letters of their name. The gray level of the pixel representing the planet is proportional to the logarithm of the flux density. The flux is scaled to the pixel size (JY/SR) and inserted in a radiance map for each planet within the field of view.

4.3.4 Moon

The Moon's geocentric mean ecliptic longitude, latitude and parallax are calculated using periodic terms obtained from "Astronomical Formulae for Calculators" by Jean Meeus. This method uses only the most important periodic terms, giving an accuracy of approximately 10 seconds in longitude and 3 seconds in latitude. The longitude and latitude of the center of the Moon are obtained, referred to the mean equator and equinox of date of the ephemeris. The equatorial horizontal parallax is obtained so that the angular diameter of the Moon and the distance between centers of the Earth and Moon can be determined. The transformation of the Moon's geocentric ecliptical coordinates into equatorial coordinates is performed.

The above equatorial coordinates referred to the equator and equinox of date are further reduced to positions referred to the equator and equinox of B1950.0. The rigorous method used in this transformation was found in "Astronomical Formulae for Calculators" by Jean Meeus.

Next subroutine LPHASE is called. This subroutine calculates the phase angle of the Moon, given the following terms:

Moon's geocentric mean ecliptic longitude & latitude;
Sun's true ecliptic longitude;
Sun's and Moon's mean anomaly;

(all positions referred to the equinox of date). The subroutine also returns the Earth-Sun distance, which is used with the phase angle of the Moon and Earth-Moon distance to calculate the radius vector of the Moon.

Subroutine SUNPOS is called to calculate the position of the Sun. First the geocentric mean longitude of the Sun is converted to equatorial coordinates referred to the equator and equinox of date. Then the equatorial coordinates are found for the equator and equinox of B1950.0 and stored in Common.

Subroutine LUNDRW is called if the center of the Moon is located within the field of view. The subsolar temperature of the Moon is determined. Also the position angle of the Moon's bright limb, and the angular separation from the subearth point to the subsolar point are determined. The later two parameters are used to calculate the coordinates of the subsolar point using a coordinate system with an origin at the subearth point. Then the coordinates of each pixel located on the disk of the Moon is determined. This method assumes an orthographic projection of the Moon onto the disk, i.e. a full hemispheric view of the Moon. With the coordinates of the subsolar point and each pixel, the central angle between the subsolar point and each pixel area can be established.

The gray level for the Moon's disk on the dark side (central angle greater than 90 degrees) is set to a low level in the image and the sunlit side of the disk is set to maximum gray level. Radiance values are computed for the radiance map array for each pixel on the Moon's disk.

4.3.5 Sun

If the center of the Sun is located within the field of view, the Sun's disk (either full or partial) is displayed in the image file at maximum brightness. No attempt has been made to convert the Sun's pixel areas to flux values and place them in the radiance map. Finally the first two letters of the name (SU) is placed below the Sun in the image, as done with the Moon and major planets.

4.4 PROGRAM OPERATION

The program requires a total of 7 parameters arranged in 4 groups. When multiple parameters are entered in response to a message, the parameters may be separated by commas, spaces, or carriage returns. The 4 groups are arranged for input as follows:

(a) message: ENTER NUMBER OF PIXELS PER DEGREE (DEFAULT 30)
parameter: PIX (real): enter "," for default or a value greater than 5

(b) message: ENTER RA,DEC OF CENTER (IN DEGREES)
parameters: RA0 (real): Right Ascension at center of FOV
Range: 0 to 360 degrees
DEC0 (real): Declination at center of FOV
Range: -90 to 90 degrees
(equatorial coordinates)

3) message: INPUT WAVELENGTH IN MICRONS
parameter: WAVE (real): Range: 12 to 100
parameter used in the thermal model

4) message: ENTER YEAR,MONTH,DAY (U.T.) YYYY MM DD.DDDD
parameters: IYR (integer) Must enter all 4 digits
MON (integer) May be 1 or 2 digits
DD (integer) The day may contain any fraction

The output from the program is contained in the following files.

1) CBAMP.LST:

Contents includes monochromatic flux, ID, right ascension, declination, radius vector (Sun-object distance) and phase angle for each asteroid in the field of view. The file also includes Sun, Moon and major planet data.

2) CBAMP.PIC:

512 by 512 byte array containing gray level values in the range of 0 to 255, representing logarithmic scaled flux density of the major and minor planets. The pixels representing the Sun and sunlit portion of the Moon are assigned values of 255.

3) CBAMP.OUT:

512 by 512 radiance map (real*4 binary) of monochromatic flux for each major and minor planet The flux densities are rescaled to the pixel size. Radiance values are included for each pixel on the Moon's disk. The Sun is not included.

A description of the input files necessary to run the program can be found in previous Sections.

4.5 PORTABILITY

The program was developed on a Concurrent 3260 computer using a Fortran VII compiler providing most of the extensions to ANSI X3.9-1978. Portability problems should be limited to I/O statements. Therefore the open statements should be modified to comply with the requirements of the Fortran compiler in use.

CBAMP has also been hosted on a COMPAQ 386 using Microsoft and Lahey F77L-EM/32 Fortran compilers. The Microsoft version had to be limited in size to less than 640K. Therefore the radiance array was eliminated in order to check the compatibility. The Lahey compiler, not constrained to the 640K limit, produced object code for the entire program. No compiler errors occurred after modifying the open statements and the write statement that outputs the image array.

Sources and Acknowledgments

(1) **Mark Sykes, Steward Observatory, Univ. of Arizona:**
Standard thermal model and method to estimate the thermal model input parameters for non-IRAS asteroids.

(2) **Edward Tedesco, JPL, Calif. Institute of Technology:**
Named and Unnamed asteroid databases.
Subroutines XYZSUB and XYZPER

(3) **National Space Science Data Center (NSSDC):**
Database from the IRAS Asteroid and Comet Survey

(4) **Astronomical Almanac:**
Orbital elements, geometric albedo and radius of the major planets. Almanac was used for partial program verification.

(5) **Spherical Astronomy, by Robin M. Green**

(6) **Astronomical Formulae for Calculators, by Jean Meeus:**
Methods and formulae for generating ephemeris algorithms

5 SUMMARY

This report has described the major algorithms and software modules now available for scene generation within the CBSD program. As indicated in previous sections, particularly Chapters 2 and 3, these modules will be undergoing continuing refinements for 3-6 months. Primary among those refinements are completion of the derivation of CBZODY vs IRAS ZOHF "best fit" parameters and full assimilation of SKY Version 3 into the point source module. Nevertheless, the existing software is sufficiently mature, debugged, and validated against IRAS data as to be available to support scene generation in a large variety of contexts.

As outlined in the introduction, extensions to the point source module for more complete treatments of nebulae and HII regions are presently in progress. In addition, the point source module will soon be expanded to include the four classes of extra-galactic "point sources" for which luminosity functions are available in the NASA/Ames SKY model: "red" normal galaxies, "blue" normal galaxies, quasars, and Seyferts. Upon completion of those extensions, the IPAC data base for large galaxies will be employed to provide CBSD with a spatially complex description capability for approximately thirty galaxies.

At present, each CBSD module exists as stand-alone software, each has its own input interface, and each generates its own binary output image. These modules have very purposefully been initially developed in this manner. Debugging and validation are obviously simplified by this approach. In addition, this approach streamlined the assimilation of early CBSD code versions into SSGM, because it made it possible to quickly "hard-wire" individual CBSD modules into SSGM without dealing with multiple code interface levels.

The final version of CBSD will include an "executive" module which will couple each of the modules to one input interface and manage the integrated operation of the modules, directed at producing one summed output image. This CBSD "executive" module will generate one FITS-formatted image file for each user scene specification. (FITS is a flexible and well-documented data standard which greatly simplifies the transfer of large binary data sets between disparate computers.) However, this CBSD architecture will still call for each module to generate its own partial output file, with a common binary format, each file representing the contribution of one phenomenology to the IR background in a given region of sky. In that manner, a user will always be able to examine the individual components of a "multi-component" scene. We believe that approach will address the largest variety of usage interests, and also simplify any future augmentation of CBSD code.